Detection and Utilization of the Information Potential of Airborne Laser Scanning Point Cloud and Intensity Data by Developing a Management and Analysis System

DISSERTATION

Bernhard Höfle

submitted to the Faculty of Geo- and Atmospheric Sciences
at the University of Innsbruck

for the degree of
Doctor of Natural Sciences (Doctor rerum naturalium)

supervised by

Univ. Prof. Dr. Johann Stötter
Institute of Geography, University of Innsbruck

Univ. Prof. Dr. Norbert Pfeifer
Institute of Photogrammetry and Remote Sensing, Vienna University of Technology

Innsbruck, August 2007

https://doi.org/10.11588/heidok.00036930

Acknowlegdements

First of all, I would like to thank my supervisors and mentors *Johann Stötter* and *Norbert Pfeifer*.

Additionally, I want to thank *Hannes Kleindienst* (Grid-IT) and *Joachim Lindenberger* (Topscan GmbH) for their support of our research project at alpS.

I would like to thank all my co-authors and article reviewers for the fruitful discussions and support to reach the final quality of the papers. Especially *Martin Rutzinger*, who was not only co-author and lead author but also a good friend and motivator throughout the years of this thesis.

Last but not least, I feel glad that I can "officially" announce big "Thanks" to *Monika Hämmerle*. Your LaTeX skills helped to finish this thesis. The future is Ours!

Bernhard Höfle
Innsbruck
August 23, 2007

Abstract

Detection and Utilization of the Information Potential of Airborne Laser Scanning Point Cloud and Intensity Data by Developing a Management and Analysis System

Keywords: Airborne Laser Scanning, Point Cloud, Signal Intensity, Correction, Segmentation, Classification, Open Source GIS, Spatial Database, Glaciology, Roof Delineation

In recent years Airborne Laser Scanning (ALS) evolved to the state-of-the-art technique for topographic data acquisition. High resolution and highly accurate digital elevation models can be produced with a high degree of automation. Especially in vegetated areas and in areas with low surface texture this active remote sensing technique surpasses traditional aerial imagery in acquiring terrain information.

Until now, primarily the rasterized elevation models (Digital Terrain and Surface Models) were used due to the simple data model (regular grid) and the multitude of existing image/raster analysis methods. The original measurements – the ALS point cloud – are generally delivered to end-users but not often used because of the lack of management and analysis strategies that can handle the incidental data volume ($>$1 pt/m^2 multiplied by scanned area). The point cloud – tuples of 3D coordinates, a value for received signal intensity and a timestamp – contains the highest degree of information as it represents the three-dimensional, ungeneralized result of ALS data acquisition.

This thesis aims to utilize the full information inherent in the ALS point cloud and the intensity value. Therefore, a new concept for spatial data management of laser points and their additional information (e.g. intensity, timestamp, scanner positions) is introduced. The Geographic Information System (GIS) is used to bridge existing raster processing methods and novel point cloud management and analysis methods. The developed information system "LISA" (LIdar Surface Analysis) integrates existing Open Source software (e.g. GRASS GIS) allowing a fast and easy implementation of new processing tools, which can make use of both, ALS elevation models and the original point cloud. Point cloud management is performed in an external spatial database management system (PostgreSQL/PostGIS). A new ALS data model was developed and the existing spatial index was extended to improve performance.

Previous research studies working with signal intensity of pulsed ALS systems stated that there is a large potential for supporting surface classification and object detection. Before making use of the intensity value, it has to be corrected for known influences (e.g. emitted power, spherical loss, topographic and atmospheric effects), which are derived from the radar equation. This thesis introduces, implements and evaluates two fully automatic approaches for intensity correction to derive a value proportional to surface reflectance, which

is well suited for surface classification. The first method, the data-driven approach, empirically determines a correction function accounting for influences correlating with range (distance scanner-target). The second method, the model-driven approach, derives individual correction factors for each laser point by applying the radar equation. The "disturbing" effects could be successfully reduced (<noise level of ca. 10%) with both methods.

Two application examples demonstrate the large potential of having concurrent access to the point cloud and its derivatives (e.g. Digital Surface Model, corrected intensity, laser range vectors). The GIS component of the LISA system allows implementing object-based analysis approaches, which overcome the "salt & pepper" problem of traditional image analysis. Additionally, geometric, topological, contextual and multi-resolution information can be regarded in the object-based methodology.

The first application example detects glacier features on basis of the original ALS point cloud. A segmentation task (region growing) utilizes the spatial and corrected intensity information of the laser points, which exhibits a good separability of the different glacier surface facies (ice, firn, snow and surface irregularities). Two-dimensional alpha shapes and a gap filling procedure (using Voronoi diagrams) are used to derive a gapless vector representation (GIS vector layer) of the glacier surface. A supervised, rule-based classification is applied to label the homogeneous segments. Further, neighboring segments of the same class are merged to the final objects. An overall classification accuracy of >90% and a delineation accuracy <2 m could be achieved.

The second application introduces a novel procedure for building detection and roof facet modeling and classification by combining object-based image and point cloud analysis. This thesis contributes the framework (LISA system) for point cloud analysis put on top of the building detection algorithm. The final roof modeling originates from a hierarchical, multi-resolution object detection. Firstly, the building polygons are derived from a fill sinks segmentation on the inverted Digital Surface Model. Secondly, these building objects are used to extract the corresponding laser points for each building. Finally, a point cloud segmentation task (region growing) using the normal vectors in each laser point (derived by plane fitting in a defined neighborhood) is applied to identify planar objects (roof patches). The 3D roof facets are further classified by their slope. This result can be used as input for a multitude of applications, such as snow load capacity modeling or photovoltaics site analysis.

This thesis concludes that efficient ALS data management integrated in a GIS environment allows moving some steps forward to the major goal of the "detection and utilization of the the full information potential". Without additional costs added value can be generated out of existing ALS datasets (e.g. intensity correction). Future research should incorporate state-of-the-art ALS data (full-waveform) as well as terrestrial laser scanning data.

Kurzfassung

Detektion und Anwendung des Informationspotenzials von flugzeuggestützten Laserscanner Punktwolken- und Intensitätsdaten durch die Entwicklung eines Verwaltungs- und Analysesystems

Flugzeuggestütztes Laserscanning (auch Airborne Laser Scanning oder kurz ALS) entwickelte sich in den letzten Jahren zu einer operationell einsetzbaren Methode zur topographischen Erfassung der Erdoberfläche. Vor allem in Gebieten mit hoher Vegetation und schwacher Oberflächentextur übertrifft diese aktive Fernerkundungsmethode traditionelle optische Verfahren (z.B. Luftbildphotographie) in der Erfassung des Geländes (Boden). Bis zum jetzigen Zeitpunkt wurden vor allem die hoch auflösenden und hoch genauen digitalen Gelände- und Oberflächenmodelle für weitere Analysen herangezogen, da es dafür bereits eine Vielzahl von Bild- bzw. Rasteranalysewerkzeugen gibt. Das eigentliche Messergebnis, die originäre Punktwolke, wird zwar oft mitausgeliefert, aber meistens nicht verwendet, da es an Verwaltungs- und Analysetools für diese große Datenmenge mangelt ($>$1 Punkt/m^2 multipliziert mit der gescannten Fläche). Diese Punktwolke setzt sich aus vielen Einzelmessungen zusammen, bestehend aus den 3D-Koordinaten, einem Wert für die Intensität des reflektierten Laserimpulses und einem Zeitstempel.

Das Ziel dieser Arbeit ist, den vollen Informationsgehalt der ALS Punktwolke zu nützen, indem ein neues Konzept für die Verwaltung dieser räumlichen Daten eingeführt wird. Das Geographische Informationssystem (GIS) wird dazu als Mittler zwischen bestehenden rasterbasierten Algorithmen und der neu entwickelten Punktwolkenverwaltung herangezogen. Das entwickelte Informationssystem "LISA" (LIdar Surface Analysis) verwendet ausschließlich bestehende Open Source Software (z.B. GRASS GIS), wodurch eine schnelle und einfache Implementierung neuer Auswertestrategien, die GIS- und Punktwolkenfunktionalität nützen, möglich wird. Die Punktwolkenverwaltung wird unter Verwendung des Datenbankmanagementsystems PostgreSQL/PostGIS umgesetzt. Hierfür wird ein spezielles Datenmodell für ALS Daten entworfen sowie der bestehende räumliche Index verbessert.

Frühere Studien sprechen dem aufgezeichneten Intensitätssignal ein großes Potenzial für die Klassifikation von Oberflächen zu. Bevor dieser Wert verwendet werden kann, müssen variable Einflussfaktoren, die in der Radargleichung erfasst sind (z.B. ausgesandte Leistung; entfernungsabhängige, atmosphärische und topographische Effekte), korrigiert werden. In dieser Arbeit werden zwei Verfahren zur vollautomatischen Korrektur der Intensität entwickelt, implementiert und evaluiert, um schlußendlich einen Wert proportional zum Reflexionsgrad der Oberfläche zu erhalten, der sich sehr gut für die Klassifikation der gescannten Oberflächen eignet. Die erste Methode (datengetriebener Ansatz) ermittelt empirisch eine globale Korrekturfunktion, die alle entfernungsabhängigen Einflüsse berücksichtigt. Die zweite Methode (modellgetriebener Ansatz) leitet sich direkt aus der vorher genannten

Radargleichung ab. Eine erfolgreiche Reduktion der variablen Einflüsse ($<10\%$) kann mit beiden Methoden erzielt werden.

Diese Arbeit soll die Möglichkeiten verdeutlichen, die durch das entwickelte Informationssystem und die Intensitätskorrektur eröffnet werden. Der volle Zugriff auf die Punktwolke sowie die gleichzeitige Einbeziehung von ALS Rasterderivaten und korrigierter Intensität stellen den Kernpunkt dieser Analysen dar. Durch die GIS-Komponente des LISA Systems ist es möglich, objektbasierte Analysemethoden umzusetzen, die mit dem in der bildbasierten Fernerkundung bekannten "salt & pepper" Effekt umgehen können. Der objektbasierte Ansatz erlaubt es zusätzlich Objektgeometrie, Nachbarschaftsbeziehungen und verschiedene Auflösungsstufen miteinzubeziehen.

Das erste Anwendungsbeispiel detektiert und klassifiziert verschiedene Gletscherfacies (Eis, Firn, Schnee sowie Gletscherspalten) auf Basis der ALS Punktwolke. Die Kombination aus räumlicher Information und korrigierter Intensität erlaubt eine gute Abgrenzung der einzelnen Oberflächenklassen. In einem ersten Schritt werden räumlich zusammenhängende, homogene Punktwolkenbereiche identifiziert ("region growing" Segmentierung). Mit Hilfe von "alpha shapes" werden diese Segmente abgegrenzt. Kleine Lücken zwischen den entstandenen Polygonen werden durch einen neu entwickelten Algorithmus gefüllt. Das Ergebnis ist ein Vektordatensatz (GIS Polygon-Layer) der segmentierten Gletscheroberfläche. Durch Anwendung einer überwachten, regelbasierten Klassifikation können benachbarte Segmente gleicher Klasse zu den finalen Objekten zusammengefasst werden. Es wird gezeigt, dass mit dem vorgestellten Ansatz eine Gesamtgenauigkeit der Klassifizierung über 90% mit einer Abgrenzungsgenauigkeit unter 2 m erreicht werden kann.

Die zweite Anwendung stellt eine neue Methode zur Gebäudedetektion und Dachflächenmodellierung vor, der ein kombinierter Ansatz aus objektbasierter Bild- und Punktwolkenanalyse zugrunde liegt. Der Schwerpunkt dieser Arbeit liegt dabei in der Bereitstellung der Entwicklungsumgebung und in der punktwolkenbasierten Auswertung, sowie in der Verknüpfung der beiden objektbasierten Ansätze. Die Dachflächenmodellierung ist das Ergebnis einer hierarchischen Objekterkennung in zwei Auflösungsstufen. Zuerst werden die Gebäudepolygone mittels "fill sinks" Segmentierung des invertierten Digitalen Oberflächenmodells abgeleitet. Darauf aufbauend werden diese Polygone dazu verwendet, die entsprechenden Laserpunkte für jedes Gebäude aus der gesamten Punktwolke zu extrahieren. Individuell für jedes Gebäude wird eine Segmentierung ("region growing") basierend auf den Normalvektoren der Laserpunkte (ermittelt durch Anpassung einer Ebene in eine definierte Punktnachbarschaft) angewandt, die es zum Ziel hat planare Dachflächenteile abzugrenzen. Abschliessend werden die ermittelten Dachobjekte nach ihrer Neigung klassifiziert. Das erreichte Ergebnis stellt einen wertvollen Input für viele Anwendungen dar, wie zum Beispiel die Modellierung der Schneelastkapazität oder die Standortanalyse für Photovoltaikanlagen.

Durch eine effiziente Datenverwaltung der ALS Punktwolke, gekoppelt mit der Funktionalität eines GIS, können wesentliche Schritte in Richtung des Ziels der “Ausnützung des vollen Informationspotenzials von ALS Daten” gemacht werden. Ohne zusätzliche Kosten kann ein deutlicher Mehrwert aus den ALS Daten (z.B. Intensitätskorrektur) generiert werden. Das entwickelte Informationssystem stellt eine gute Basis dar, “full-waveform” ALS Daten sowie terrestrische Laserscannerdaten zukünftig miteinzubeziehen.

Contents

List of Figures

List of Tables

1 Introduction

1.1 Motivation

At all times spatial information has played a vital role in human life, from knowing where to find food in prehistory up to make a round-the-world trip in a few seconds using Google Earth. Even in times of global networking and Web 2.0, space and time are the major dimensions in human interaction. Hence, spatial information is necessary for driving decisions on all kind of levels (from an individual up to public decision-makers). Nowadays, using remote sensing techniques (terrestrial, airborne or spaceborne) a high amount of spatial datasets in a variety of domains can be acquired in a very short time. A challenging problem is to transform this huge amount of data into useful information without losing accuracy or information itself. These large amounts of spatial datasets make manual processing impossible and it is therefore necessary to develop efficient and effective techniques for semi or fully automatic information extraction. Taking into account the dimension time, i.e. with the availability of multi-temporal datasets, the need for standardized and repeatable extraction methods even increases. For example, in natural hazard management fast access to spatial information extracted from high resolution spatial data is crucial. Basically, data availability plays a key role. Not only the pure existence of spatial data with high information content is sufficient but data accessibility is even more fundamental.

This work concentrates on spatial data acquired by means of Airborne Laser Scanning (ALS). This active remote sensing technique is mainly used for topographic data acquisition resulting in high resolution elevation models of the Earth's surface (Kraus, 2004). Country-wide ALS datasets already exists, as Switzerland (Luethy and Stengele, 2005), Federal State of Vorarlberg/Austria (Würländer et al., 2005) and the Autonomous Province of Bolzano/Italy (Wack and Stelzl, 2005) show. ALS data is characterized by high data density (namely point density) and high accuracy (Baltsavias, 1999a; Kraus et al., 2004), also in vegetated areas where ALS clearly exceeds the quality of competing acquisition methods (Kraus and Pfeifer, 1998). The primary result of ALS, which is also delivered to end-users, is called point cloud. The point cloud consists of single point measurements of x, y, z coordinates and a value for signal strength, called intensity (cf. Chapter 3). In general, the point cloud is further processed with a high degree of automation to Digital Terrain and Surface Models (DTMs and DSMs) continuously representing space (e.g. raster data). But nevertheless the original point cloud, discontinuously representing space (vector data), contains the highest degree of information, as it is three-dimensional, not modified by any

algorithm or aggregated in any dimension. As mentioned before, ALS data is mainly used for topographic data acquisition but nowadays many fields of applications, such as forestry (Hyyppä et al., 2004; Hollaus et al., 2006), road and building detection (Clode et al., 2005; Kaartinen et al., 2005; Rutzinger et al., 2006a), and glaciology (Geist et al., 2003; Arnold et al., 2006), give a good impression of the high information content included in the spatial distribution, variation and relationship of single laser points.

1.2 Research methods and objectives

The scope of research evolved from the necessity to extract highly accurate spatial information contained in ALS data but not yet operationally used. It was chosen to concentrate on ALS data only, to better evaluate the potential given by using just this data source, in comparison to approaches combining ALS with other data sources, such as optical data (e.g. Rottensteiner et al., 2005a).

The ALS point cloud contains the highest degree of information but problems arise if standard Geographic Information Systems (GIS) and remote sensing software are used for processing and analysis of this huge amount of single point measurements. The major problems are i) that only few algorithms working on the ALS point cloud are implemented and ii) that the implemented vector data models are not designed for billions of points (e.g. reaching file size limits of the operating system). Not only 3D coordinates and intensity are important information sources but also time, number of reflections/echoes and corresponding sensor position are useful additional attributes for each single laser point, which should not be disregarded if available.

1.2.1 Spatial data management

Fig. 1.1 compares the general workflow of remote sensing data processing with the main ALS data processing tasks utilized in this thesis. Spatial data management is the most important component for fast and successful spatial data analysis. Due to the lack of existing software supporting the management of more than only coordinates and intensity, a new data management strategy tailored to the data model of laser points is needed.

The first and fundamental objective of this thesis is to *develop a spatial database management system designed for ALS point clouds* employing solely Open Source components and strictly following open standards (OGC Inc. – Open Geospatial Consortium, 1999). Open Source means having full insight into the algorithms used in a software, optimally described by the source code (OSI – Open Source Initiative, 2006). By means of “Open Source”, fully

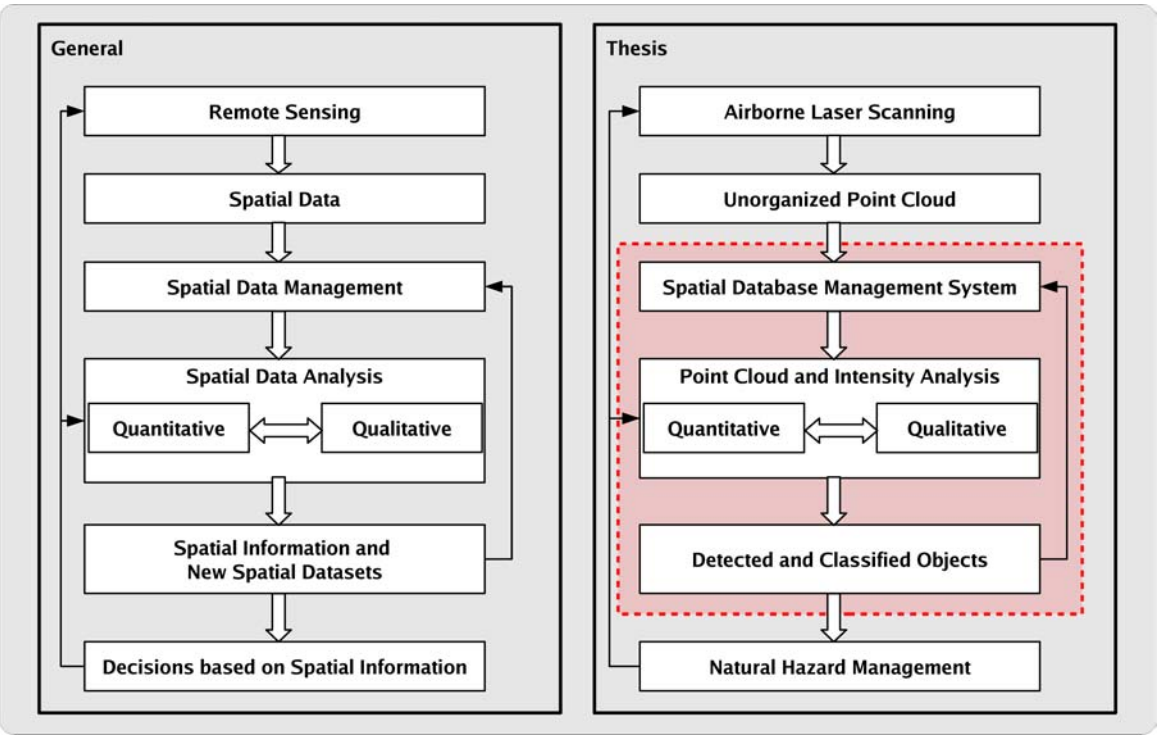

Figure 1.1: *General workflow of remote sensing data processing compared with ALS data processing treated in this thesis. The red square emphasizes the scope of research.*

transparent scientific work is made possible in comparison to proprietary software with its unpublished algorithms (Boulanger, 2005). The main requirement for such a management system is the integration into a GIS, which provides good usability and access to the full functionality of a standard GIS software. Exactly the combination of a GIS with an ALS data management system generates a multitude of new analysis possibilities, i.e. enabling to extract "new information" from ALS data.

1.2.2 Intensity analysis

Most ALS sensors – commercially in use – record the signal intensity of each backscattered reflection (Baltsavias, 1999b). Images generated out of the recorded intensity are often used as assistance in interpreting objects and phenomena that can be found in the scanned area because intensity images may surpass shaded relief images of flat, texture-less terrain. The intensity value is related to the reflectance (in the laser wavelength) of the scanned surface, but first it has to be corrected for known influences; such as range-dependency, topographic and atmospheric effects (cf. Chapter 3). Just a few attempts to correct laser intensity can be found in literature (e.g. Ahokas et al., 2006; Coren and Sterzai, 2006) and others only consider range-dependency and try to normalize intensity on a certain range level (e.g. Luzum et al., 2004; Donoghue et al., 2006). Reasons for the rare amount of research in intensity

correction but a variety of existing applications using intensity can be that i) the data situation does not allow for intensity correction (e.g. no information about emitted energy or scanner position available) or ii) the stated influences are found to be almost similar in the area of interest (e.g. flat terrain, same flying heights and scanner settings), which leads to only small disturbance in the image representation.

The second research objective aims to *generate and evaluate the added value of using ALS intensity* on a theoretical but also applied level of research by means of an extensive state-of-the-art report, examination of the physical principles of ALS intensity, development of model- and data-driven correction procedures (cf. Chapter 3), as well as demonstrating the potential of using corrected intensity by specific surface analyses (cf. Chapter 4).

1.2.3 Object-based point cloud analysis

In recent years Object-based Image Analysis (OBIA), a subdiscipline of GIS science (Goodchild, 1992), has evolved to a new concept for geographic information generation, mainly based on remote sensing imagery (Lang and Blaschke, 2006; Blaschke and Lang, 2006; Blaschke et al., 2007). The major strengths of the OBIA concept, such as organizing the landscape following the human perspective (experience and knowledge), suppressing the influence of noise and reduction of data by intelligently grouping primitives to objects (Hay and Castilla, 2006), clearly demonstrate the advantages compared to traditional pixel based approaches. The major components – segmentation, object-modeling and classification (Benz et al., 2004) – can also be applied in principle to laser scanning point clouds. The Object-based Point Cloud Analysis (OBPA) – as defined by Rutzinger et al. (accepted) – does not only consider the spatial domain of the point cloud, but also integrates object and topological properties, as well as neighborhood relations on higher levels (segment and object levels in multiple scales). The main advantages of OBPA are that it works directly on the point cloud (no rasterization necessary) but can be combined, if necessary, with OBIA working on raster data. Especially the hierarchic combination of OBIA followed by OBPA is suitable for large areas where the point cloud data volume does not allow efficient computation anymore but highly accurate object detection is needed. This means that the advantages of both, raster and vector-based analysis, is utilized.

The third research objective arises as *applications of object detection and classification using ALS point cloud data* according to the concepts of OBIA and OBPA. This third objective can be seen as the synthesis of the previous two objectives because it is based on point cloud data management and corrected intensity. Two examples, one for natural and one for human environments, will be developed and tested. These two applications will

show how spatial information can be obtained and provided as GIS-ready datasets useful for simple users. In principle, the developed methods can be applied to a multitude of other applications not investigated further in this thesis, e.g. applied to other land cover classes, such as roads, water bodies or vegetation (e.g. Brennan and Webster, 2006).

Fig. 1.1 additionally indicates a connection between surface classification and data management. The classification can be assigned to the point cloud, which was used for object extraction. As the connection between a stored laser point and the point used in analysis is never lost, the classification result can be used to label and classify, respectively, the corresponding elements in the data management system, i.e. additional attributes to laser points are generated and stored. These attributes provide a highly valuable input for supplementary point cloud analyses, i.e. selected classes of laser points can easily be extracted, which then serve as input dataset for further classifications or delineations. For example, if all raised objects are classified in the point cloud, DTM generation is straightforward without the need for filtering.

1.3 Summary of research goals

The aim of this research is to provide a tool that allows using the full information content of ALS point cloud data by bringing together new strategies of data management, intensity analysis and surface object detection into a newly developed information system, called "*LISA (LIdar Surface Analysis)*" (Fig. 1.2). As a consequence added value is generated by using original ALS point cloud data in comparison to traditional approaches working on elevation models, as well as by raising data availability and hence spatial information access.

Figure 1.2: *LISA (LIdar Surface Analysis) system logo.*

The goals of the thesis can be pointed out as following:

1. to improve handling of very large ALS point cloud datasets
2. to establish better understanding of ALS intensity, as well as introduce and evaluate new methods for intensity correction
3. to apply OBIA concept on ALS point clouds, i.e. OBPA, and show potentials of this new concept by implementing two examples covering the human and natural environment
4. to incorporate all developed algorithms and methods in one framework guaranteeing full GIS functionality and compatibility

1.4 Thesis outline

1.4.1 alpS project 1.5A

The thesis was performed in cooperation of the Institute of Geography, University of Innsbruck (`http://uibk.ac.at/geographie`), and the alpS-Centre for Natural Hazard Management, Innsbruck (`http://www.alps-gmbh.com`). Within the alpS Project 1.5A "*Determination of surface properties from laser scanner data*", the scientific results of this thesis are daily in use and applied to solve problems in natural hazard management (e.g. process modeling and damage potential assessment; (Geist et al., accepted)). alpS also stands for an international platform bringing together basic and applied research. alpS provided the author with a good framework for discussing and exchanging research know-how with an international community, as presentations on conferences (e.g. Salzburg, Aalborg, Helsinki) and scientific visits (e.g. Coimbra, Utrecht, Vienna) show.

1.4.2 Structure

The cumulative thesis comprises four reviewed papers (Chapters 2-5; cf. Fig. 1.3). Furthermore, many additional publications have been carried out complementing the outline of this thesis. To faciliate finding the full citations, the reference lists of the selected papers have been put into the overall reference chapter attached to the main text.
Chapter 2 describes the development of a management and analysis system for ALS point cloud and raster data. This system is the basis for all further analyses because it offers fast and easy access on all relevant information coming along with the unorganized ALS point cloud (ALS raw data). Based on the functionality evolved in Chapter 2, two methods for signal intensity correction (data-driven and model-driven) could be developed, presented

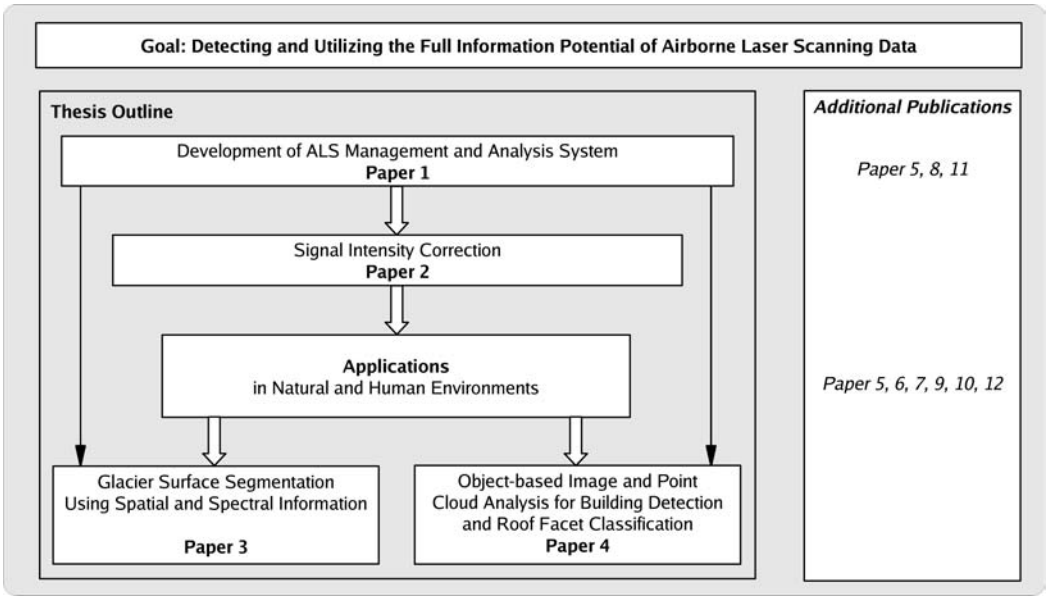

Figure 1.3: *Outline of the thesis. Papers are listed in detail below.*

in Chapter 3. Chapter 3 also gives an extensive state-of-the-art report concerning recent correction strategies and applications, and gives a good impression of the potential of ALS (and TLS respectively) signal intensity for future applications. Chapter 4 explains a workflow for glacier surface segmentation and classification using both, the spatial and spectral information (i.e. corrected signal intensity) of the ALS point cloud. Chapter 4 can be seen as an explicit application of the methods developed in Chapter 3. Chapter 5 combines the strength of raster and point cloud based analysis methods for detecting buildings and reconstructing roof facets. Both applications (Chapter 4 and 5) make use of the object-based analysis concept (raster and/or point cloud based), which is technically made available by the system developed in Chapter 2. Chapter 6 complements the most important findings of the single papers with the latest developments, discusses the cumulative results of this thesis, and additionally underlines the inherent connection between the papers (Fig. 1.3). Finally, Chapter 7 concludes the contributions of this thesis and points out the next steps for future work.

1.4.3 Selected publications

All four selected papers have multiple authors. It has to be clarified that Bernhard Höfle is the lead author of three of four papers. He independently designed, implemented the research ideas and wrote down the results while fruitful discussions took place with the co-authors. In the fourth paper Martin Rutzinger is the main author. Bernhard Höfle contributed the design and implementation of the object-based point cloud analysis (mainly

object modeling, feature calculation and classification) but Martin Rutzinger developed the OBIA building detection and the overall workflow.

Paper 1
Höfle, B., Rutzinger, M., Geist, T., Stötter, J. (2006): Using airborne laser scanning data in urban data management – set up of a flexible information system with open source components. *Proceedings of UDMS 2006: 25th Urban Data Management Symposium*, Aalborg, Denmark, pp. 7.11-7.23, (on CDROM).

Paper 2
Höfle, B., Pfeifer, N. (in press): Correction of laser scanning intensity data: data and model-driven approaches. *ISPRS Journal of Photogrammetry and Remote Sensing*, doi:10.1016/j.isprsjprs.2007.05.008.

Paper 3
Höfle, B., Geist, T., Rutzinger, M., Pfeifer, N. (2007): Glacier surface segmentation using airborne laser scanning point cloud and intensity data. *International Archives of the Photogrammetry, Remote Sensing and Spatial Information Sciences 36*, Espoo, Finland, (on CDROM).

Paper 4
Rutzinger, M., Höfle, B., Pfeifer, N. (accepted): Object detection in airborne laser scanning data – an integrative approach on object-based image and point cloud analysis. In: *Blaschke, T., Lang, S., Hay, G. (eds.): Object-Based Image Analysis – Spatial concepts for knowledge-driven remote sensing applications*, Springer.

1.4.4 Additional publications

Paper 5
Geist, T., Höfle, B., Rutzinger, M., Pfeifer, N., Stötter, J. (accepted): Laser scanning – a paradigm change in topographic data acquisition for natural hazard management. In: *Veulliet, E., Stötter, J., Weck-Hannemann, H. (eds.): Sustainable natural hazard management in alpine environments*, Springer.

Paper 6
Kodde, M.P., Pfeifer, N., Gorte, B.G.H., Geist, T., Höfle, B. (2007): Automatic glacier surface analysis from airborne laser scanning. *International Archives of the Photogrammetry, Remote Sensing and Spatial Information Sciences 36*, Espoo, Finland, (on CDROM).

Paper 7

Rutzinger, M., Höfle, B., Pfeifer, N., Geist, T., Stötter, J. (2006): Object-based analysis of airborne laser scanning data for natural hazard purposes using open source components. *International Archives of the Photogrammetry, Remote Sensing and Spatial Information Sciences 36 (Part 4/C42)*, Salzburg, Austria. URL: `http://www.commission4.isprs.org/obia06/papers.htm`

Paper 8

Edelmaier, F., Höfle, B., Heller, A. (2006): Konzepte zur 3D Visualisierung von Laserscanner-Daten mit VTK und Python. *Angewandte Geoinformatik 2006. Beiträge zum 18. AGIT-Symposium Salzburg*, Wichmann Verlag, Heidelberg, pp. 128-134.

Paper 9

Rutzinger, M., Höfle, B., Geist, T., Stötter, J. (2006): Object-based building detection based on airborne laser scanning data within GRASS GIS environment, *Proceedings of UDMS 2006: 25th Urban Data Management Symposium*, Aalborg, Denmark, pp. 7.37-7.48, (on CDROM).

Paper 10

Geist, T., Höfle, B., Rutzinger, M., Stötter, J. (2005): Der Einsatz von flugzeuggestützten Laserscanner Daten für geowissenschaftliche Untersuchungen in Gebirgsräumen. *Photogrammetrie, Fernerkundung, Geoinformation 3/2005*, 183-190.

Paper 11

Höfle, B., Geist, T., Heller, A., Stötter, J. (2005): Entwicklung eines Informationssystems für Laserscannerdaten mit OpenSource-Software. *Angewandte Geoinformatik 2005. Beiträge zum 17. AGIT-Symposium Salzburg*, Wichmann Verlag, Heidelberg, pp. 277-286.

Paper 12

Geist, T., Höfle, B., Rutzinger, M., Stötter, J. (2004): Analysis of Laser Scanner Data with Remote Sensing Techniques for Determining Surface Characteristics. *International Archives of the Photogrammetry, Remote Sensing and Spatial Information Sciences 36 (Part 8/W2)*, 297.

2 Using airborne laser scanning data in urban data management – set up of a flexible information system with open source components

Published as:
Höfle, B., Rutzinger, M., Geist, T., Stötter, J. (2006): Using airborne laser scanning data in urban data management – set up of a flexible information system with open source components. *Proceedings of UDMS 2006: 25th Urban Data Management Symposium*, Aalborg, Denmark, pp. 7.11-7.23, (on CDROM).

Abstract

*In recent years airborne laser scanning has evolved into the state-of-the-art technology for topographic data acquisition. Applications for urban areas are recently growing to a greater extent (e.g. building extraction). Airborne laser scanning produces large datasets of point measurements, which demand for new strategies in data management. LISA (**LI**dar **S**urface **A**nalyses) is a concept for combining existing Open Source software for an efficient data management and analysis. The core components are the spatial database PostgreSQL/PostGIS, the geographical information system GRASS GIS and the statistical software R. Interfaces between the system components exist and therefore time-consuming data transfers are avoided. The open structure allows for developing workflows from simple applications to complex analysis. LISA is operationally used at the alpS-Centre for Natural Hazard Management. A large potential is given, for scientific applications as well as for operational tasks of public authorities.*

2.1 Introduction

Public planning processes on all levels have a strong demand for high quality topographic data (e.g. road construction, large building projects, natural hazard management). With Airborne Laser Scanning (ALS) a well accepted operational method for the acquisition of topographic data exists, allowing the construction of both high resolution and high accurate digital elevation models. Fundamental knowledge about the technical accuracy of this method (Baltsavias, 1999c) and the quality of produced digital elevation datasets (Kraus et al., 2004) has evolved in recent years and thus has opened the use of ALS to a wide range of applications (Wever and Lindenberger, 1999).

Airborne laser scanning is used to acquire country-wide digital elevation models, e.g. the entire Netherlands, Switzerland or Baden-Wuerttemberg/Germany. A growing number of

companies offer ALS campaigns (Baltsavias, 1999b) and deliver different ALS products (e.g. digital elevation models, classified land cover maps) but also the original point data which are archived, but often not used anymore, as standard GIS or CAD software packages are not able to manage billions of vector points in an efficient and easy-to-use way.

This paper presents a new concept to store, process and visualize vector and raster products of ALS up to a country-wide level. Emphasis is laid on the storage of the laser points without loss of information and on a fast and simple retrieval of defined laser scanner datasets and their descriptive statistics. The information system – "LISA" (**LI**dar **S**urface **A**nalyses) – is entirely built in an Open Source environment with components (OSI – Open Source Initiative, 2006), which can be downloaded from the Internet for free. It will also be shown how the functionality of LISA is integrated into a Geographic Information System (GIS) and how multiple users can work with laser data through server-client applications, for example the Internet.

2.2 Airborne laser scanning

The primary products of ALS campaigns, the so-called "raw data" or "primary data", are numbers (time, x, y, z, intensity) for one or more reflections of the emitted laser beam. Secondary, raster models can be derived from this raw data. The higher the point density the more accurate elevation models can be achieved (Kraus, 2004). Several sophisticated filter methods allow for separating object points from ground points (Sithole and Vosselman, 2003). Traditionally gridded digital terrain models (DTMs) without objects and digital surface models (DSMs) with objects are produced. While raster datasets are a) easier to handle and b) offer a significant reduction of data and information, vector points represent the unstructured, original point measurements with the highest degree of information. But large areas and high point densities lead to a large number of points.

Due to the fixed scanning pattern of the laser scanning systems – the beam is usually redirected orthogonally to the flight direction – the laser beam cannot be pointed on particular objects directly (Brenner, 2005). If a high shape accuracy of objects (e.g. buildings) is needed, a high point density has to be chosen (Maas and Vosselman, 1999; Würländer et al., 2005).

While there are a number of commercial ALS systems on the market with quite different technical properties (Baltsavias, 1999b), the great variety of data formats can be reduced to the characteristics of ALS data (cf. Wehr and Lohr, 1999). A laser shot can have none, one

or more reflections (echoes). Every echo is located in time (timestamp) and space (x, y, z) in a given coordinate system. Most of the scanners save additional attributes for each point (e.g. intensity, pulse width or number of the echo). ALS campaigns are organized in flight strips. Every laser point belongs to a strip. Every point is connected to the plane positions, which are recorded in a much lower frequency (e.g. 2 Hz) than the laser points (e.g. 50 kHz).

State-of-the-art scanners also provide the digitized full-waveform of the reflected laser beam (Wagner et al., 2004), which allows to use scanner independent echo detection algorithms (Persson et al., 2005). For current operational use full-waveform data still has to be reduced to distinct echoes. One attempt for defining a standard for ALS data can be seen in the LAS format (LAS Specification, 2005). The LAS format is a public binary file format for the interchange of ALS data between customers and ALS vendors, but also between software packages and between operating systems. The LAS format both includes metadata definitions and definitions for classified laser points (e.g. ground, non-ground, building or vegetation points).

2.3 Information system LISA

2.3.1 Reasons for an Open Source information system

Nowadays the term “Open Source” gains more and more attention (European Commission – IDABC work programme, 2006; Boulanger, 2005; Wheeler, 2005). Open standards and fully transparent software solutions lead to a stronger cross linking of knowledge and data itself. Existing ALS software tools are built for particular tasks, e.g. point classification, object recognition and modeling, ALS data correction or DTM generation. Most packages are proprietary stand-alone solutions or add-ons for commercial GIS software.

Blaschke (2005) states that “the users and especially the potential users of remote sensing data are not interested in the data as such, but rather in information”. Mainly public authorities own huge ALS datasets, of which the overall information is relevant for one application, while a controlled reduction is necessary for another application. The information system LISA combines the advantages of Open Source software with the functionality of a spatial database management system (DBMS), a geographic information system (GIS) and a statistical software package. The use of open standards (OGC Inc. – Open Geospatial Consortium, 1999) in a central data management system plays the key role in providing ALS data and extracted information to a broad public. Keywords as interoperability, data vendor independency, multi-user support, data security, data integrity and cross-platform

support emphasize the importance of intelligent data management strategies. Commercial database systems support spatial data types as well (e.g. Oracle Spatial). Additionally to the know-how, which is needed in general for the administration of DBMSs, license fees have to be paid for commercial systems and spatial add-ons. Cost-saving solutions are especially required by institutions with low budget.

2.3.2 System architecture

The demands on a flexible information system for ALS data and its derivatives described in the previous chapters dedicate the system design to a large degree. The key principle is to use existing functionality and combine it in an optimized way for the requirements of ALS data handling. The idea is to use the advantages of every single component (e.g. raster capabilities of the GIS). The system architecture is modular with well-defined interfaces. Every system component (cf. Sec. 2.3.3) can be run on various operating systems (Windows, UNIX, Linux). The client-server architecture minimizes both data storage and administration efforts. Time-consuming data transfer within LISA is avoided. Every application of LISA can directly access the original laser points in the spatial database. The data models for vector and raster datasets include the dimension "time", which makes multi-temporal analyses possible. Further processing, analysis and visualization of the ALS data can be performed in both the original point cloud and the generated raster datasets.

2.3.3 Components

The main components of the information system are

- the *object relational database management system PostgreSQL* (version 8.1; PostgreSQL Global Development Group, 2006) with its spatial add-on *PostGIS* (version 1.1.0; Refractions Research Inc., 2006),
- the *geographic information system GRASS* (version 6.1; GRASS Development Team, 2006) and
- the *statistical software R* (version 2.1.1; R Development Core Team, 2006).

Workflows and applications are constructed using the scripting language Python (version 2.4.1; Python Software Foundation, 2006). Python was chosen because of its rich pool of scientific modules (Jones et al., 2001) and its connectors to PostgreSQL and R (Cain, 2006; Lang, 2006). Interfaces connect all components to each other. GRASS can read and write spatial layers in a PostgreSQL/PostGIS database (Neteler and Mitasova, 2004). The

statistical software R has full access to GRASS layers (Pebesma and Bivand, 2006) and can be implemented into the DBMS as the procedural language PL/R (Conway, 2006). There are in fact no important limitations for the storage of huge amounts of data in a PostgreSQL database. The database size is unlimited and the maximum table size is approximately 32 Terabyte (cf. PostgreSQL Global Development Group, 2006). The 3D visualization of point cloud subsets is managed with the Open Source program VTK (VTK, 2006), which offers a PostgreSQL interface.

2.3.4 Data management and data model

The spatial DBMS PostgreSQL/PostGIS is used for the storage of the ALS primary data. PostgreSQL is a database server, which provides user access management and multi-user capabilities. The ALS vector data is therefore stored only once with assured access control and data availability. For operational use the raster datasets (e.g. DTMs) are organized on the client side in GRASS GIS. Internet applications with raster support may be realized with the help of UMN MapServer (UMN MapServer, 2006) or the GRASS SWIG interface, which is presently under development (GRASS Development Team, 2006; Beazley et al., 1995).

The chosen DBMS offers a spatial object type defined by the OpenGIS "Simple Features Specification for SQL", which is used to store the Cartesian coordinates of a laser point as a geometry object in a single table field. Hence, the Structured Query Language (SQL) is used to apply geometric functions and spatial queries on the geometry objects. The internal storage format of spatial objects corresponds with the OpenGIS Well-Known Binary (WKB) specification (OGC Inc. – Open Geospatial Consortium, 1999; Refractions Research Inc., 2006). Three-dimensional point geometry consists of a description of byte order and WKB type (5 bytes), the three coordinates (3x8 bytes), additional information about the spatial referencing system identifier (SRID, 4 Bytes) and the bounding box (4x8 bytes). The SRID allows on-the-fly reprojection of features. The SRID can be defined with the help of EPSG codes (European Petroleum Survey Group, 2006). Due to the large overhead the bounding box and the SRID are not saved for every point. The SRID is only saved once per flight campaign, which in general consists of only one coordinate system. The WKB description (type, byte order) is used by external applications to recognize the geometry object.

The characteristics of ALS data (cf. Sec. 2.2) lead to the data model shown in Fig. 2.1. ALS campaigns consist of flight strips. Every campaign has uniform parameters (e.g. SRID, scanner calibration), which are stored in a separate metadata table. Area-wide laser scans are made by overlapping strips. Every laser point belongs to a unique strip. A recorded laser

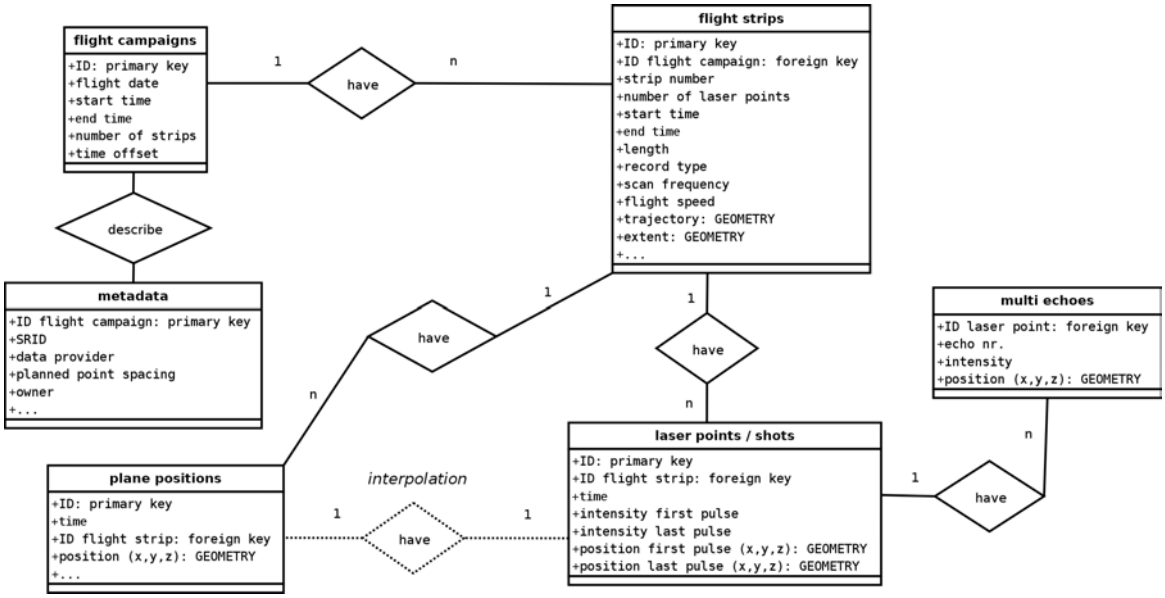

Figure 2.1: *Simplified ALS primary data model.*

shot has at least one echo, defined as last pulse. If two or more echoes are recorded, the first echo is defined as first pulse. The echoes between first and last pulse are stored in a separate table because only recent ALS systems provide multiple echo detection. Furthermore, the percentage of multiple echoes depends on the predominant land cover distribution. More than two echoes mainly occur in areas with high vegetation. Every echo belonging to one laser shot has the same timestamp. The time attribute is a relative date (seconds since start of week), which can easily be converted into an absolute date format as the time offset is stored for each flight campaign. A linear interpolation approach over time connects a laser point with its plane position.

Security and data integrity are important issues for client-server systems. PostgreSQL offers a comprehensive user access management. Different access privileges can be defined for every database item, for example database access for specified IP addresses, editing privileges for administration users or read-only access for ordinary users. Data integrity and consistency are guaranteed by PostgreSQL's transaction management and by the defined foreign keys (constraints). Each laser point is related with its flight strip, which is connected with its flight campaign. During the data import the relationships between the data model entities are built and all indices are updated. GRASS GIS also supports a user and right management, which is based on the UNIX/Linux file system.

A B-tree index is used to speed up queries on the time attribute. Paul Ramsey states that "indexes are what make using a spatial database for large data sets possible" (Refractions

Research Inc., 2006). PostGIS uses an R-Tree index implemented on top of a Generalized Search Tree (GiST) for indexing geometry columns. The spatial index is for example more robust than a normal PostgreSQL R-tree index; also columns containing null geometries can be indexed. GiST supports indexing some different geometry types as lines, polygons, multi-geometries (e.g. multi-points) and geometry collections, but also non-extended objects (e.g. multidimensional points). Only bounding-box operators, for example window queries, take advantage of GiST (cf., Bartunov and Sigaev, 2006; GiST Project, 2006; Brinkhoff, 2004). The advantage of GiST of saving only the 2D bounding box of large geometries, leads to a disadvantage for point geometries as an extensive overhead is produced.

A laser point consists of 4 bytes for ID, 2 bytes for ID flight strip, 8 bytes for timestamp, 2 bytes for intensity and 29 bytes for the position. The indices for a laser point are ca. 25 bytes for the B-tree on ID, ca. 42 bytes for the B-tree on timestamp and ca. 43 bytes for the GiST on geometry. In total 155 bytes (244% index overhead) are necessary for a laser shot with one echo and 229 bytes (201% index overhead) for a laser shot with first and last echo. A flight campaign for Tyrol (12649 km^2) with approx. 1 point per m^2 would lead to a database with ca. 1900 Gbytes. The indices require a lot of disk storage but guarantee a reasonable performance, also for large ALS datasets.

```
-------------------------------------------------------------------------
SELECT geom_last FROM laser_points WHERE geom_last &&
MakeBox2d('POINT(551612 244880)','POINT(551602 244890)') AND
distance(MakeBox2d('POINT(551612 244880)','POINT(551602 244890)'),
geom_last)<=0 AND intens_last>5 AND
abstime(time,idstrip)>'2003-11-05 11:00:00'::TIMESTAMP AND
abstime(time,idstrip)<'2003-11-05 12:00:00'::TIMESTAMP;

#time: 1.0 ms -> 71 laser point records (database with 2 million points)
#time: 9.7 ms -> 859 laser point records (database with 96 million points)
-------------------------------------------------------------------------
```

Figure 2.2: *SQL statement for the selection of last pulse laser points.*

The chosen data model makes complex queries possible with any combination of spatial, temporal or attribute search criteria. Spatial queries consist of a prior bounding box query followed by a distance query. Fig. 2.2 shows an example for selecting the coordinates of last pulses in a given area and time interval, limited to points with an intensity value greater than 5.

2.3.5 Data processing and workflows

Workflows and applications for LISA are constructed in a hierarchical approach (Fig. 2.3). The spatial database enables not only data storage and retrieval, but also data manipulation (e.g. coordinate transformation, plane position interpolation, signal intensity correction). Many methods are written in PostgreSQL's procedural languages. For example PL/pgSQL is used to generate cross-sections through the 3D point cloud, PL/Python for constructing orthogonal distance regression planes for local point neighborhoods, and PL/R for correlation analyses. The resulting SQL functions deliver ordinary records, which are used in the next higher level. Apart from the ALS primary data also other vector layers (e.g. flight lines) are stored in the spatial database, but also external vector data sources (e.g. cadastral maps, building delineations) can be made available for every client.

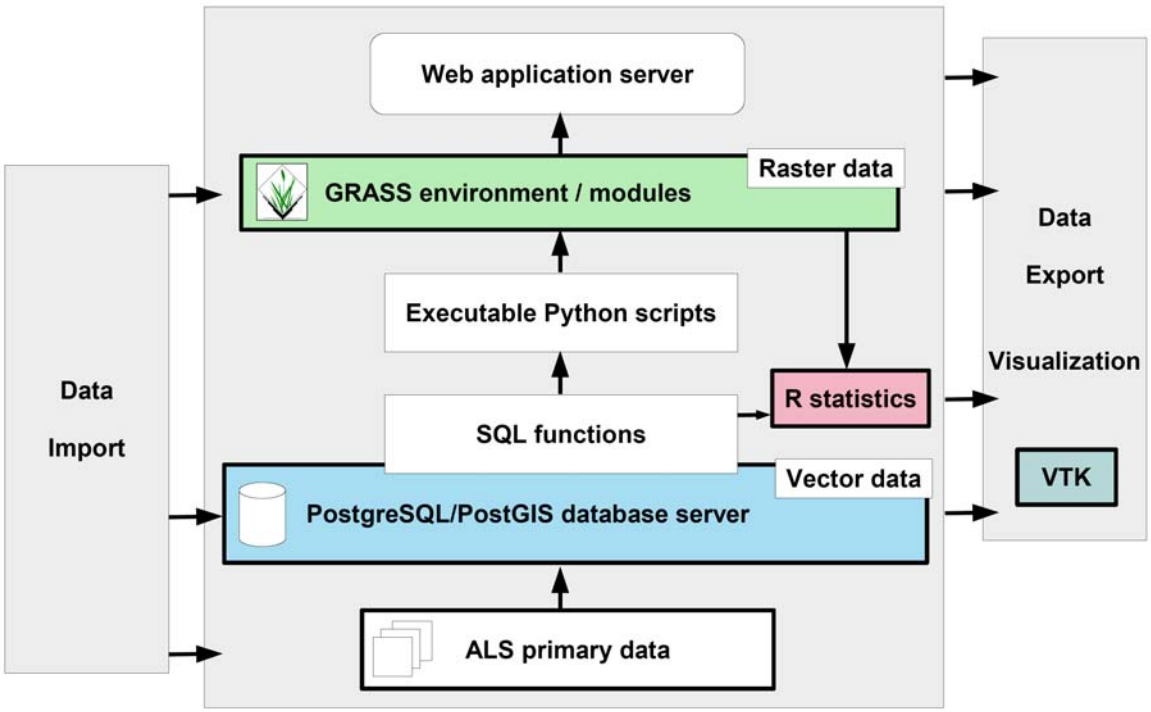

Figure 2.3: *LISA system architecture and workflow.*

The Python scripting language was chosen for programming the applications. Most of the work load is already done by the SQL functions. Python functions can easily be re-used in other scripts. The resulting scripts are platform independent. Every script can be executed locally or by a web application server supporting the Python language.

The GRASS GIS environment offers an easy way to develop so-called "GRASS modules" (GRASS commands). A module corresponds to the underlying Python script but with in-

creased usability. The modules can be used by both command line and graphical user interface (GUI) of GRASS. Within the GRASS environment the new LISA modules ([l.*] laser commands) can be combined with the existing modules of GRASS ([r.*] raster and [v.*] vector commands) for writing batch processing workflows. GRASS also supports the DTM generation algorithm of Brovelli et al. (2002). The LISA modules are fully integrated into GRASS, for example they make use of the current "region" settings (e.g. work area extent and resolution). The ALS database server definition is configured once for every "location" (l.db.connect), which is a GRASS internal working environment with unique projection settings. The database definition is automatically used for every LISA command.

The hierarchical workflow allows for a multitude of data access and data processing possibilities from client and server side. Web applications are good examples for direct access to all levels. For example PostGIS vector layers can directly be visualized through a MapServer application. Another example is to interactively select a profile line on a web map and send the instructions to the Python application, which returns the ready image of the point cloud profile to the client's browser.

2.3.6 Data interchange and interoperability

Due to the different scanning systems and the large number of ALS vendors, the primary data are delivered in a variety of formats. A translation tool is only needed for the import into the LISA system. Thereafter the primary data is stored in the defined data model. The import procedure is also used to check the inner consistency of the ALS data. Only complete ALS campaigns which fit with the data model are imported. As a consequence a trouble-free use of all applications is guaranteed. It is not practical to build import utilities for a multitude of vendor specific data formats. The LAS format, which includes all necessary information, should operate as exchange format in the future.

One major advantage of Open Source software is the support of many exchange formats and interfaces to other programs. As mentioned before many GIS clients support a direct connection to PostgreSQL/PostGIS data sources, for example ESRI ArcGIS (ESRI, 2006), GRASS GIS or MapServer. The client-server architecture enables a platform independent access through standard Internet protocols. The export of the ALS data and its derivatives into most common data formats is supported (e.g. ESRI Shapefile, DXF, GML, SVG, ASCII raster, image formats). As a consequence spatial software packages (GIS, CAD programs) can still be used to work with small ALS datasets, which are provided by LISA. PostgreSQL/PostGIS and GRASS databases are easy to backup, and therefore easy to distribute en bloc.

2.4 Application examples

The LISA information system is operationally used at the alpS-Centre for Natural Hazard Management in Innsbruck/Austria in an applied research project, which aims on the use of ALS data for different aspects in natural hazards management. In the project emphasis is laid on the qualitative assessment and the quantification of surface properties (e.g. surface roughness which is a key parameter in e.g. hydrological modeling) and the temporal change of these properties. Derived surface properties are useful for the extraction and classification of objects (e.g. buildings, roads). The GIS component of LISA allows the combination of the objects extracted from the laser scanning data with existing datasets (e.g. cadastral maps). The comparison of datasets from different sources or dates gives the opportunity to enhance and update existing datasets (e.g. tree inventory) or draw conclusions with regard to temporal changes. LISA has been tested with various laser scanning datasets. Urban areas were acquired with a high point density ($>$8 pts/m^2). Test sites in Vorarlberg/Austria larger than 200 km^2 and with more than 800 million laser points were successfully imported into the system. The one-time job of importing 1 million laser shots with existing first and last pulse (in total 2 million point geometries) takes about 5 minutes. The import algorithm scales linearly with the number of laser points.

2.4.1 Raster generation

The point cloud is overlaid with an analyzing grid. The laser points are attached to individual raster cells. The spatial sorting of the points and the aggregation of the attribute values can be performed either in the database (SQL function) or in the Python script, which writes the ASCII raster file. The latter is faster and offers more aggregate functions (e.g. min., max., average, sum, median, skew, standard dev., percentile). Attributes can be defined by SQL syntax. Additionally, a point density raster is written, which is a quality measure for each cell (cf. Kraus et al., 2004). In the next step different filters and algorithms (e.g. median filter or spline interpolation) are used to fill the gaps (empty cells). The highly detailed information of the original points is lost in the raster format but also outliers and noise are removed. In Fig. 2.4 the “where clause” limits the laser points in the temporal dimension, but it can also be used to limit points to a specific attribute (e.g. only ground points).

```
-------------------------------------------------------------------------
#generate first pulse maximum raster and import (-i) into GRASS

l.rast -i north=246513.0 south=245795.0 east=551201.0 west=550686.0 \
resolution=1.0 pulse=first aggr=max column='z(geom_first)' \
file=/tmp/raster1 \
where="abstime(time,idstrip)>'2003-11-05 11:04:47'::TIMESTAMP" input=raster1

#time: 2 min 46 s, 3 183 190 laser points processed
-------------------------------------------------------------------------
```

Figure 2.4: *GRASS command for raster generation within LISA.*

2.4.2 Retrieval of laser point subsets

The fast and simple retrieval of laser point subsets is essential for many applications. The raster generation algorithm, the histogram module, as well as the profile function query the laser points spatially. LISA offers many possibilities to extract laser points, for example 2D profiles, 3D point subsets, selection of valley or ridge points, spatial window queries combined with attribute limitations and an interactive selection tool for GRASS.

The profile function is an example for the combination of all workflow levels (cf. Sec. 2.3.5). A SQL function delivers the distance on the profile line and the corresponding Z-value for each point within a given buffer. A Python script is used for the visualization of the profile. The LISA profile module in GRASS enables an interactive creation of the profile line on screen or the use of a given line vector layer. But also an Internet client is able to pass the parameters for the function (line coordinates, buffer size, and Z-value) and receive the resulting profile image or ASCII values.

Fig. 2.5 shows a Z-coded DSM of the main building of the University of Innsbruck and its surroundings. Additionally the laser points for one building were retrieved and classified by elevation with the help of the corresponding histogram (green: $<$640 m, blue: $\geq$640 m). The profile shows colored laser points (red: first pulse, blue: last pulse) and an estimated terrain line. The high degree of information in the ALS primary data is visualized in Fig. 2.6. The point cloud profile contains not only the surface, but also terrain points and points in the middle vegetation layers.

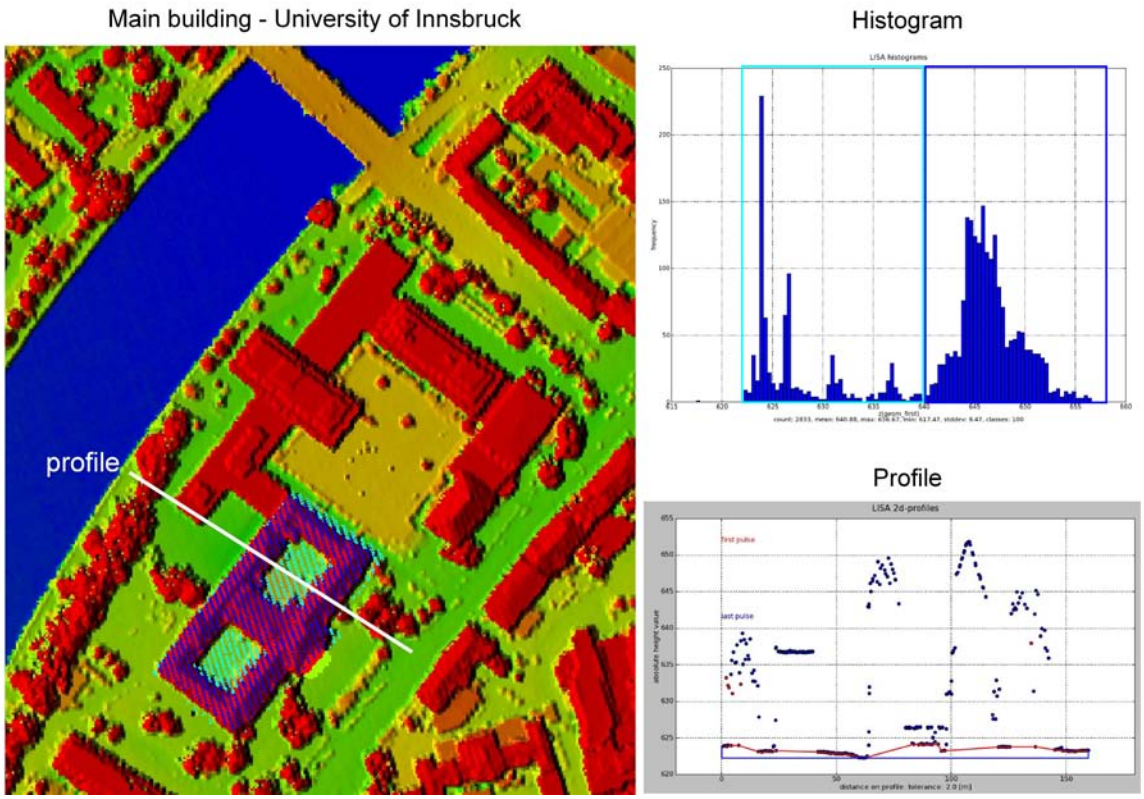

Figure 2.5: *Z-coded DSM with selected laser points (left), elevation histogram of selected laser points (upper right) and 2D profile (lower right).*

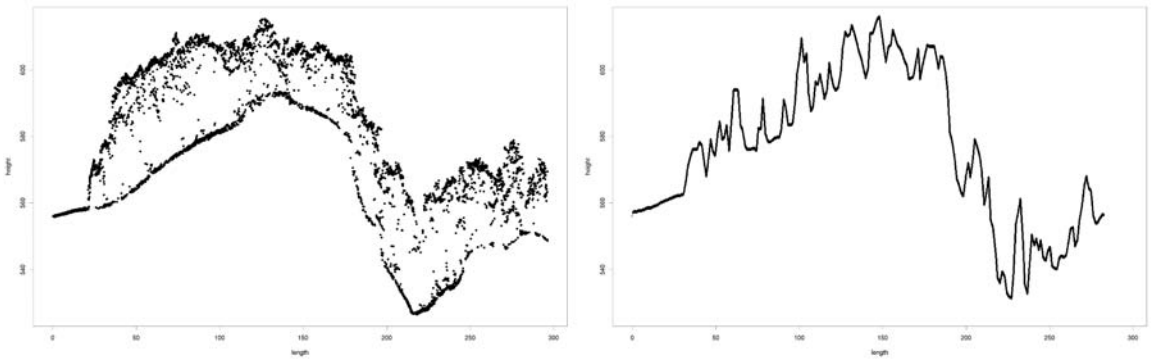

Figure 2.6: *Profile through a forested area: point cloud (8 pts/m^2) (left) compared with 1m DSM raster generated with SCOP++ (right).*

2.5 Conclusions and future work

The intention of this paper is to show how existing Open Source software can be combined for the special purpose of ALS data management. Large sets of ALS primary data can be

managed efficiently, and even more advantage can be taken of laser scanning data, which already exists for many regions. As the primary ALS data has to be stored in any way, it stands to reason to make it easily available for all users with higher data security. The Open Source community assures for persistent improvements of the single system components and everyone can take part in this development. The architecture of LISA is extensible, e.g. including full-waveforms similar to the multiple echo extension. The implementation of additional software components and the development of new workflows within LISA are possible. Thin-client applications (e.g. web profile function) do not demand GIS or database knowledge of the user, and no special hard- and software requirement is given on the client side.

Further strategies have to be tested to increase performance and decrease disk storage. The overhead of the spatial index could be reduced by grouping all reflections of a laser shot into a single geometry object (multi-point object) with exactly one appearance in the index, or even group a multitude of adjacent points to one geometry object (cf. Dorninger, 2004). The distribution of database portions on different computers (cluster environment) reduces the depth (tree levels) of the indices and work load is spread.

Rutzinger et al. (2006a) present a method for building extraction based on ALS data only. The workflow of building detection is fully integrated into LISA. The input layers for the raster-based method are provided by LISA. The aim is to extract buildings in the raster data, but also classify the point cloud and draw exact borders based on the laser points.

The unordered ALS primary data is not useful for multitemporal analysis because of the missing identification. Two common ways are a) to extract objects in every time step and b) to generate raster datasets or TINs out of the primary data (e.g. DTMs). Both methods are appropriate for natural hazard management, which can be seen as a special task of urban data management. LISA currently supports raster-based multitemporal studies at the Hintereisferner, a glacier in the Ötztal valley, Tyrol (cf. Geist et al., 2003). LISA will also be used for object-based change detection strategies, for artificial (e.g. buildings) but also natural objects (e.g. rock glaciers).

The modular framework and the open interfaces of LISA stimulate to think of many new applications. One possible field can be the combined management of airborne and terrestrial laser scanning data. Particularly for urban regions terrestrial laser scanning becomes more and more important. LISA is the fundament for a variety of urban data management applications using laser scanning data.

3 Correction of laser scanning intensity data: data and model-driven approaches

Published as:
Höfle, B., Pfeifer, N. (in press): Correction of laser scanning intensity data: data and model-driven approaches. *ISPRS Journal of Photogrammetry and Remote Sensing*, doi:10.1016/j.isprsjprs.2007.05.008.

Abstract

Most airborne and terrestrial laser scanning systems additionally record the received signal intensity for each measurement. Multiple studies show the potential of this intensity value for a great variety of applications (e.g. strip adjustment, forestry, glaciology), but also state problems if using the original recorded values. Three main factors, a) spherical loss, b) topographic and c) atmospheric effects, influence the backscatter of the emitted laser power, which leads to a noticeably heterogeneous representation of the received power. This paper describes two different methods for correcting the laser scanning intensity data for these known influences resulting in a value proportional to the reflectance of the scanned surface. The first approach – data-driven correction – uses predefined homogeneous areas to empirically estimate the best parameters (least-squares adjustment) for a given global correction function accounting for all range-dependent influences. The second approach – model-driven correction – corrects each intensity independently based on the physical principle of radar systems. The evaluation of both methods, based on homogeneous reflecting areas acquired at different heights in different missions, indicates a clear reduction of intensity variation, to 1/3.5 of the original variation, and offsets between flight strips to 1/10. The presented correction methods establish a great potential for laser scanning intensity to be used for surface classification and multi-temporal analyses.

3.1 Introduction

Airborne Laser Scanning (ALS) provides a well accepted operational method for the acquisition of topographic data. Fundamental knowledge about the accuracy of this method (Baltsavias, 1999c) and the quality of produced digital elevation data sets (Kraus et al., 2004) has evolved in recent years and thus has opened the use of ALS to a wide range of applications. A lot of research effort has been put into the development of new algorithms for processing the primary result of ALS – the 3D point cloud (x, y, z). A great variety of filter algorithms has been published for the derivation of digital terrain models (DTMs)

and for the segmentation and classification of laser points based on the spatial relationship, i.e. purely the geometrical component, in the 3D point cloud (Filin and Pfeifer, 2006; Sithole and Vosselman, 2004). Algorithms and methods, also including optical information, for building extraction resulting in 3D city models as well as forest measurements, were developed (Hyyppä et al., 2004; Kaartinen et al., 2005).

This active remote sensing technique delivers not only detailed information about the geometry, but also about the reflectance characteristics of the Earth's surface in the laser wavelength, which is typically in the near infrared (NIR) spectra between wavelengths 800 nm to 1550 nm. Most ALS systems currently record the return amplitude of each received echo and a growing number of systems already provide full-waveform digitization (Persson et al., 2005). The emitted laser shot interacts with the surface, generating the backscatter, and the received signal is recorded as function of time. This signal can contain one or more peaks, which correspond to distinct reflections of the laser beam. In the field of ALS the terms signal intensity, reflectance intensity and pulse reflectance are often used as synonym for the return amplitude or energy of one echo. Our aim is to correct the value referred to as "intensity", typically not well specified by the laser scanner manufacturers, in order to obtain a value proportional or equal to surface reflectance.

The benefit of ALS intensity has been studied in several different fields of applications, for example in forestry and glaciology, where the signal intensity is already used as additional data source for surface classification and object detection. As well as the fact that the intensity is already delivered to most end-users, the advantages of the active sensor system and its specific wavelength in the NIR also generates potential for using ALS intensity. The intensity values are available as attributes for the geometry (x, y, z, I) and in comparison to raw digital images typically already georeferenced (Filin, 2003; Kager, 2004). Orthorectified intensity images can be easily produced; they are insensitive to light conditions to a great extent, e.g. solar irradiation, clouds, illumination shadows, and support surface classification where a good spectral separability is given in the NIR (Wolfe and Zissis, 1993).

Most ALS systems recording the intensity are small-footprint scanners, which operate with a beam divergence in the range of 0.3 to 0.8 mrad and a flying altitude above ground up to 3500 m. With a beam divergence[1] of 0.8 mrad and a flying height of 1000 m, the laser footprint diameter would be 0.8 m (and 2.8 m for 3500 m flying height). The illuminated area covered by the footprint can be seen as the maximum achievable spatial resolution in terms of reflectance information. As for cameras, the spatial resolution, i.e. the footprint area, may vary strongly with different ranges and scan angles of the laser beam caused by changes in the flying altitude and the topography of the scanned surface, as the beam

[1] Assuming a Gaussian profile the beam divergence is defined via those points where the energy drops to a factor of $1/e^2$ of the maximum energy in the beam middle.

divergence is constant within one flight mission. The variations in scan geometry lead to a scanning pattern, i.e. the point spacing along and across track, which does not allow for a homogeneous sampling of the whole area and results in a concurrent under-sampling (gaps) and over-sampling (overlapping footprints) (Baltsavias, 1999a). For further processing of the intensity in both the point cloud and in rasterized image formats, the intensity has to be corrected for the influences of topography and flying altitude.

The intensity data provided by current commercial systems offer a resolution of 8-bit, 12-bit or 16-bit. There is no detailed insight given into the proprietary pulse detection algorithms. The intensity may correspond to a specific amplitude of the detected echo, e.g. its maximum, but also to the integral of the returned signal over the pulse width. In full-waveform system echo detection, however, the backscattered signal is digitized, with e.g. 1 ns sampling. Such full-waveform datasets allow for applying individual detection algorithms and waveform modeling (Jutzi and Stilla, 2006). Additionally to the determined amplitude, pulse width and returned energy are also provided for each echo. Therefore, full-waveform ALS data is also suitable for calibration, i.e. the observed laser intensities can be converted to values proportional to surface reflectance (Kasaalainen et al., 2005; Wagner et al., 2006). However, with full-waveform laser scanning the target cross section, i.e. the quantity σ in Eq. (3.3), can be determined free of assumptions, such as the assumption of Lambertian reflectors.

The need for normalized intensity values and images, respectively, is most obviously given for large ALS data sets containing strong elevation differences, as for example in high mountainous areas where uncorrected intensity images can hardly be used. Furthermore, multi-temporal analysis based on intensity requires a strategy to convert intensity to a relative but comparable measurement for different epochs with different conditions (e.g. ALS system, scan geometry, atmospheric conditions, etc.). A correction technique on point basis takes the advantage of the higher degree of information in the original data, such as the timestamps saved for every shot and relationships between laser points and plane positions. Time tagging does not only allow linking a ground reflection to the corresponding emitter position along the flight path, but also offers – in principle – the potential of considering time dependent changes of surface properties, e.g. due to water content. The original intensity value is not lost in the correction process but the corrected value is saved as additional attribute for every echo. Once the intensity attribute of the laser points is normalized, the interpolation of undistorted images is straightforward.

The objectives and contributions of this paper are:

- to give a short but broad review of recent works and applications considering ALS intensity (Sec. 3.2.1),
- to summarize the basics of the physical principles of ALS systems for understanding intensity values and reflectance, respectively (Sec. 3.2.2),
- to introduce an empirical correction technique with data-driven parameter estimation, as well as a model-based correction technique exploiting the physical principles (Sec. 3.4),
- to identify and quantify the factors for intensity variations over areas with the same surface cover/material, to determine, for example, how the signal intensity of ALS systems is affected by scan geometry (Sec. 3.5)
- to assess the potential of corrected laser return intensity as independent and additional variable for surface classification and multi-temporal analyses (Sec. 3.6).

Contrary to other papers treating the intensity and range measurement in detail (e.g., Jutzi and Stilla, 2006), this paper starts from a practical point of view. Given unknown environmental conditions during the acquisition of data as well as undisclosed details of the commercial airborne laser scanning systems, this paper details which procedures are to be applied in order to correct intensity measurements for subsequent utilization. In Sec. 3.3 the data used is presented and Sec. 3.7 concludes the findings.

3.2 Background

3.2.1 Recent work considering ALS intensity

Ever since the works of Hug and Wehr (1997); Thiel and Wehr (1999), based on a continuous-wave ranging system, in which "the reflectance criterion proved to be the most reliable of the discriminators" for the automatic detection and identification of topographic surface objects (Hug and Wehr, 1997), a number of authors concentrated on evaluating the use of pulsed ALS system intensities. Progress can be found in many different fields, which can be divided into two major scopes a) sensor related procedures (particularly estimation of planimetric offsets) and b) surface segmentation and classification methods (e.g. land-cover classification, forestry, glaciology and urban applications). The studies presented below cover both 1) algorithms that process the original point cloud directly and 2) image processing techniques based on interpolated intensity raster data.

Several authors propose methods for the estimation of planimetric offsets between ALS strips with the help of reflectance data. For these approaches no calibration is required because only relative values from the first to the second strip or between neighboring pixels are of interest. Additionally, an offset and a scale factor between the intensities can, e.g., be estimated during matching procedures. Matching of local intensity texture assists the determination of planimetric strip discrepancies in flat areas with non-existent height contrast. Burman (2000) uses height and reflectance images simultaneously to match strips and determine the offsets. Maas (2001, 2002) introduces a least-squares matching strip adjustment method that allows searching for tie points in ALS reflectance data. The intensity value simply replaces the height value in the least-squares matching for the determination of horizontal shift parameters. Vosselman (2002) suggests using the reflectance for the estimation of edge locations. Initial edges are detected by a straight line growing algorithm on a median filtered reflectance image. These initial values (edge location and reflectance values on either side of the edge) are used as input for reducing edge location errors by analytical modeling of the response of a laser beam to a gray value edge in the original laser point cloud.

Oude Elberink and Maas (2000) show the use of reflectance data in segmentation tasks with image processing techniques. As for strip adjustment, the reflectance complements the procedure for classifying ground level objects with low contrast texture and no extension into z-direction. Up to 70% detection accuracy could be reached for the classification of road, grassland and agricultural land. In the study of Song et al. (2002) the usability of ALS intensity data for land-cover classification is tested. The separability of the classes asphalt, grass, roofs and trees is shown for three different intensity images calculated from the point cloud through a) Inverse Distance Weight (IDW) interpolation, b) IDW with following median filtering and c) Kriging. The interpolation and filtering helps to overcome noise and enhances the spectral separability of the chosen classes. Song et al. (2002) state the potential of intensity for land-cover classification, but better results could be reached if disturbing effects of scan geometry on the intensity are removed through normalization by the angle of incidence. In Matikainen et al. (2003) the classification of homogeneous areas segmented in the height image is assisted by the Gray Level Co-occurrence Matrix (GLCM) homogeneity of intensity. Building segments are separated from tree segments by assuming a higher homogeneity in the GLCM of height, GLCM of intensity and a longer average length of segment edges for buildings.

In the supervised parametric classification algorithm of Charaniya et al. (2004) the intensity is used as a feature describing the four surface categories; roads, grass, buildings and trees. Using the intensity feature along with height and height variation, i.e. geometric features, caused an improvement in the classification results. Using the luminance of a gray-scale

aerial image as a forth feature slightly improves the results. One step in the method of Clode et al. (2004) for automatic road extraction makes use of the intensity to limit the candidate last pulse laser points to a subset, which fulfills the defined threshold for minimum and maximum intensity depending on the road material characteristics. Clode et al. (2005) additionally introduce an *intensity density* function that describes the ratio of number of points fulfilling the threshold to all points in the local neighborhood. Thus, the intensity density value reduces problems caused by noise in the intensity. The characteristics of power lines, i.e. low return intensities due to their small effective reflecting area, have been used by Clode and Rottensteiner (2005) as criteria to differentiate between first pulses on power lines and vegetation. Rottensteiner et al. (2005a) fused laser intensity data with multi spectral images to create a pseudo-NDVI image from the intensity and the red band of the digital orthophoto. The calculated NDVI is used as indicator for vegetation. Also man-made objects, such as roofs, have high reflectance characteristics in the laser wavelength and therefore cause errors in the NDVI. Luzum et al. (2005) use elevation and intensity measurements of first and last returns to discriminate between two object classes, buildings and trees. Mean intensities and standard deviations of intensities are found to provide the largest distances in feature space, the best separability respectively for the two classes. A correlation between geometrically related parameters, particularly the scan angle, and other features (e.g. mean intensity of first pulse) is stated by the authors but nevertheless the overall separation and therefore the classification accuracy remain high.

In Lutz et al. (2003) the potential of intensity imaging to classify glacial surface types is explained and the influence of scanning geometry (range, angle of incidence, footprint size) on the intensity is evaluated. The use of maximum intensity values in strip overlapping areas eliminates the cross-path fading effects in laser infrared images, as stated by the authors. The chosen surface classes (snow, ice, rock, water) can be distinctly identified in the intensity images and surpass the orthophotos in distinguishing surface features.

Moffiet et al. (2005) give an overview of literature dealing with ALS intensity in the field of vegetation/forest analysis. The main objective is to find reliable correlations between tree species and forest biophysical properties on the one hand and return amplitudes on the other (Lim et al., 2003; Persson et al., 2006). Due to the characteristic of laser shots to be partly reflected in different parts of the vegetation, the emitted energy is distributed to multiple reflections. As they point out, the derivation of reflectance from the return amplitude is wrong if the effective target area (backscattering cross-section) of each echo is not considered. Moffiet et al. (2005) also show how the return intensity statistics, for example average and standard deviation, are affected by forest structure and how variables based on intensity statistics could be used for characterizing closure, spacing and type of foliage components within tree crowns. Despite the fact that the intensity is not radiometrically calibrated Watt

and Wilson (2005) find "LiDAR intensity is the best single measure for identifying different species and species mixtures".
The DTM filter comparison of Sithole and Vosselman (2004) does not mention any method which makes use of reflectance data. Nevertheless, the intensity assists surface classification and therefore is of interest to the generation of DTMs.
Most studies listed above do not use the intensity data of laser points directly but derive variables from it (e.g. mean, standard deviation, "intensity density" in a local neighborhood (as defined by Clode et al., 2005)) describing the target object features. Basically, the accuracy and quality of reflectance-based surface classification is limited by the low spatial resolution of intensity images, i.e. under-sampling with low point densities, and the noisy characteristics due to several factors affecting this value (Charaniya et al., 2004; Jonas, 2002; Song et al., 2002; Vosselman, 2002; Watt and Wilson, 2005).
Attempts at normalizing intensity data are presented in Donoghue et al. (2006) and Luzum et al. (2004). They compensate for variations in path lengths (ranges), i.e. the signal strength diminishes with larger ranges. Luzum et al. (2004) apply a signal loss of one over range squared (which is justified for extended targets as detailed in Sec. 3.2.2). The values are normalized to a user-defined standard range (Eq. (3.1)).

$$I(R_s) = I\frac{R^2}{R_s^2} \tag{3.1}$$

with $I(R_s)$ as normalized intensity value to standard range R_s, I as measured intensity value and R as range between sensor position and reflection surface of a laser shot. The corrected intensities are equivalent to the intensity values that would have been recorded if the range were the same, the defined standard range, for all points. Donoghue et al. (2006) observe only small surface elevation and therefore range changes (around 80 m) in the study area. A linear regression correction approach for intensity and range is chosen to remove the assumed linear trend for intensity versus range in the given ALS data set.[2] Coren and Sterzai (2006) suggest a method, referred to as radiometric calibration, which is done in three steps a) laser spreading loss b) incidence angle and c) air attenuation correction. An asphalted road is used as homogeneous reflecting area. After removing the geometrical influence factors on the laser amplitudes, which is not explained in detail, the atmospheric attenuation coefficient is determined by best fit of an exponential decay function including the laser-target double distance and a coefficient for the total atmospheric extinction per unit length. The used data set includes a maximum double distance difference of around 150 m, which results in a weak atmospheric effect and therefore in an uncertain parameter estimation. Coren and Sterzai (2006) generate a pseudo-reflectance map out of the corrected

[2]This model is an oversimplification from the physical point of view, but proved to be sufficient for the data of that study.

intensity values, and directly and solely use this information for classifying the surface into 4 groups (bare ground, grass, sparse and dense vegetation).

3.2.2 Physical principles of ALS intensity

The basic measuring principle of Laser Scanning (LS) refers to LaDAR (Laser Detection And Ranging), more generally known as LiDAR (Light Detection And Ranging). Laser Scanning, whether airborne or terrestrial, operates on the same physical principles as microwave radar but at shorter wavelengths (Jelalian, 1992). The radar range equation (Eq. (3.2)), described in Jelalian (1992) comprises the three main factors a) sensor, b) target and c) atmospheric parameters, which diminish the transmitted signal power P_t.

$$P_r = \frac{P_t D_r^2}{4\pi R^4 \beta_t^2} \eta_{sys} \eta_{atm} \sigma \tag{3.2}$$

where the received signal power P_r is a function of the transmitted signal power P_t, the receiver aperture diameter D_r, the range from sensor to target R, the laser beam width β_t, a system η_{sys} and atmospheric transmission factor η_{atm} and the target cross section σ. In Eq. (3.2) it is assumed that i) the receiver field of view matches the beam divergence and that ii) emitter and detector have the same distance to the target.
The effective target cross section (backscattering cross section) σ contains all target characteristics and is defined as:

$$\sigma = \frac{4\pi}{\Omega} \rho A_s \tag{3.3}$$

where σ is a function of the scattering solid angle of the target Ω, the target reflectance ρ and the target area A_s. The direction of the reflection is determined by the angle between the laser beam and the target area; the angle of incidence α. It is defined as the angle enclosed by the surface normal and the laser shot direction. The reflectance is the portion of reflected to incident radiation from the target area in the laser wavelength, a value averaged over the total target area. The type of reflection (e.g. specular or diffuse) influences both the direction and the strength of the backscattering cross section. The target size is the effective area illuminated by the laser beam, i.e. the size of the orthogonal-to-ray projected area of the scatterer (Wagner et al., 2004).
Under the following assumptions Eq. (3.3) can be simplified (Jelalian, 1992). Firstly, the entire footprint is reflected on one surface (extended target) and the target area A_s is circular, hence defined by the laser beam width β_t and the range R. Secondly, the target has a solid angle of π steradians (Ω=2π for scattering into half sphere). Thirdly, the surface has Lambertian scattering characteristics. If incident angles are greater than zero ($\alpha > 0^\circ$), σ

has a proportionality of $\cos\alpha$ (Jutzi and Stilla, 2006; Rees, 2001).

$$A_s = \frac{\pi R^2 \beta_t^2}{4} \tag{3.4}$$

$$\sigma = \pi \rho R^2 \beta_t^2 \cos\alpha \tag{3.5}$$

Substituting this into the radar range equation (Eq. (3.2)) leads to an inverse range square dependency of the received signal power (Eq. (3.6)), independent of the laser beam width.

$$P_r = \frac{P_t D_r^2 \rho}{4R^2} \eta_{sys} \eta_{atm} \cos\alpha \tag{3.6}$$

The areas of non-extended diffuse targets show different range dependencies, as for example point targets (e.g. a leaf) with an area smaller than the footprint are range independent, and linear targets areas (e.g. wire) are linear range dependent (Jelalian, 1992). As a consequence the received power reflected from non-extended targets underlies an inverse range-dependent function with higher power ($1/R^4$,$1/R^3$).

Most ALS systems do not record the emitted power or even the emitted waveform. Hence, *stability* of the emitted laser power is the prerequisite for modeling the external factors influencing the received power. The system transmission factor η_{sys}, the *optical transmission efficiency* of all optical components in the ALS system, is assumed to be constant for a certain ALS system but may vary with different systems (and over time). The aperture diameter D is also set to be a constant factor within an ALS campaign using the same system. The system-independent atmospheric effect expressed by η_{atm} stands for the average atmospheric conditions at the time of flight. Even if we assume the atmospheric conditions, i.e. the loss of energy primarily due to scattering and absorption of the laser photons in the atmosphere between scanner and target, to be constant for a LS campaign the range strongly influences the total amount of extinction. For a wavelength of 1.06 μm the effect of scattering considerably exceeds the contribution of absorption (Kim et al., 2001). For horizontal propagation, the attenuation a can range from 0.2 dB/km for extremely clear conditions to 3.9 dB/km for haze conditions (Jelalian, 1992). Regarding vertical paths, the atmospheric transmittance typically increases with higher altitudes, which results in lower average attenuation coefficients in comparison to horizontal paths. For flying heights of 1000 m, 2000 m and 3000 m above ground and above sea level, the average vertical attenuations are 0.22, 0.17 and 0.14 dB/km, respectively. These values hold for mid-latitude summer and rural aerosol conditions with a visibility of 25 km. For the flying height of 1000 m η_{atm} becomes 0.91 according to Eq. (3.7).

$$\eta_{atm} = 10^{-2Ra/10000} \tag{3.7}$$

with a as atmospheric attenuation coefficient in dB/km and R in meters[3].
The noise in the intensity measurement is around 10%, which is derived from practical experience, looking at the distribution of intensities in homogeneous regions (also reported by Ahokas et al., 2006). Under very clear atmospheric conditions and small ranges η_{atm} could therefore be neglected. On the other hand, intensities have to be corrected, particularly when large range differences appear. Therefore, the model has to consider the range dependency of η_{atm} as well. Due to the lack of detailed meteorological data of the atmospheric layers (e.g. temperature, water vapor or aerosol concentration) and the high spatial variability of these parameters, an approximated value for a has to be chosen, which should represent the average atmospheric conditions at time of flight. This leads to the equation in the following form:

$$P_r(R) \propto \frac{\rho}{R^2} 10^{-2Ra/10000} \cos\alpha \cdot C \tag{3.8}$$

with factor C representing the sensor parameters (e.g. P_t, D, system losses), which are assumed to be constant within a flight campaign using the same ALS system settings.
Except for full-waveform digitizing systems a further specification of the processing steps of the received power P_r is not delivered. The left side of Eq. (3.8) is converted into a voltage, amplified in the ALS system and finally transformed into a digital number (DN), i.e. scaled integer value, through an unknown proprietary function. Assuming *linearity in this transformation* and the *intensity always to be the peak amplitude of the received signal*, it is further possible to compare intensity measurements. With a Gaussian pulse waveform the amplitude at a certain percentage of the pulse width delivers comparable values. The peak of a Gaussian can e.g. be found at 50% of the width. Extended single targets with almost Lambertian reflectance characteristics and unchanged reflectance have to be identified, which allows for estimating differences in the constant C between time shifted ALS campaigns. Having target areas with a defined reflectance ρ, e.g. measured by a spectrometer on the ground, would even allow a direct determination of parameter C. The normalization of the intensity to an average range and the estimation of C offer a reasonable approximation of surface reflectance under the conditions explained above.

[3]The factor 10000 originates from a given in *deci*Bel per *kilo*meter, whereas R is in meters as before.

3.3 Data sets

The study area, about 7 km^2 of the airport of Münster/Osnabrück, is located in Northwestern Germany. The ALS campaign was carried out in the end of August 2005 by TopScan GmbH (www.topscan.de) with Optech's ALTM 3100 (www.optech.on.ca), a pulsed small-footprint system with multiple echo recording. An overview of the 18 flight lines is given in Fig. 3.1 and a detailed description is listed in Table 3.1. The ALS system employed works with a laser wavelength of 1064 nm and the intensity is digitized by 12 bit. The beam divergence was constantly set to 0.3 mrad, the maximum scan angle to $\pm 25^\circ$ and the scan frequency varies between 40 and 70 Hz. The ALTM 3100 system provides pulse repetition rates of 33, 50, 70 and 100 kHz, which are specified with different maximum flying altitudes above ground level, for example 2500 m for 50 kHz and 1100 m for 100 kHz. The ALS data is stored and processed in a database with spatial indexing, which provides fast access to spatially distributed data (Rigaux et al., 2001). This spatial database also allows for full access to all relevant information for each ground measurement, including for example intensity, corresponding interpolated plane position and pulse repetition rate (cf. Höfle et al., 2006).

Table 3.1: *Description of flight strips at Münster/Osnabrück airport used for correction experiments.*

strip	shots	length [m]	scan freq. [Hz]	PRR [Hz]*	avg. intens. [DN]	avg. range [m]
1	308391	630.94	40	50000	8.93	2542.93
2	4031970	5614.16	40	50000	8.61	2557.43
3	320162	586.93	40	50000	7.28	2551.24
4	2528142	3590.61	40	50000	8.60	2554.89
5	3359139	4643.69	40	50000	8.91	2536.01
6	3599554	3616.55	40	70000	17.64	1737.76
7	122968	242.87	40	70000	15.99	1737.68
8	181351	294.01	40	70000	16.83	1735.10
9	485826	577.35	40	70000	17.34	1739.82
10	3005008	2952.80	40	70000	17.22	1733.79
11	4581332	4539.55	40	70000	16.61	1735.78
12	10048091	7258.68	40	100000	35.83	1027.87
13	9356560	7219.90	40	100000	36.00	1022.33
14	4540815	3212.75	40	100000	33.60	1018.79
15	5220352	3721.22	40	100000	32.86	1027.35
16	6335042	4407.87	45	100000	33.46	1006.26
17	4811324	3832.15	50	100000	34.37	1012.31
18	6177849	4352.60	70	100000	34.36	991.08

* with PRR as pulse repetition rate of the laser scanner

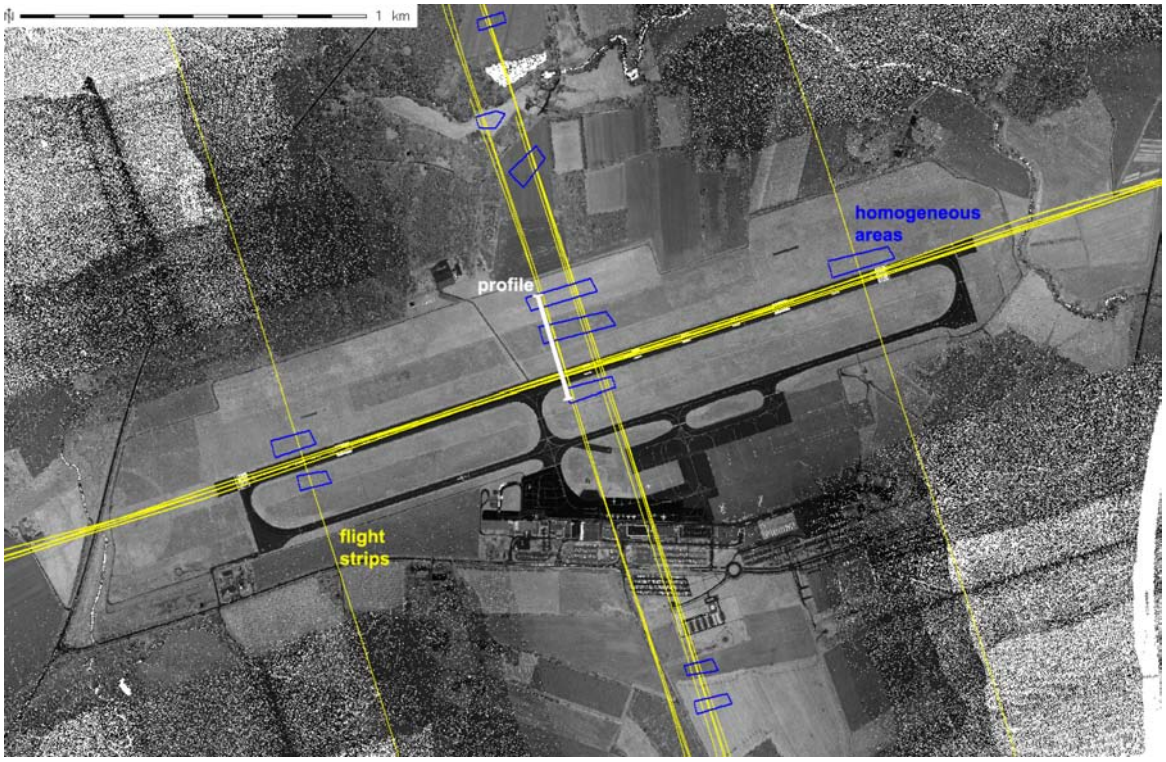

Figure 3.1: *Overview of study area airport Münster/Osnabrück: i) raster with maximum value of recorded intensity per cell (1 m cell size, empty cells left blank) as background image – lower point density (fewer overlapping strips) in image corners can be clearly seen; ii) flight strips, iii) selected homogeneous areas and iv) selected profile line.*

3.4 Methods

Two different methods for intensity correction were developed, which have different requirements for their input data sets. For both approaches the laser points (x, y, z, I) together with their corresponding plane position (x, y, z) are required for reconstruction of the laser shot vector (direction and length), which is used for calculating range and angle of incidence. The first method – data-driven correction – is suitable for flight campaigns where multiple flying altitudes are given for a part of the scanned area, not necessarily for the whole area of interest. These over-represented areas are used to estimate the parameters for the empirical correction model, which is further applied to the whole data set. Alternatively, correction parameters derived for a standard campaign may be applied to similar missions. The second method – model-driven correction – which is based on the physical model of ALS (Eq. (3.8)) has less demands on the ALS data set itself but requires information about the atmospheric conditions during data acquisition.

3.4.1 Mathematical model and parameter estimation for data-driven correction

For the data-driven correction it is assumed that the recorded intensity is proportional to the ground reflectance and related to the flying height via a monotonic function, e.g. inversely quadratic (cf. Table 3.2). With this assumption, all physical effects, e.g. extinction in the atmosphere, will have an influence on the estimated parameters. This means that all effects are (partly) compensated for, too. The value of such a model is that once the parameters are obtained, the parameters can be used for further missions (with the same system settings, comparable atmospheric conditions, etc.). Additionally, error analysis can show the capabilities and limitations of the method and give hints on the validity of the assumption. Also, the method allows for the compensation of unknown or unmeasured physical effects.

Table 3.2: *Tested empirical models (cf. Eqs. (3.9), (3.10) and (3.11)).*

model no.	$f(r)$
1	$\frac{1}{ar^2+br+(1-1000^2a-1000b)}$
2	$ar^2+br+(1-1000^2a-1000b)$
3	$ar^3+br^2+cr+(1-1000^3a-1000^2b-1000c)$
4	$ar+(1-1000a)$
5	$\frac{1}{ar+(1-1000a)}$

For the estimation of the function parameters, only measurements to extended targets may be used. This means that laser shots where more than one echo was returned may not be included in the test, because it is not known which proportion of area was struck by the emitted energy. The area covered and its reflectance are two parameters that are not distinguishable in the received echo. Furthermore, it has to be assumed that the target has uniform reflectance. Therefore points measured on the border of two different materials, as well as shots with more than one echo, must not be used. The angle of incidence of the laser beam onto the reflecting surface has an influence on the backscattered energy and should therefore be constant throughout the experiment.
The general mathematical model is:

$$i(r) = i^{1000} f(r), \quad f(r) < f(r+\Delta r) \quad \forall \Delta r > 0, \quad f(1000) = 1 \tag{3.9}$$

The above equation depicts the relation between observed intensity i and range r and the intensity that would be observed with a range of 1000 m i^{1000}. The requirement that the

value of the function f for a range of 1000 m is one is introduced to overcome an over-parametrization. Possible models for the function f are

$$f(r) = \frac{1}{ar^2 + br + (1 - 1000^2 a - 1000b)} \tag{3.10}$$

$$f(r) = (1 - 1000c_1 - 1000^2 c_2 - \dots) + c_1 r + c_2 r^2 + \dots \tag{3.11}$$

Eq. (3.10) shows the inversely quadratic relation between observed intensity and flying height, whereas Eq. (3.11) can be seen as estimating the coefficients of the Taylor expansion of the physical function relating intensity to flying height.

In order to estimate the function parameters, points are selected in cells with homogeneous intensity within one flying strip to guarantee the requirements. For such a cell, measurements from different heights (more precisely: ranges) have to be available. If the functional relationship is quadratic, at least three notably different ranges are required. Those cells, e.g. laid out in a regular quadratic grid, which fulfill the homogeneity criterion (low standard deviation of intensities) and the different ranges requirement will be called fields in the following. The fields are indexed by the letter k.

For each field a number of observations of intensity obtained at a specific range are given:

$$\text{Field } k: \quad (i_{k,l}, r_{k,l}), \quad l = 1, \dots b_k, k = 1, \dots f$$

Where f is the number of fields, b_k the number of observations in field k, and $i_{k,l}$ an observed intensity in that field. The observation equations now read:

$$\widehat{i_{k,l}} = \frac{\underline{i_k^{1000}}}{\underline{a}(r_{k,l}^2 - 1000000) + \underline{b}(r_{k,l} - 1000) + 1} \tag{3.12}$$

$$\widehat{i_{k,l}} = \underline{i_k^{1000}}(1 + (r_{k,l} - 1000)\underline{c_1} + (r_{k,l}^2 - 1000^2)\underline{c_2} + \dots) \tag{3.13}$$

In Eqs. (3.12) and (3.13) the unknowns are underlined, the stochastic observation is displayed with a hat and the range is a known, not stochastic parameter. These are the observation equations used for estimating the unknown parameters of the functions Eq. (3.10) and (3.11), respectively. The parameter $\underline{i^{1000}}$ is estimated per field, whereas the function parameters are global. It is also noted that with flying heights of around 1000 m the factors next to the unknowns are kept small. As the equations are not linear they have to be linearized and approximate values have to be determined for least-squares adjustment (LSA). Approximations for i_k^{1000} can be obtained by investigating the measurements in each field independently, again applying a model as Eq. (3.1) with $R_s = 1000$ or Eq. (3.12) with a and b determined for each field separately.

The number of unknowns is $2 + f$, and the number of observations is the total number of

all points in all fields $\sum_{k=1}^{f} b_k$.

3.4.2 Theoretical intensity correction – model-driven correction

For correcting the recorded intensity values on theoretical grounds, a number of assumptions are also made; namely, that 1) the reflectors are assumed to be extended Lambertian reflectors, 2) the surface slope can be estimated from a neighborhood of points, 3) the atmospheric conditions are known (and constant), 4) the transmitted laser power P_t is assumed to be constant (or changes in time or due to different scanner settings are known), and 5) the receiver maps incoming power linear to the recorded intensity values.
The first two assumptions are fulfilled over open terrain and can be enforced to a large extent by eliminating shots with multiple echoes. In forested areas multiple reflections are the norm, not the exception, and obtaining measures close to physical properties of the reflecting surfaces becomes impossible. If all assumptions are fulfilled, the result is a value directly proportional to ρ as defined in Sec. 3.2.2.

$$\rho_{\text{diffuse}}(R_s, \alpha) \propto I \frac{R^2}{R_s^2} 10^{2Ra/10000} \frac{1}{\cos \alpha} \tag{3.14}$$

with $\rho_{\text{diffuse}}(R_s, \alpha)$ as value proportional to ρ normalized on range R_s, I as recorded intensity, R as recorded range and α as angle of incidence defined as angle between surface normal and incoming laser shot ray.
With ALS data the geometry of the reflector has to be approximated. In general, the footprints of the laser shots do not overlap and therefore only one geometrical measurement (x, y, z) within the reflecting area is given. By calculating an orthogonal regression plane for a certain point neighborhood (e.g. fixed distance, k-nearest neighbors) an estimation for the real surface geometry can be used to calculate the angle of incidence of the laser ray.
In Eq. (3.14) the atmospheric attenuation is summarized by the coefficient a. The coefficient a has to be seen as an average value for the atmosphere between airplane and ground. One may have complex and variable atmospheric conditions during a flight campaign as well as different atmospheric layers the laser ray travels through. For simplicity and computational reasons the determination of a for each single measurement is not included in the intensity correction model. A more sophisticated meteorological model could be used to derive an average atmospheric attenuation coefficient for each laser shot, for example if information about different atmospheric layers is given. The coefficient a could be a function of R but also of the absolute elevation z, for example as the concentration of scattering particles decreases with altitude.

3.5 Experiments

3.5.1 Evaluation method of intensity correction

The primary objective of the intensity correction – to reduce variations and systematic errors due to influences of scan geometry and atmosphere – is evaluated a) on basis of a raster where the reflectance is assumed to be homogeneous for each field and b) for the flight strips where the effect of correction can be seen as *strip adjustment* for intensities. The standard deviation of the intensities within one field shows the degree of variation. The different data scaling when normalizing on a standard range leads to significant spreading or narrowing of the standard deviations. Therefore, the coefficient of variation c_v (std.dev./mean) of the intensities before and after correction is chosen as measure of quality. Furthermore, the quality of the empirical model used in the data-driven approach is described by the root-mean-square error of the LSA. All in all, the visual inspection of the corrected intensity images clearly show the reduction of disturbance.

3.5.2 Data-driven correction

The data-driven correction consists of three major steps a) select fields that fulfill the criteria described in Sec. 3.4.1, b) perform the global LSA with the data collected from the accepted fields and c) apply the correction formula to all measurements. First, the whole test area has to be restricted to areas where homogeneous reflectance is expected. This can be done either manually (e.g. digitize areas, cf. Fig. 3.1) or automatically, for example excluding areas with multiple echoes (and therefore not extended targets, e.g. vegetation), extremely high (e.g. to avoid specular reflectors) or extremely low intensities (e.g. to avoid partial reflectors). The selected areas must include the whole spectrum of ranges and intensities to reach representative results. The size of the fields mainly depends on the given point density and on the land cover characteristics. The fields should not be too large to cover more than one surface class but should be large enough to contain a respective sample size, i.e. number of points and distinguishable flying altitudes. For all fields that are within the expected homogeneous areas the intensity homogeneity (relative standard deviation, respectively coefficient of variation) and the number of points ($>$10 pts/strip) are checked per strip. Additionally, only fields with more than three different flying altitudes are accepted. For each field the empirical model (cf. Table 3.2) is preliminary fitted (local LSA) and analyzed by evaluating the fraction of variance in the data that is explained by the model, termed *r-square*.[4] Fields with r-square < 0.9 are rejected. Generally, low r-square

[4] In statistics r-square is defined as r-square = 1 - (residual sum of squares / total sum of squares) (cf. Stein et al., 2002).

values mainly occur where different surface reflectances are within a field or the ranges of the laser points are poorly distributed (Fig. 3.2).

Figure 3.2: *r-square of the local LSA for an empirical model. Low r-square values in the image corners are mainly due to the small number of strips covering these areas, hence resulting in a small number of points and few distinguishable ranges per cell (3 m cell size).*

A maximum number of accepted fields is reached for a field size of 3 m (cf. Table 3.3). For the parameter estimation only intensities of single echo points[5] that do not exceed an angle of incidence of 10° are used. This minimizes the impact of the angle of incidence on the echo ($\cos(10°) > 0.98$, therefore below noise level). The result of the parameter estimation is a correction formula to normalize all intensities to a certain *range level*, a mean r-square for all accepted fields and the corresponding global LSA quality parameters (e.g. root-mean-square errors).

Performing a global LSA in comparison to the overall averaged least-squares solutions from each field shows only small differences in the derived model parameters. The correction functions are quite similar (Fig. 3.3) and therefore analogous results are achieved. The threshold for incidence angle in the parameter estimation process should lead to a correction function not considering the effects of terrain slope (cf. Table 3.3). Taking into account α, i.e. topographically correcting the intensities in the evaluation process, only small changes in the results can be seen (for model 2 (5 m): $\bar{c}_v$/field=8.90% (vs. 9.02% without α), $\bar{c}_v$/strip=5.20% (vs. 5.11%)) due to the relatively flat terrain at Osnabrück airport. So far the evaluation process has been done for the homogeneous fields used in the estimation step

[5]Selection of shots with single echoes does not guarantee selecting extended targets only, as there is a potential of having small or dark reflectors that may generate an echo below detection threshold. In any case distinct non-extended targets are excluded.

(cf. Table 3.3). Applying the intensity correction function to the whole scene, i.e. also to inhomogeneous fields, leads as expected to higher average variation per field but still shows a significant reduction of variation (for model 2 (3 m): $\bar{c}_v$/field=24.07%, $\bar{c}_v$/strip=10.79%; for model 2 (5 m): $\bar{c}_v$/field=26.42%, $\bar{c}_v$/strip=8.81%).

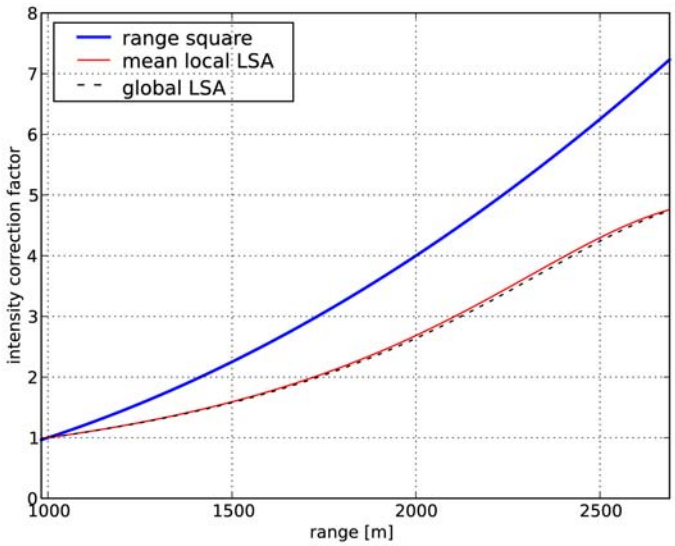

Figure 3.3: *Correction functions $f(r)$ a) range square (Eq. (3.1)), b) averaged local and c) global least-squares adjustment for model 2 and field size 5 m.*

Table 3.3: *Comparison and evaluation of different empirical models (cf. Table 3.2) and field sizes for one flight campaign at Osnabrück airport, area of interest for evaluation are limited to previously selected homogeneous areas (Fig. 3.1). The angle of incidence is not considered both in the estimation and evaluation process.*

	Estimation process				*Evaluation process*	
field size	model	fields accept.	points accept.	$\bar{r}$-square	$\bar{c}_v$/field [%]	$\bar{c}_v$/strip [%]
5 m	$I_{obs}{}^*$	2254	647277		30.98	50.22
	1	2254	647277	0.97	10.69	7.79
	2	2050	569801	0.94	9.02	5.11
	3	2053	571004	0.94	9.76	7.26
	4	1251	295750	0.92	21.08	29.19
	5	1255	283177	0.92	12.12	10.99
	$\frac{R^2}{1000^2}$				21.50	20.69
3 m	$I_{obs}{}^*$	6266	646549		30.91	50.17
	1	6263	646276	0.97	10.56	8.50
	2	5738	576503	0.94	8.87	6.03
	3	5746	577579	0.94	9.97	9.08
	4	3803	340545	0.92	21.33	30.01
	5	3909	341531	0.92	12.06	11.53
	$\frac{R^2}{1000^2}$				21.40	21.02
1 m	$I_{obs}{}^*$	56341	645932		28.51	31.73
	1	2046	42853	0.98	9.40	9.10
	2	1935	40563	0.95	7.75	6.86
	3	1964	41159	0.95	11.56	12.23
	4	1608	33736	0.93	13.69	14.84
	5	1599	33421	0.94	10.92	11.07
	$\frac{R^2}{1000^2}$				19.05	20.18

*Observed, uncorrected intensities.

3.5.3 Model-driven correction

The model-driven correction consists of four major parts: a) emitted energy b) spherical loss c) topographic and d) atmospheric correction. The effect of these variables on the correction results is examined. The model-driven approach is insensitive to the intensity data itself, i.e. in comparison to the empirical approach it does not compensate for systematic errors, which are in some way related to R. Hence, this correction separates the effects of scan geometry and atmosphere from other effects that influence the signal intensity. The physical-based approach can be applied to all laser points but it has to be considered that only corrected intensities of laser points, which fulfill the assumptions in Sec. 3.4.2, can be related to surface reflectance.

3.5.3.1 Emitted energy

The emitted energy is typically related to the pulse repetition rate (PRR). The higher the PRR the lower the emitted pulse energy and therefore the observed intensity value. This applies to the scanning system used in this study. It has also been reported by Chasmer et al. (2005) and Baltsavias (1999c). Assuming a constant average power and pulse duration leads to a decreasing peak power indirectly proportional to the PRR settings. Therefore, Eq. (3.14) has to be completed by a term that corrects the influence of the PRR on the emitted power.

$$P_r(R) \propto \frac{\rho}{R^2} 10^{-2Ra/10000} \cos\alpha \frac{1}{f_{sys}} \cdot C \tag{3.15}$$

with f_{sys} as factor accounting for the emitted energy. Following the equation of Baltsavias (1999c) the correction factors are f_{sys} = 1.0 for PRR of 50 kHz, 1.4 for 70 kHz and 2.0 for 100 kHz. The values reported by Chasmer et al. (2005) for the ALTM 3100 result in correction factors of 1.0 for 50 kHz, 1.349 for 70 kHz and 1.898 for 100 kHz, which differ up to 5% from the linear approach of Baltsavias (1999c). We decided to use the values reported by Chasmer et al. (2005) as those are specific to the laser scanner model also used in our study.

3.5.3.2 Spherical loss

The inverse range-squared dependency of the received power of extended targets plays the major role for intensity variation in the study area because multiple flying altitudes overlap (Fig. 3.4), but is even evident for areas with high relief intensity and relatively constant absolute flying altitudes. Following Eq. (3.14) the effect of spreading loss can be removed by multiplying the original intensities by range squared divided by the normalizing range squared (e.g. R_s = 1000 m).

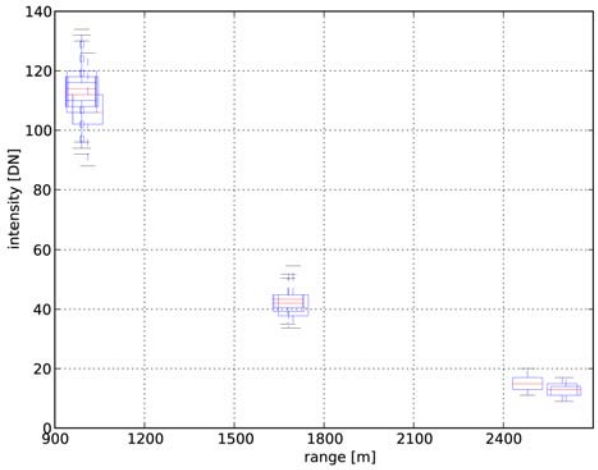

Figure 3.4: *Boxplots of recorded intensity versus range for single flight strips for a close-cropped grass plot. The range-dependency of the intensity can be clearly seen. In this example the recorded intensities range from 9 to 136, whereas the maximum range we observed is 0 to 5100.*

3.5.3.3 Topographic effects

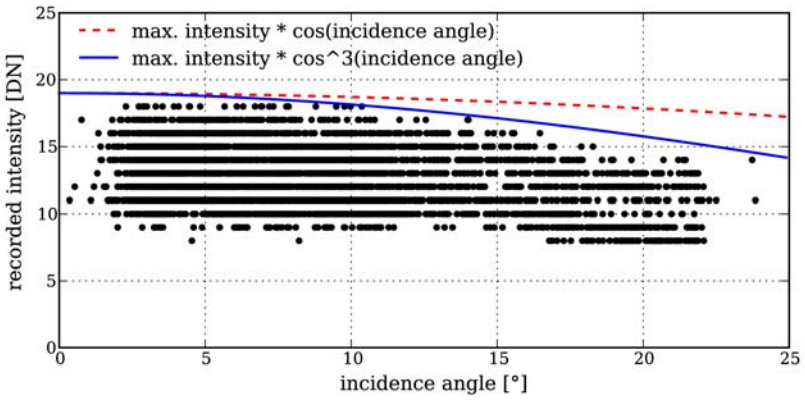

Figure 3.5: *Effect of incidence angle on recorded intensity for a selected cross-section of a single flight strip with constant flying altitude above ground level. Dashed line shows change of reflectance with* $\cos\alpha$ *and solid line additionally includes change of range (resulting in* $\cos^3\alpha$*).*

The topography is expressed by the angle of incidence of the laser ray. The incidence angles are also between $\pm$max. scan angle for flat terrain. For ideal Lambertian scatterers the reflected intensity is proportional to $\cos\alpha$. The higher the portion of non-Lambertian reflectance properties (specular scattering) the smaller the amount of light coming back to the sensor if $\alpha \neq 0$. That means the assumption of having simply Lambertian scatterers can lead to a topographic over-correction of intensities. It would be necessary to have information about the reflection characteristics of each measurement, i.e. using a high resolution land cover classification with reflection estimates for each class, but a realistic determina-

tion still remains difficult. Following Eq. (3.14) the topographic effects are corrected by multiplying with $1/\cos\alpha$. Fig. 3.5 shows the decrease of intensity towards higher incidence angles.

3.5.3.4 Atmospheric effects

In general, information about atmospheric conditions (e.g. Rayleigh and aerosol scattering transmittance) during a flight campaign are not available but information about the atmospheric visibility can be obtained from airport or weather data much more easily. The visibility parameter (in km) can be used as input parameter for modeling the atmospheric effect as for example with the radiative transfer model MODTRAN (Berk et al., 1998), which outputs an estimate for the integrated total atmospheric transmittance. Running MODTRAN3 with the recorded visibility of 25 km (meteorological data of airport Münster/Osnabrück), the options mid-latitude summer atmosphere and rural aerosol conditions for the three predominant flying altitudes (1070 m, 1760 m and 2560 m a.s.l. with an average target altitude of 50 m a.s.l.) results in atmospheric attenuation coefficients of 0.21 dB/km, 0.18 dB/km and 0.15 dB/km. These independent determinations can be compared to the atmospheric attenuation coefficient a (in dB/km) extracted from the data itself by selecting the ranges and topographically corrected intensities of a homogeneous area (Eq. (3.16)). By dividing two equations (3.15) to the same target from two different flying heights R_1 and R_2 and corresponding angles of incidence, a can be estimated:

$$a = 5000\log_{10}\left(\frac{I_1 R_1^2 \cos\alpha_2 f_{sys1}}{I_2 R_2^2 \cos\alpha_1 f_{sys2}}\right)\frac{1}{R_2 - R_1} \tag{3.16}$$

Using Eq. (3.16) for the flying altitudes 1070 m and 2560 m, an average value of a = 0.20 dB/km was determined. Using multiple fields, a standard deviation of $\pm$0.058 dB/km was derived. Comparison of values and their agreement is shown in Table 3.4.

Table 3.4: *Comparison of atmospheric transmittance values for two flying altitudes: i) extracted from the data with Eq. (3.16) and ii) calculated with MODTRAN.*

altitude [m]	η_{atm} empirical	η_{atm} MODTRAN	rel. difference [%]
1070	0.904	0.899	-0.55
2560	0.787	0.831	5.33

3.6 Results and discussion

The data-driven correction approach, exemplified by empirical model 2, shows a significant reduction of disturbance in the intensity signal (Fig. 3.6). After correction the variation within the homogeneous fields is reduced to $\bar{c}_v$/field $< 10\%$ of the average value and the displacement between the flight strips ($\bar{c}_v$/strip) attains about 5%.

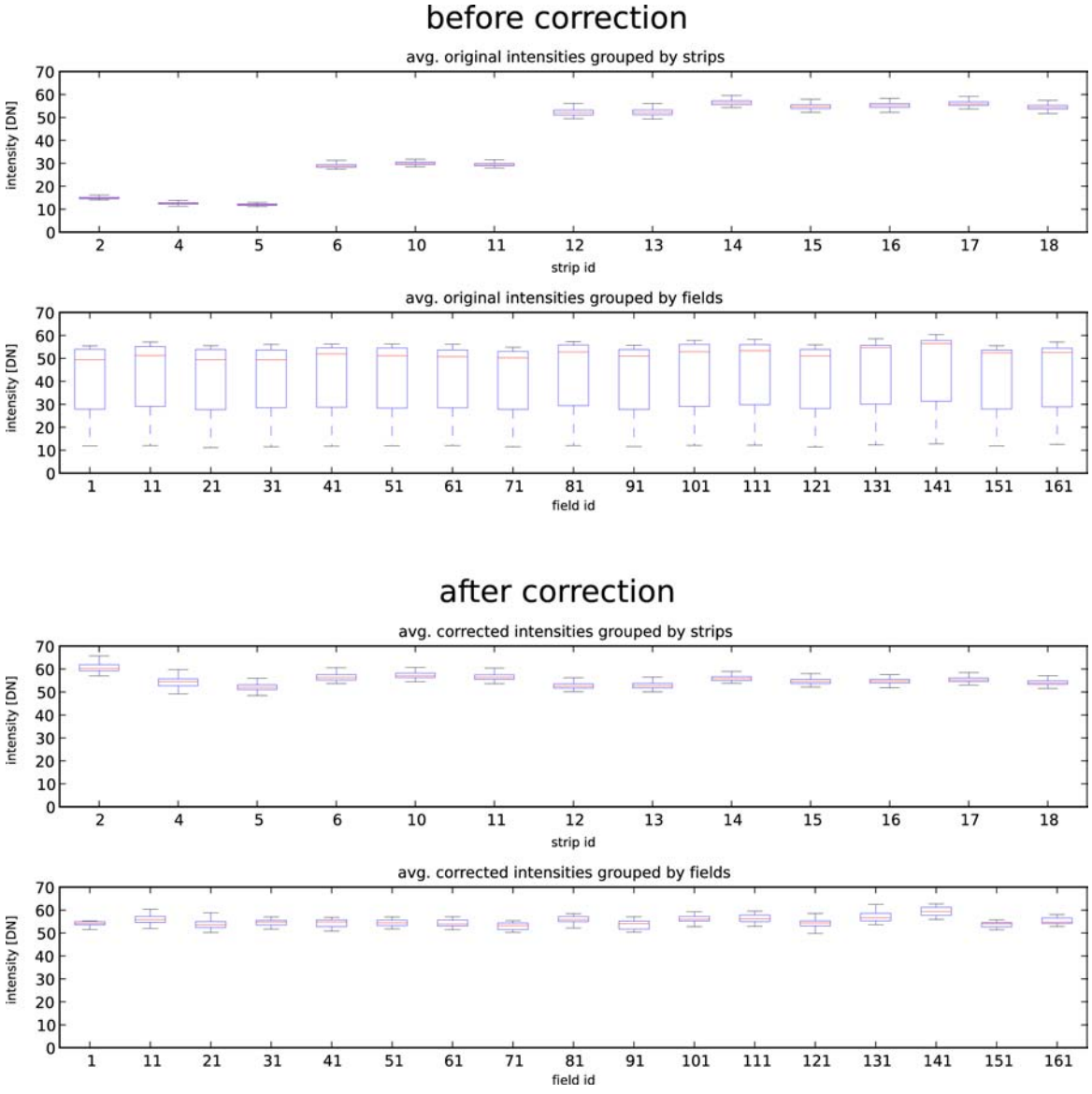

Figure 3.6: *Comparison of recorded and empirically corrected intensities (model 2), every 10th field (5x5 m) of a single homogeneous area.*

The second order polynomial model accounts for all influences correlating quadratic loss (e.g. spherical) and linear loss with range. Effects related to the PRR settings, which are changed with different flying altitudes, are also compensated for. The lower PRR have higher ranges and therefore partially compensate the losses due to distance. Introducing a

PRR correction factor before the parameter estimation delivers a correction function which has similar function values to the model-driven corrections (Fig. 3.7).

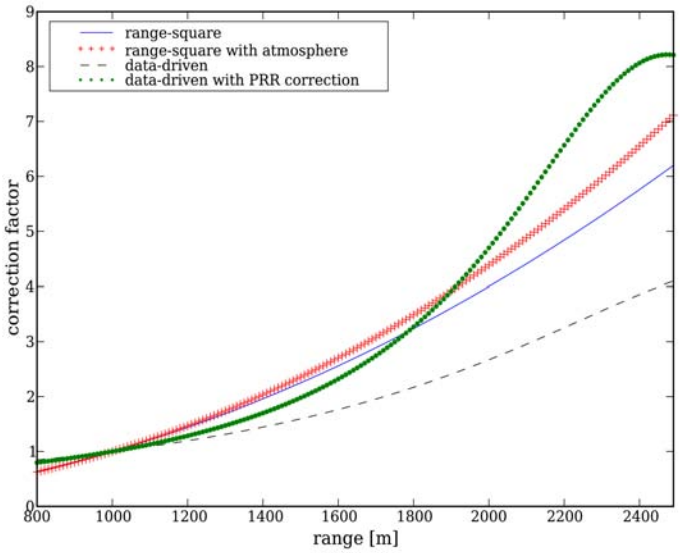

Figure 3.7: *Comparison of correction functions: Empirical functions are based on empirical model 2; atmospheric attenuation a set to 0.20 dB/km.*

In the cross-sections of Fig. 3.8 through grass (bright) and an adjacent airstrip (dark) the successful adjustment of the single flight strips can be seen. The remaining variation originates from the inherent random noise in the intensity measurement, especially for short ranges with a small sampling area, but also from the present surface characteristics. One can easily distinguish between grass land, road and road marking. A few points from the road lying within the intensity domain of grass seem to be partially reflected from the bright marking and the dark road. In this special case calculating a mean intensity image can cause problems for surface classification, but additionally using an image with the std. deviations could provide support. The averaged intensity images (Fig. 3.9) clearly demonstrate the effect of intensity correction. The highest correction factors are reached for areas covered with only one high flight strip (at image corners). In Fig. 3.10 one can also see the boundaries of the flight strips indicated by a higher correction towards higher scan angles (cf. Fig. 3.1).

Performing the evaluation process with the model-driven correction procedure, considering only the spherical loss, shows a decreasing variation (1 m fields: $\bar{c}_v$/field=19.05%, $\bar{c}_v$/strip=20.18%) in comparison to the original intensities, but a significantly higher variability than the empirical correction. Using PRR correction factors in the correction for spherical loss and topography, as well as applying an atmospheric attenuation coefficient of 0.20 dB/km, which was estimated from the data, results in $\bar{c}_v$/field=9.08% and $\bar{c}_v$/strip=8.56%.

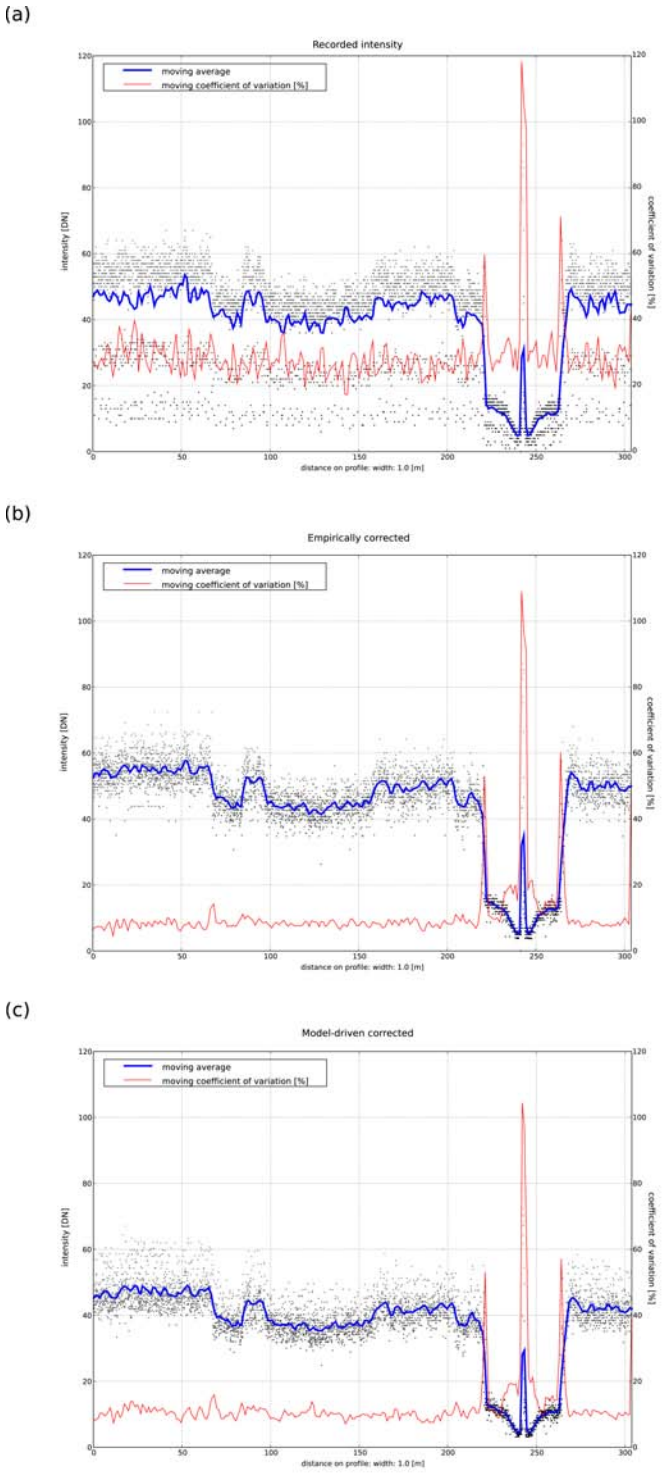

Figure 3.8: *Selected profile line (cf. Fig. 3.1) through a) recorded intensity, b) empirically corrected intensity and c) model-driven corrected intensity with moving average and coefficient of variation for each cross-section.*

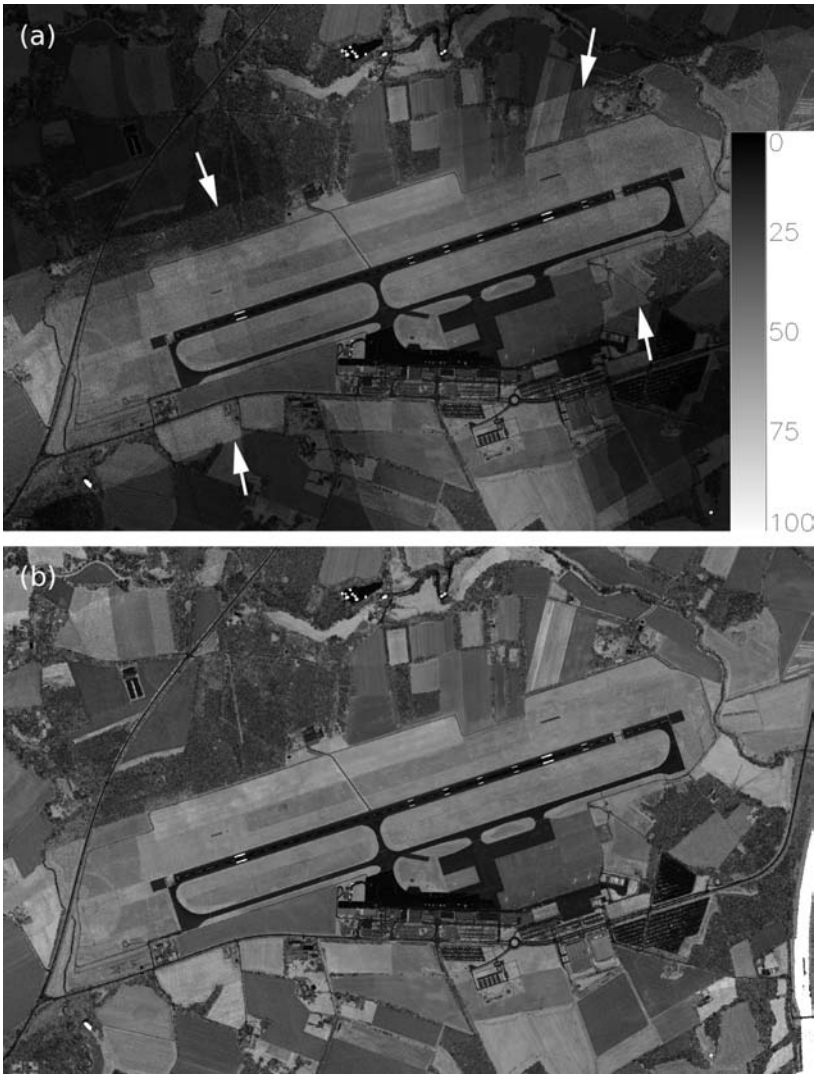

Figure 3.9: *Averaged intensity rasters (gray-scaled), empty cells filled with a median filter: a) original recorded intensity and b) data-driven corrected intensity.*

Intensity outliers directly influence the model-driven corrected intensity value. In comparison to the empirical parameter estimation process that suppresses the influence of intensity outliers, the model-driven correction does not check the values for reliability because every measurement is treated individually. Hence, using the same evaluation process as for the data-driven results further checks have to be considered (e.g. variation of intensity within each strip).

The theoretical correction can be developed further by using *radiometric control points*. This is one method of obtaining absolute ρ values. An alternative would be recording the emitted shot with the same method and obtaining ρ via the quotient of the emitted and received intensity. In order to make two campaigns, possibly with different scanners using the same wavelength, comparable, *radiometric tie points* are sufficient.

Both presented correction methods show similar results according to the reduction of in-

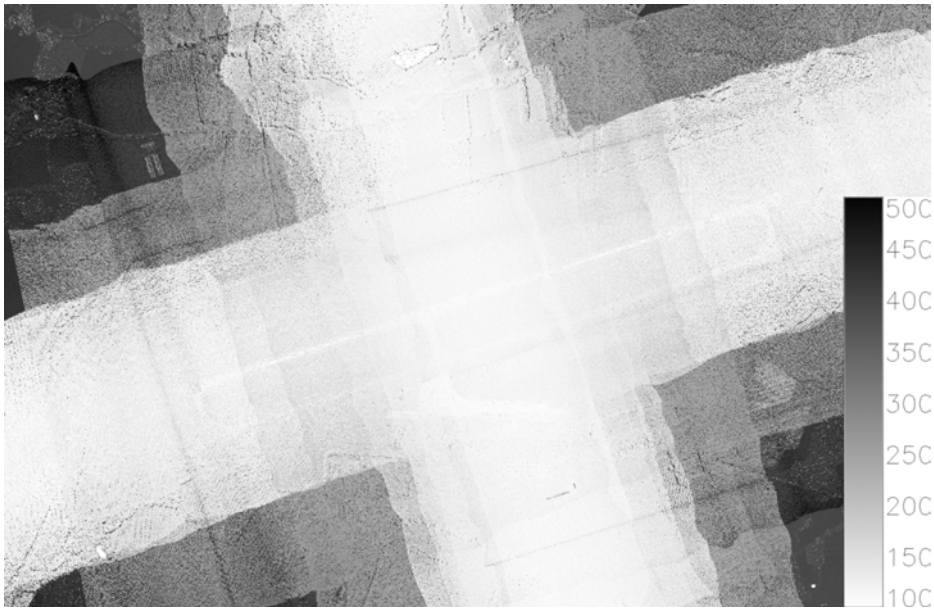

Figure 3.10: *Corrected intensity in percentage of original intensity.*

tensity variation. The main differences are the data requirements. Both methods obviously need the plane position to derive the *range* and the surface normal vector to derive the *angle of incidence* for each laser shot. The data-driven correction only succeeds if multiple flying altitudes over relatively homogeneous areas are given. No further knowledge about system settings and atmospheric conditions have to be available. However, applying the correction formula is only reliable if an ALS mission is accomplished where the conditions are in the domain of the parameters used for the correction formula derivation (flying height envelope, system used, etc.). The model-driven approach primarily handles each measurement individually. Good results are achieved if P_t is constant or known, the atmospheric model reproduces the predominant atmospheric conditions at time of flight and the reflectance properties are similar to single extended Lambertian scatterers, i.e. the type of reflection and the effective reflecting area can be modeled.

The corrected intensity values are used to generate intensity images with lower systematic errors (Fig. 3.9). For the rasterization further constraints can be introduced to minimize the influence of intensity outliers (e.g. partial or specular reflectors), such as giving higher weight to values with lower incidence angles or ignore values outside an accepted homogeneity criterion (e.g. deviation to median value) for calculating the average cell value. Complementary to the undisturbed intensity images the information about intensity variation and outliers could be used as an additional variable for describing and classifying surface characteristics.

3.7 Conclusions

In this paper two independent methods for correcting airborne laser scanning intensities were presented. The first approach – data-driven method – performs a least-squares adjustment for a given empirical model including intensity and range, the major variable influencing the received signal intensity. The best results were achieved with a model representing a range-square dependency. The second approach – model-driven method – is derived from the radar equation, which describes the loss of emitted pulse power. Both correction methods achieve a significant reduction of local intensity variation within cells of a regular grid (1 m, 3 m and 5 m size) spanned over the study area and an even more significant global adjustment of the single flight strips.

The evaluation of the theoretical correction showed comparable results with the empirical method. Which method to choose primarily depends on the existing ALS data set. Both methods are designed to work on large data sets. The data-driven approach solely requires multiple flying altitudes over relatively homogeneous areas. By contrast, the model-driven approach can be applied without any special requirements on the design of the flight campaign. It is therefore preferred. Eq. (3.15) can be used with values from atmospheric models to obtain values proportional to surface reflectance from laser scanning intensity values. Additionally, Eq. (3.15) can be used to estimate a (the atmospheric attenuation coefficient) or f_{sys} (a factor accounting for the emitted power) by a least squares adjustment if measurements over homogeneous areas are available from different systems or flying heights.

In high mountainous glaciated areas where optical imagery has its problems (e.g. shadows, lack of texture) intensity images have great potential to support the primary topographic information for surface classification. With the help of intensity correction the influence of relief changes are removed from the intensity value leading to an intensity map useful for glacial surface classification (Lutz et al., 2003). Having a standardized intensity correction method makes it possible to compare multi-temporal intensity data sets flown with the same scanner (e.g. monitoring of snow cover changes). If unchanged and homogeneous reflecting areas are available in the temporal shifted data sets, adjusting the intensities of different epochs is straightforward (e.g. linear regression of expected homogeneous areas to determine difference in factor C in Eq. (3.8)).

The paper has demonstrated that intensity values that come from ALS sensors using an unknown proprietary function to preprocess the signal can be successfully corrected. This can potentially support surface classification and monitoring of surfaces which have a good separability in the wavelength of the ALS system. Better technical information from the manufacturers should overcome the problem of changes in emitted power. However, as the power (and pulse shape) may not necessarily be constant from one shot to the next,

simultaneous recording of the emitted pulse energy distribution and full-waveform digitization of the received pulse will improve the correction of airborne laser scanning intensity measurements.
With full-waveform ALS data more explicit insight into the received pulse energy is available. The peak amplitude and the pulse width can be extracted in the post-processing step with a function visible for the user. Together with the recorded emitted waveform the target reflectance ρ can be calculated with less assumptions concerning the system parameters. But the effective reflecting area (e.g. occluded areas with multiple echoes) and the scattering characteristics (e.g. Lambertian, quasi-Lambertian, specular) of the targets still remain unknown and may cause uncertainties in deriving area-wide reflectance maps from ALS.
Concerning laser range data acquired from terrestrial platforms, it has to be noted that current commercial systems do not offer the option to record more than one echo or the full-waveform. Therefore, the selection of homogeneous areas with exclusively extended targets would have to be adapted. Apart from that, and considering that the methods described in this paper work on the original point cloud, the methods can be applied to Terrestrial Laser Scanning as well.

3.8 Acknowledgments

The authors would like to thank TopScan GmbH, especially J. Lindenberger, for their cooperation in the data acquisition campaigns and providing detailed insight into ALS data processing steps.

4 Glacier surface segmentation using airborne laser scanning point cloud and intensity data

---

Published as:
Höfle, B., Geist, T., Rutzinger, M., Pfeifer, N. (2007): Glacier surface segmentation using airborne laser scanning point cloud and intensity data. *International Archives of the Photogrammetry, Remote Sensing and Spatial Information Sciences 36*, Espoo, Finland, (on CDROM).

Abstract

As glaciers are good indicators for the regional climate, most of them presently undergo dramatic changes due to climate change. Remote sensing techniques have been widely used to identify glacier surfaces and quantify their change in time. This paper introduces a new method for glacier surface segmentation using solely Airborne Laser Scanning data and outlines an object-based surface classification approach. The segmentation algorithm utilizes both, spatial (x, y, z) and brightness information (signal intensity) of the unstructured point cloud. The observation intensity is used to compute a value proportional to the surface property reflectance – the corrected intensity – by applying the laser range equation. The target classes ice, firn, snow and surface irregularities (mainly crevasses) show a good separability in terms of geometry and reflectance. Region growing is used to divide the point cloud into homogeneous areas. Seed points are selected by variation of corrected intensity in a local neighborhood, i.e. growing starts in regions with lowest variation. Most important features for growing are (i) the local predominant corrected intensity (i.e. the mode) and (ii) the local surface normal. Homogeneity is defined by a maximum deviation of $\pm$5% to the reflectance feature of the segment starting seed point and by a maximum angle of 20° between surface normals of current seed and candidate point. Two-dimensional alpha shapes are used to derive the boundary of each segment. Building and cleaning of segment polygons is performed in the Geographic Information System GRASS. To force spatially near polygons to become neighbors in sense of GIS topology, i.e. share a common boundary, small gaps (<2 m) between polygons are closed. An object-based classification approach is applied to the segments using a rule-based, supervised classification. With the application of the obtained intensity class limits, for ice<49% (of maximum observed reflectance), firn 49-74% and snow$\geq$74%, the glacier surface classification reaches an overall accuracy of 91%.

4.1 Introduction

The cryosphere is a component of the Earth system that presently undergoes dramatic changes. Glaciers and ice sheets as important features of the cryosphere are sensitive to climate fluctuations and their mass balance can be used as an indicator of regional-scale climate change. Next to the quantification of glacier geometry and mass, the qualitative analysis of the glacier surface is important, as for example the identification of the snow line for subsequent parametrization of glacier mass balance or the classification of different glacier surface facies (e.g. ice, firn, snow). Glaciological research is fundamentally based on field observations, which are rather costly and time-consuming. During the last two decades numerous studies have tested and discussed the possibilities offered by optical and radar remote sensing (summarized e.g. in Rees, 2005; Bamber and Kwok, 2004). Airborne Laser Scanning (ALS) allows for detailed mapping of glacier topography and the quantitative analysis of glacier geometry, such as changes in area and surface elevation, and subsequently mass. Not yet explored is the potential of ALS data for qualitative analysis (e.g. object detection, surface classification).

This paper presents a new method for glacier surface segmentation based on the unstructured point cloud using the full information of ALS data, namely geometry (x, y, z) and signal intensity. The proposed algorithm is fully implemented in a Geographic Information System (GIS). Hence, the GIS vector data model and its topological processing tools can be used. The paper describes in detail the processing and segmentation steps and outlines an object-based classification. While this paper presents an application to glaciers, it shows that a common exploitation of geometry and radiometry provided by laser scanning can be jointly used to successfully segment and classify objects, where neither information source alone would suffice.

4.1.1 Related work

The last decade has seen increasing interest in the use of ALS for mapping and monitoring glaciers and ice sheets. One motivation was the ability of the technology to map areas of low surface texture (e.g. snow and firn) at high accuracy and resolution. To date, laser scanning for glaciological purposes has been widely and successfully applied in Antarctica and on the Greenland ice sheet (e.g. Abdalati et al., 2002), but only a few attempts have been made to utilize ALS or airborne laser profiling on mountain glaciers (e.g. Kennett and Eiken, 1997; Baltsavias et al., 2001). Geist et al. (2003) and Arnold et al. (2006) give an initial overview on potential applications of ALS in glaciology.

ALS intensity has been utilized in many fields of applications (e.g. road and building detection, strip adjustment, forestry) but only a few studies investigated its value for glaciological research (e.g. Lutz et al., 2003; Hopkinson and Demuth, 2006). Point cloud segmentation is mostly used for anthropogenic objects/surfaces (e.g. Filin and Pfeifer, 2006; Rabbani et al., 2006). Natural surfaces, such as vegetation or glacier ice, are more likely to have a great variation in terms of geometry and reflectance characteristics. Thus, segmentation of such surfaces into homogeneous regions may be difficult. But separating homogeneous from heterogeneous surfaces already delivers valuable information, as for example the detection of glacier surface irregularities (e.g. crevasses, melt water channels, moulins, debris) surrounded by relatively homogeneous areas.

4.1.2 Glacier surface characteristics

The paper concentrates on the prevalent glacier surface classes ice, firn, snow and surface irregularities. The reflection characteristics of the glacier surface classes in the near-infrared wavelength of the laser scanner used in this study (1064 nm) exhibit a good spectral separability (Wolfe and Zissis, 1993). Due to the decrease of reflectance with age – metamorphosis from new to granular snow and increasing amount of absorbing particles (dirt) – different stages of snow/firn can be distinguished. Typical reflectance values are: glacier ice$<$0.2, firn 0.5-0.7 and fresh snow$>$0.7 (Rees, 2005; Hook, 2007). After correcting the laser signal intensity for spherical loss, topographic and atmospheric effects (Section 4.3.1), it can be used as a value proportional to surface reflectance (Ahokas et al., 2006; Höfle and Pfeifer, in press). Lutz et al. (2003) and Hopkinson and Demuth (2006) state that the intensity is a good indicator for glacial surfaces (Fig. 4.1).

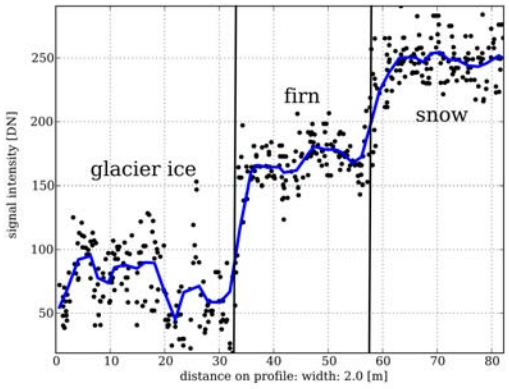

Figure 4.1: *Corrected intensity cross-section along different surfaces: glacier ice, firn and snow. Moving average line clearly shows steps in intensity between the surface classes. Also high variability in intensity of glacier ice areas can be seen.*

Additionally to the corrected intensity, surface roughness can be used to describe the different classes. In general, terrain variation is increasing with proceeding melting from snow to uncovered glacier ice where irregularities due to glacier dynamics reach the upper surface, and hence are visible for the laser scanner.

4.2 Study area and datasets

4.2.1 Test site and data acquisition

Hintereisferner (Fig. 4.2) is a typical valley glacier with a length of approximately 6.5 km along the flow line (determined in 2005). The glacier shows a longitudinal profile with a relatively flat tongue and a steeper accumulation area. For the study described here data from 12 August 2003 is used, when most of the glacier, except the uppermost parts, was free of snow. The ALS flight campaign configurations are summarized in Table 4.1.

Table 4.1: *ALS flight campaign parameters.*

ALS campaign	
date, time	12.08.2003, 6:30 - 9:21
scanning system	Optech ALTM 2050
laser wavelength	1064 nm
avg. height above ground	1150 m
pulse repetition frequency	50 kHz
scan frequency	30 Hz
scan angle	$\pm 20^{\circ}$
swath width	837 m (with 40% overlap)
avg. point density	1.7 pts/m^2

4.2.2 Reference data

Traditional aerial images were taken at the same day as the ALS campaign. These images were processed to orthophotos (0.5 m resolution). In order to obtain ground truth for validation, reference data for evaluating the results was created by a glaciologist aware of the local conditions. The classes ice, firn and snow were digitized using the orthophoto and the corrected intensity image. Surface irregularities were identified in the shaded relief of the ALS elevation model.

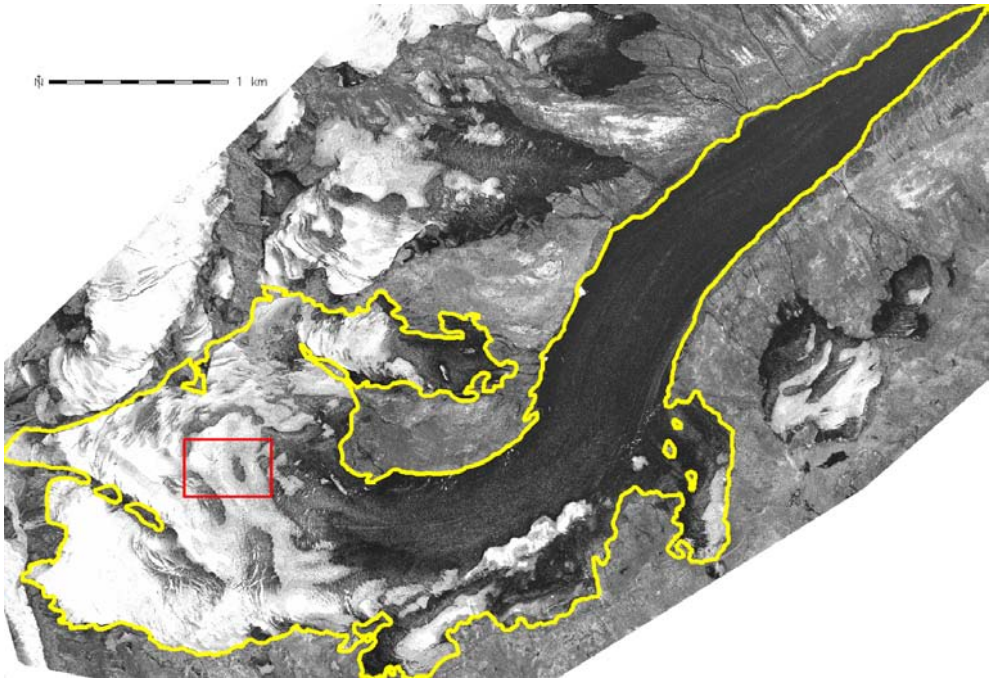

Figure 4.2: *Corrected intensity image of Hintereisferner with glacier borders and rectangular test site.*

4.2.3 Datasets and data management

The ALS point cloud is managed within the LISA (LIdar Surface Analysis) framework (Höfle et al., 2006), which integrates full GIS functionality provided by the Open Source GIS GRASS. The results of the segmentation (segment polygons) are stored in the GRASS vector data model providing topologic geometry storage and attribute data management. For the glacier surface segmentation only single echo points are used. Plane positions, needed for intensity correction, are made available by LISA for each laser shot using linear interpolation of the GPS positions. A test site representing all target classes with 485 m x 318 m extent and 335.104 laser points was selected (Fig. 4.2).

4.3 Methodology

The developed methodology for glacier surface classification is shown in Fig. 4.3. The major processing steps will be described in detail below.

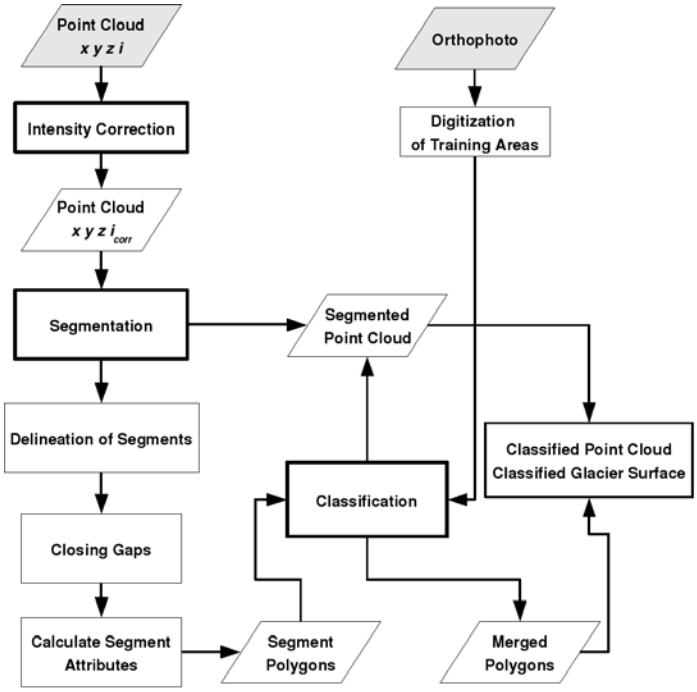

Figure 4.3: *The workflow of glacier surface classification using the original, unstructured ALS point cloud.*

4.3.1 Intensity correction

To get a value proportional to surface reflectance, a correction procedure accounting for spherical loss, topographic and atmospheric effects has to be applied. The emitted power is assumed to be constant for the chosen flight campaign because scanner settings, such as pulse repetition frequency, are not changed. The existing data situation allows only for applying a model-driven correction approach (Eq. (4.1)), due to the lack of multiple flying altitudes over homogeneously reflecting areas.

$$\rho \propto I \frac{R^2}{R_s^2} 10^{2Ra/10000} \frac{1}{\cos \alpha} \tag{4.1}$$

where

ρ = reflectance
I = signal intensity [digital number (DN)]
R = range [m]
R_s = standard/normalizing range [m]
a = atmospheric attenuation coefficient [dB/km]
α = angle of incidence [°]

Further details concerning intensity correction are described in Ahokas et al. (2006) and Höfle and Pfeifer (in press).

The intensities are normalized to 1000 m range. Under the assumption of Lambertian scattering characteristics of the surface this value is proportional to surface reflectance and will be called *corrected intensity* in the following. The surface normal is estimated by fitting an orthogonal regression plane to the 30 nearest neighbors and a vertical atmospheric attenuation coefficient of 0.15 dB/km was derived by modeling the atmospheric conditions at time of flight. Fig. 4.4 shows the evident reduction of disturbance in intensity after correction and Fig. 4.2 the corrected intensity image of Hintereisferner.

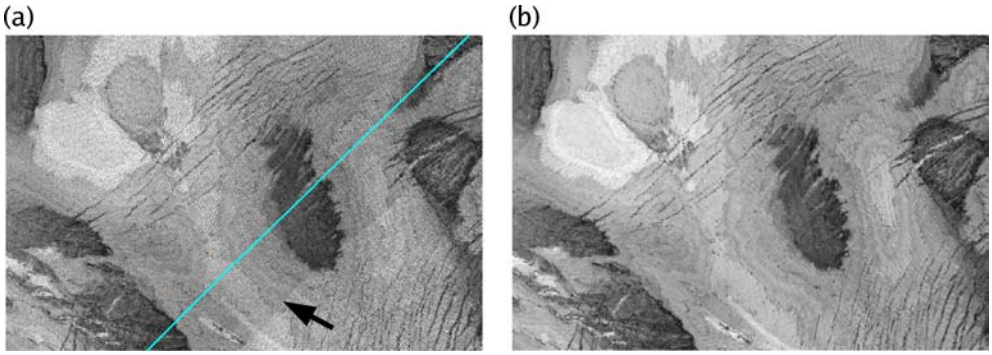

Figure 4.4: *a) Image of mean recorded intensity with flight path (cyan): strip offsets can be clearly seen (arrow), b) mean corrected intensity image.*

4.3.2 Segmentation

The point cloud is subdivided into homogeneous segments using a geometrical and intensity homogeneity criterion. Segments are defined as spatially connected regions, allowing only smooth terrain transitions (break at step edges, such as crevasses, water channels and glacier borders) and similar intensities. The segmentation steps are (i) point feature calculation, (ii) seed point selection and (iii) region growing.

4.3.2.1 Feature calculation

For each laser point the features are calculated from its 2D k nearest neighbors (kNN). The surface normal is estimated by fitting an orthogonal regression plane. Additionally, the standard deviation (SD) of the orthogonal fitting residuals is used as parameter for surface roughness. A representative corrected intensity value is found in the histogram by choosing the most frequent value (mode) for a given bin size. Hence, the predominant surface is selected and the influence of noise and outliers is reduced. Additionally, the coefficient of

variation (c_v) of the corrected intensity is used as parameter for surface homogeneity in the local neighborhood.

4.3.2.2 Seed point selection

The laser points are sorted by homogeneity (c_v). The lower the variation, the more likely the point lies within a homogeneous area, representing a single surface class, well suited as start point for growing a segment. The seed points could be limited by a certain c_v threshold. Due to the inherent reflectance variation of natural surfaces and to reach an area-wide segmentation, all laser points are accepted as seed points ordered ascending by c_v.

4.3.2.3 Region growing

The local connectivity of segments is forced by using a small local neighborhood (e.g. k=15) and a maximum growing distance, as well as a maximum distance of a neighbor to the current adjusting plane of the segment (either the local surface plane of the starting seed, the current seed or the fitted plane to all current region points). To maintain similarity in terms of smoothness, the angle between the current segment plane and the surface normal of a candidate point is checked. The similarity in terms of reflectance is checked by comparing the current segment corrected intensity (either intensity feature of starting seed, current seed or mean of all current region points) with the corrected intensity feature of the candidate point. The difference must be lower than a defined percentage of the current segment intensity, i.e. for brighter objects higher absolute variation is allowed.

4.3.3 Delineation of point cloud segments

To be able to use an object-based classification procedure, the delineation (polygonization) of point cloud segments is necessary. The segment boundary line is derived individually for each segment by calculating a 2D basic alpha shape (i.e. based on the Delaunay triangulation of the point set) for a given alpha value (Edelsbrunner and Mücke, 1994; Da, 2006). Small alpha values not necessarily produce a convex shape. If alpha is chosen very large (alpha $\rightarrow \infty$), the alpha shape represents the convex hull. Before calculating the alpha shapes a minimum segment size threshold (no. of points) is applied, which removes small, isolated points/regions, such as small snow spots or debris. The alpha value has to be chosen such that a connected exterior boundary can be produced. The alpha complex consists of non-ordered boundary line segments. Using GIS tools a clean polygon boundary is built (connect line segments; remove duplicate vertices and small islands; Fig. 4.5).

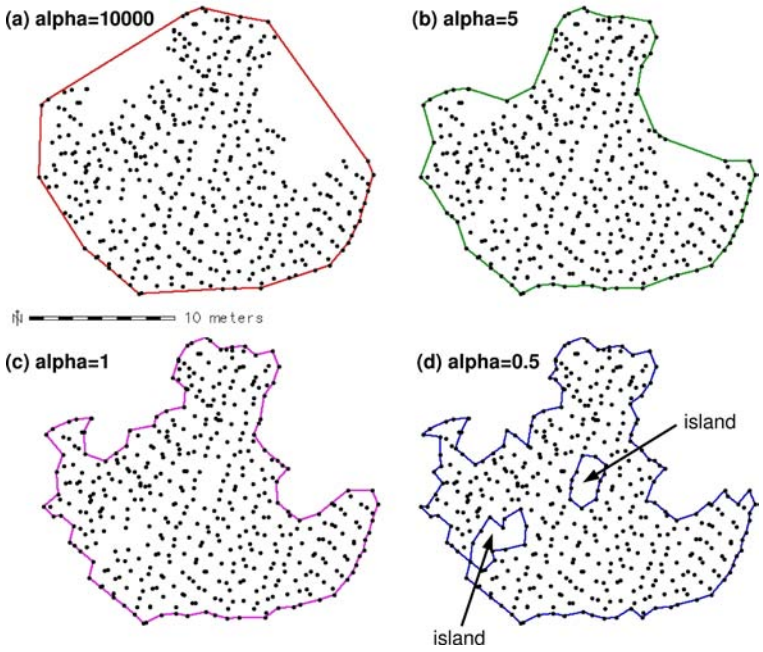

Figure 4.5: *Segment boundary derived from point cloud alpha shape using different alpha values. a) With alpha = 10000 the convex hull is reached, d) with small alpha values islands can occur.*

4.3.4 Removal of overlaps and closing of gaps between segment polygons

As the segment polygons are derived individually small overlaps and gaps may occur between the single segment polygons. With higher alpha values, more overlapping is necessarily produced. The lower the density of acquired points, the more areas are not covered by a polygon. Cleaning of segment polygons is proceeded as following (Fig. 4.6):

1. Buffer polygons (define max. gap size) and intersect with gap areas (areas not covered by any polygon).
2. Create Voronoi diagrams of segment boundary vertices. Voronoi polygons get ID of corresponding segment.
3. Intersect gap areas within buffer size with Voronoi diagrams. Assign segment ID to intersection polygons.
4. Merge intersection polygons with segment polygon sharing same ID.
5. Merge overlapping areas (intersections) and very small areas ($<$2.0 m^2) with adjacent segment sharing longest boundary.

The buffer size should not be too large (e.g. half of estimated gap size) because the segments also grow into the areas not covered by any segment, which are later used to identify surface

irregularities. After closing small gaps spatially near polygons share a common boundary line and therefore agree with the definition of neighbor in sense of GIS vector topology.

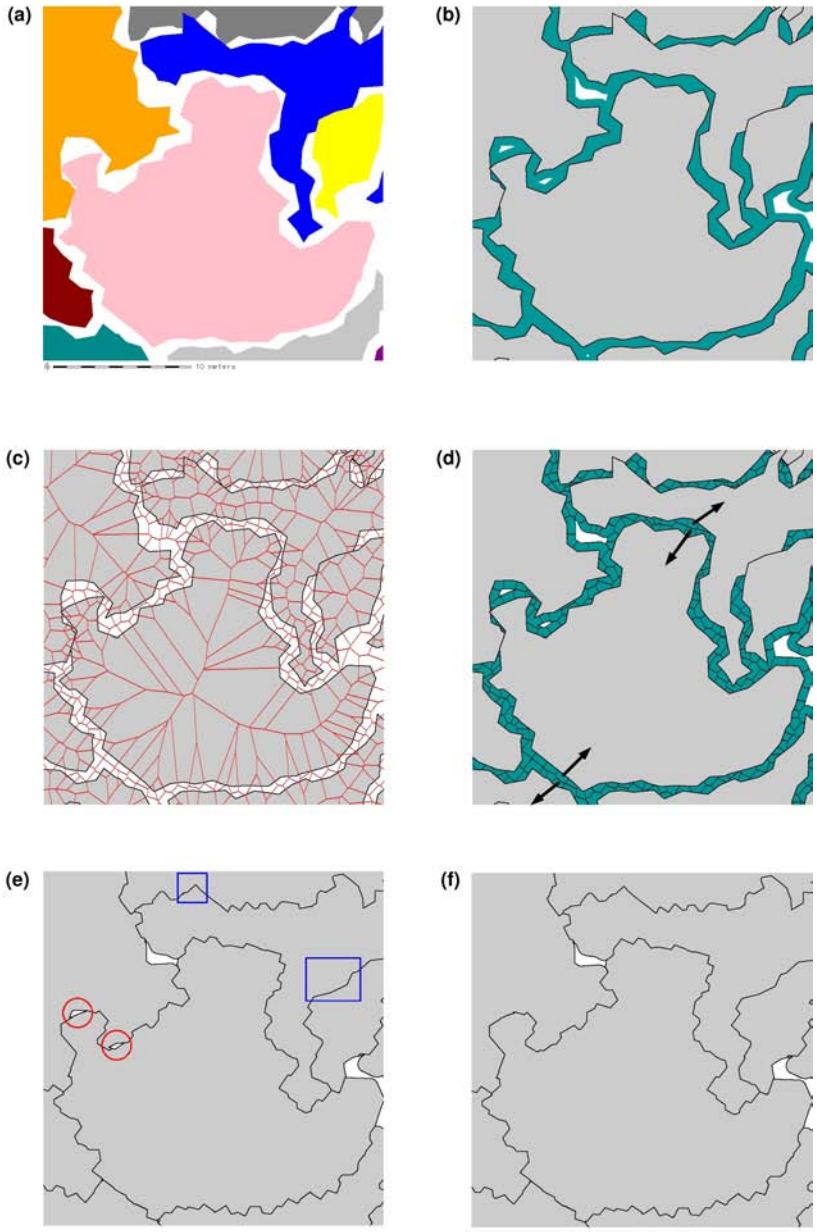

Figure 4.6: *a) Segment polygons derived from alpha shapes, b) 1.0 m buffer (green) c) Voronoi diagrams (red lines) of boundary points, d) intersection of Voronoi diagrams with buffer area, e) intersection areas attached to segment polygons; overlaps are already removed (blue squares), small leftover areas to be removed (red circles), f) resulting segment polygons after filling gaps and removing overlaps.*

4.3.5 Calculate segment attributes

The segment attributes are directly derived from the point cloud (Sec. 4.3.2.1) but also from the segment polygon. Most important attributes are number of points, descriptive statistical values (e.g. min, mean, max) for elevation, corrected intensity, roughness (SD of plane fitting), as well as polygon area, point density and compactness (perimeter / (2 * sqrt(PI * area)).

4.3.6 Classification

To show the potential of the proposed segmentation for glacier surface mapping, a simple rule-based classification with manually defined training areas is applied. Training areas are digitized on basis of the orthophoto (Fig. 4.7b). In a first step the range of corrected intensity values for each target class is derived from the segments spatially selected by the training areas. The second classification feature roughness is preliminary grouped into three classes: low$<$0.1 m, medium 0.1-0.25 m, and high$\geq$0.25 m (Kodde et al., 2007). In a second step the segments are labeled according to the classification (e.g. snow with low roughness, ice with medium roughness). Polygons of areas not covered by any segment are derived and labeled as class surface irregularities. Using the compactness of the polygon shape the irregularities could be further divided into "longish" (e.g. if high roughness: crevasses, low roughness: superficial stream) and "compact" (e.g. moulins). Using the segment ID the classification can be assigned to the laser points resulting in a classified point cloud.

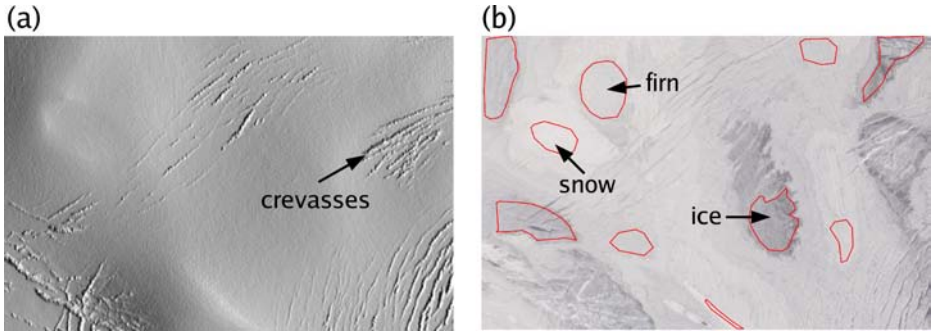

Figure 4.7: *Test site: a) shaded relief b) orthophoto with training areas.*

4.3.7 Merge of segments – dissolving of common boundaries

Due to the cleaning of the vector topology (e.g. close gaps, remove overlaps) neighboring segments falling into the same class can be easily dissolved along shared boundary lines to larger polygons. The IDs of the segments are stored and therefore the connection to the segment attributes is kept.

4.4 Results

A fundamental result of the proposed algorithm is the corrected intensity, which can be used to produce undistorted intensity images (Figs. 4.2 and 4.4b). Intensity offsets between flight strips and topographic effects have been successfully removed. Using the intensity mode of a given neighborhood for segmentation leads to a removal of outliers and small surface structures (e.g. debris), but also results in a certain classification of the intensity dependent on the chosen bin size of the histogram. A bin size of 5% of the total value range (max. 20 classes) for 50 *k*NN delivers appropriate values. If the bin size is too small, the mode is not representative anymore. If it is chosen too large, spectral classes are lost. To guarantee defined intensity homogeneity a maximum deviation of $\pm$5% to the intensity of the segment starting seed point is set for growing. To allow smooth terrain transitions but stop growing at step edges, a maximum angle of 20° between the surface normals of current seed and candidate point is specified. The angle criterion is set low enough to get segment boundaries fitting well to the edges of crevasses (Figs. 4.7 and 4.8). The alpha shape value for segment delineation should be larger than the double average point spacing else too many islands are produced. An alpha value of 1.5 m was set due to the 0.7 m avg. point spacing of the test site. A larger alpha value would lead to more overlapping segments. Closing gaps between adjacent segment polygons is necessary because the boundaries are individually derived. The double of the buffer around the polygons determines the maximum gap size that is closed. A buffer size of 1.0 m was chosen, and hence gaps of max. 2.0 m are closed but also non-covered areas are shrinked or even fully closed, such as narrow crevasses. Filling gaps and cleaning of polygons is computationally very expensive (a lot of intersection with many polygons). If contextual information is not needed for classification, one could first classify the point cloud, merge the points of adjacent segments of the same class and then derive the boundaries and close gaps. But in comparison to our approach, the question of how to define a clear adjacency of point cloud segments can be more ambiguous.

The classification rules are determined using the manually delineated training areas. The distributions of the three classes partly overlap. The following corrected intensity values (in percentage of maximum observed value in test site) were extracted: ice 38% (11.3% SD), firn 64% (6.7% SD) and snow 85% (6.2% SD). In the ice areas of our test site also small snow and firn spots can be found, which results in a high SD for ice areas. The upper ice class limit is set to class mean+1 SD, whereas for firn and snow a class limit of mean$\pm$1.5 SD is used. Hence, the classification rules are: ice$<$49%, firn 49-74% and snow$\geq$74%. The roughness feature is not used to identify the surface classes but to independently subdivide the objects into the roughness classes low, medium and high (Sec. 4.3.6). The areas remaining uncovered even after filling gaps emerge from areas with no

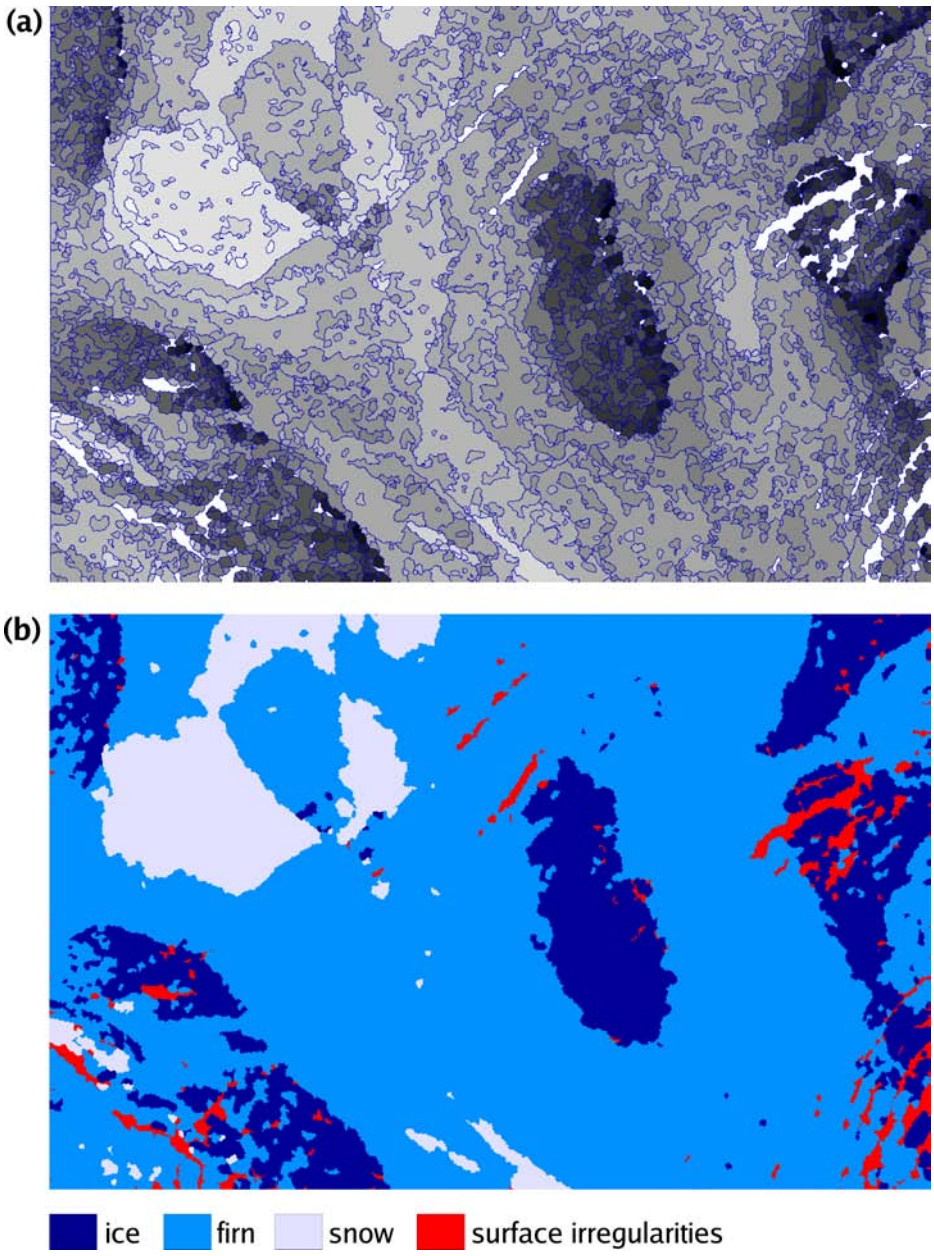

Figure 4.8: *a) Segments colored by mean corrected intensity (black: low intensity, light gray: high intensity, white: unsegmented), b) glacier surface classification.*

laser points or areas with a high variability in intensity or elevation. These areas are summarized as "surface irregularities". Once the segments are classified, the building of larger units by merging neighboring segments is straightforward.

Error assessment was performed using a point wise comparison method. For that purpose the classified point cloud was additionally labeled according to the reference map. The overall classification accuracy turned out to be 90.92%, whereas the spatial accuracy of the object boundaries strongly depends on point density and distribution. The given average

point spacing of 0.7 m and closing of gaps <2.0 m fully agree with the state-of-the-art requirements for operational tasks in glacier monitoring, which state a min. horizontal accuracy of ±2 m, in most cases even lower, to be sufficient (Jackson et al., 2001). Ice areas were found to have a good separability but there is a weak transition between firn and snow (Fig. 4.8), which can be explained by the advanced age of the snow (in August).

4.5 Conclusions

The paper has presented a new workflow for glacier segmentation and classification using spatial and intensity information of the unstructured ALS point cloud. Most ALS sensors already record signal intensity, hence available without additional costs. Homogeneous objects concerning reflectance could be successfully derived. ALS intensity data surpasses the orthophoto in distinguishing between ice and firn (or snow), and in areas with shadows, which are very often in high mountainous areas. The accuracy of the classification is certainly sufficient for glacier inventory mapping but should be assessed for applications in detailed scales, as for example collect GPS data of distinct objects (e.g. ice and snow spots, crevasses). The segmentation, i.e. the zoning of the glacier into areas with homogeneous surface characteristics, highly reduces data with defined loss of information (homogeneity criteria), and already represents a valuable input for energy balance and melt process models. For the conversion of corrected intensity (DN) to reflectance values defined reflectance targets are needed (Ahokas et al., 2006). The surface classification supports glacier monitoring and facilitates the creation of glacier inventories solely using ALS data. The class "surface irregularities" is important for multitemporal analyses, such as feature tracking of objects for flow velocity estimation or glacier dynamics monitoring (e.g. closing and opening of crevasses).

Future work will concentrate on

- applying the methodology to larger areas with more surface classes (e.g. debris, water). Additional classification features have to be selected (e.g. use roughness for surface identification).
- utilization of geometrical and contextual relationships provided by the segment vector topology
- object-based error assessment (spatial and qualitative accuracy) of the classification. Ground truth data has to be collected.
- improving the intensity correction by applying individual reflectance functions for the detected surface classes (e.g. anisotropic reflectance for snow)

5 Object detection in airborne laser scanning data – an integrative approach on object-based image and point cloud analysis.

Published as:
Rutzinger, M., Höfle, B., Pfeifer, N. (accepted): Object detection in airborne laser scanning data – an integrative approach on object-based image and point cloud analysis. In: *Blaschke, T., Lang, S., Hay, G. (eds.): Object-Based Image Analysis – Spatial concepts for knowledge-driven remote sensing applications*, Springer.

Abstract

In recent years object-based image analysis of digital elevation models acquired by airborne laser scanning gained in importance. Various applications for land cover classification (e.g. building and tree detection) already show promising results. Additionally to elevation rasters the original airborne laser scanning point cloud contains highly detailed 3D information. This paper introduces an integrative approach combining object-based image analysis and object-based point cloud analysis. This integrative concept is applied to building detection in the raster domain followed by a 3D roof facet delineation and classification in the point cloud. The building detection algorithm consists of a segmentation task, which is based on a fill sinks algorithm applied to the inverted digital surface model, and a rule-based classification task. The 340 buildings of the test site could be derived with 85% user's accuracy and 92% producer's accuracy. For each building object the original laser points are further investigated by a 3D segmentation (region growing) searching for planar roof patches. The finally delineated roof facets and their descriptive attributes (e.g. slope, 3D area) represent a useful input for a multitude of applications, such as positioning of solar-thermal panels and photovoltaics or snow load capacity modeling.

5.1 Introduction

High resolution imaging in satellite and airborne remote sensing led to the development of Object-Based Image Analysis (OBIA), in order to overcome problems of noise and misclassification, which occur in classification results if conventional pixel-based approaches are applied. Concerning Airborne Laser Scanning (ALS) data, OBIA has mainly been restricted to approaches using rasterized ALS data, often in combination with multi-spectral data. First and last echo Digital Surface Models (DSM) and Digital Terrain Models (DTM),

Digital Intensity Models (DIM), as well as their derivatives from ALS, provide important additional information, such as surface geometry, topography and surface reflectance, which open new possibilities in land cover classification (e.g. Brennan and Webster, 2006).

ALS systems in operational use measure x, y, z coordinates and intensity values for several reflections stored as 3D point cloud with intensity attribute. While the platform position is recorded with the Global Positioning System (GPS), deviations in position and angular attitude between linearly connected GPS positions are determined with the records of the Internal Measurement Unit (IMU). The point coordinates on the reflecting surface are measured taking into consideration all flight parameters and the travel time of the laser beam (Wehr and Lohr, 1999).

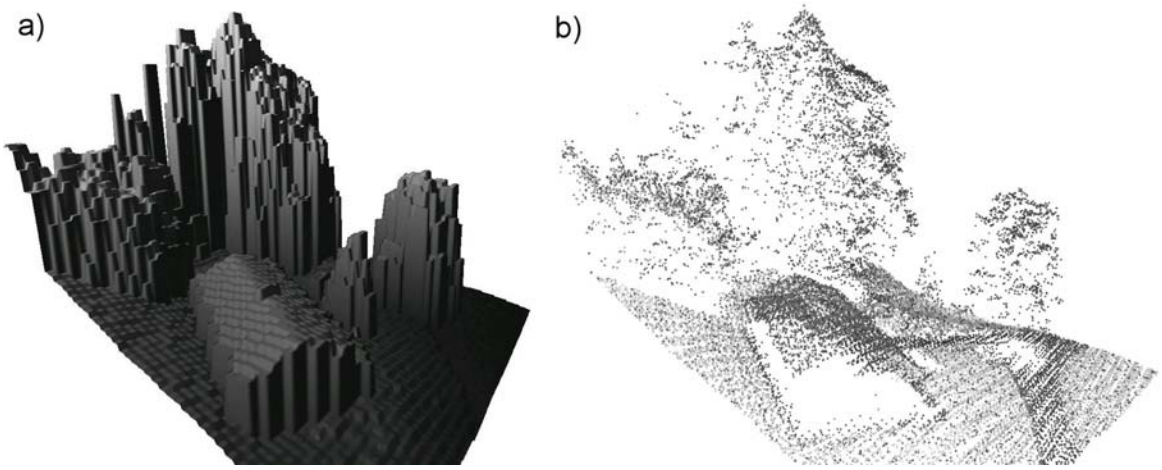

Figure 5.1: *Comparison of level of detail for a) 2.5D DSM (1 m cell size) and b) 3D raw data point cloud (ca. 8 shots/m^2).*

For common applications, the ALS point cloud (raw data) is converted into regular cells so that common image analysis algorithms as well as object-based image analysis workflows can be applied. The rasterization of data can be seen as a first abstraction in the sense of the multi-resolution representation of objects. The degree of abstraction depends on the relation between point density and raster resolution (Fig. 5.1). Additionally, the method of aggregation (e.g. minimum point height) and interpolation applied in the rasterization step are essential for the resulting raster. Furthermore, raster data can model only 2.5D surfaces, but not 3D objects, such as a bridge. The rasterization of the point cloud is an irreversible processing step and is therefore accompanied by a loss of information. The fact that the DSM and the DTM as well as the raw data point cloud are often delivered to the customer, and the fact that there are several efficient algorithms to classify rasterized data, lead to the development of an integrative analysis approach, combining the advantages of OBIA and Object-Based Point Cloud Analysis (OBPA) handling the high level of detail in the ALS

raw data point cloud.

In Sec. 5.2 related work will be presented and Sec. 5.3 explains the methodology for the integrated OBIA-OBPA approach. The concept of the integrated approach of OBIA and OBPA is applied to 3D roof classification (Sec. 5.4), which has several applications. The results can be used to determine potential areas for solar-thermal panels and photovoltaics (Vögtle et al., 2005). The roof type of a building defined by the extracted roof segments can be used for the reconstruction of buildings in 3D city modeling (Brenner, 2005). In natural hazard research the roof type is one input for estimating the snow load capacity of buildings in damage potential calculations. On the one hand, the snow load capacity depends on the building construction, roof area and slope, and on the other hand on the snow pack-properties and meteorological conditions.

5.2 Related work

5.2.1 Object-based image analysis on airborne laser scanning data

Several authors show the advantage of using ALS data in addition to other rasterized remote sensing images in order to classify the data applying an OBIA approach. Most studies from different research areas use the multi-resolution segmentation and fuzzy classification approach, implemented in the commercial software eCognition (Benz et al., 2004).
Asselen and Seijmonsbergen (2006) use this OBIA approach to classify geomorphologic landforms such as alluvial fan, fluvial terrace, talus slope, incised channel, rock cliff and glacial landform. The segmentation is based on a slope map derived from a rasterized DTM. The rule-base is built by statistical values such as mean, standard deviation, minimum and maximum elevation derived from the DTM for geomorphologic units in a training dataset.
Hollaus et al. (2005) combine a normalized Digital Surface Model (nDSM) from ALS with a Normalized Difference Vegetation Index (NDVI) from a high resolution Composite Infrared (CIR) image to define different land cover classes, which are then used to apply hydrological roughness values for hydrological flood modeling.
Maier et al. (2006) classify forest units according to their height by segmenting single tree crowns and forest stands respectively. The inputs are an nDSM and an aspect and slope map derived from a DTM representing the varying forest growth conditions. They derive different landscape metric indices in order to describe forest structure and stability.
Tóvári and Vögtle (2004) present a method to classify buildings and high vegetation. An nDSM calculated from ALS data is segmented. The segmentation starts at a seed point and includes all objects defined by a certain minimum object height threshold. Subsequently for these segments the features first-/last echo difference, area, shape index, height texture, gra-

dients on segment borders and intensity are calculated for each object. Then they compare a fuzzy rule-base, and a maximum likelihood classification.
Further applications of OBIA using ALS data with focus on natural hazard management are described in Rutzinger et al. (2006b).

5.2.2 Segmentation and classification of 3D point clouds

Concepts to segment and classify 3D point clouds collected by either Terrestrial Laser Scanning (TLS) or ALS follow the idea of an object-based analysis workflow. For each field of application only the most recent references are cited.
Tóvári and Pfeifer (2005) present a segmentation-based method to separate high object points from terrain points in order to generate a DTM. The method works partly in 3D (point cloud segmentation) and in 2.5D (ground surface interpolation). The points are first grouped by a region growing segmentation using random seed points. Then a surface is interpolated for all points. The single segments are weighted by the mean least square distance from the interpolated surface. Then a new surface is calculated in several iterations, taking into account that segments with a low weight contribute less to the surface calculation, and are therefore high objects.
Sithole (2005) presents different algorithms to segment and classify ALS data. In the sense of a multi-resolution approach, he distinguishes between micro (local surface roughness) and macro objects (predominant landscape objects) and classifies man-made (buildings, bridges) and natural objects (vegetation and bare Earth).
Filin and Pfeifer (2006) present a segmentation algorithm based on a clustering approach, taking into account features calculated on the basis of an adaptive neighborhood. The neighborhood parameters depend on point density, measurement accuracy, and horizontal and vertical point distribution. The features used are the point coordinates and the surface normal vector in each point, estimated from the neighboring points. The segmentation distinguishes noisy points representing vegetation and plane areas like vertical walls, bare Earth and roof facets.
Vosselman et al. (2005) show the possibilities for 3D mapping using ALS data. The software eCognition is used to segment and classify buildings with a rasterized DSM and nDSM for change detection analysis. The classified buildings are compared to a vector ground-plan in order to detect newly constructed, demolished and unchanged buildings. Furthermore a 3D city model is derived using ground-plan information to select the point cloud and to extract the roof surface type. The final model contains buildings, trees, and streets with the corresponding height from the ALS point cloud.
Reitberger et al. (2006) classify tree species using full-waveform ALS data. Full-waveform systems detect not only the first and last reflection of a laser shot, but record the whole

backscattering cross-section. This gives insight into the inner structure of vegetation, as well as additional information to derive features for the classification of 3D objects. The working steps are the segmentation of individual tree crowns, the derivation of describing features, and the final classification of tree species.
An application of OBPA for glacier surface classification is described by Höfle et al. (2007). After a region growing segmentation in the 3D point cloud based on corrected intensity values the segment outlines are modeled using alpha shapes. The classes snow, firn, ice, and surface irregularities (mainly crevasses) are assigned to the segments using a supervised rule-based classification.

5.3 Methodology

5.3.1 Airborne laser scanning point cloud data management

5.3.1.1 LISA system

ALS delivers a dense 3D point cloud of the scanned surface (typically >1 pt/m^2). For large areas (e.g. country-wide acquisition campaigns) a high amount of single point measurements arises. The LISA (LIdar Surface Analysis) system incorporates the strength of a GIS and the strength of an external data model, developed specifically for ALS data, implemented in an external spatial database (Höfle et al., 2006). Exclusively Open Source components are in use, which is enabled as many sophisticated free available programs with well-defined interfaces and open data formats already exist. LISA integrates management, processing and visualization of large ALS datasets.

5.3.1.2 Point cloud data model

Each area-wide ALS flight campaign typically consists of many single flight strips. Each flight strip holds the corresponding single point measurements, which are described by a timestamp, 3D coordinates (x, y, z) and a measure for the strength of the received signal (signal intensity). The developed data model accounts for this structure of ALS data. Additionally the data model supports unlimited multi echoes (reflections) per laser shot, as well as the storage of the air plane trajectory, which can be linked to each measurement. This allows the reconstruction of the scan geometry, which is, for example, required for the correction of signal intensities (Höfle and Pfeifer, in press).
Data management is designed to provide a fast and simple retrieval of data subsets. For large data volumes, performance is guaranteed by spatial indexing of the single flight strips (i.e. data partitioning by flight strip), as well as the spatial indexing of the laser points belonging to a strip (Bartunov and Sigaev, 2006). Consequently, query performance mainly depends

on the data volume, which is requested/selected, and only to a small portion on the total size of the database.

5.3.1.3 System components and implementation

The LISA framework consists of two main components: i) the geographical information system GRASS (GRASS Development Team, 2007) and ii) the object-relational database management system (DBMS) PostgreSQL (PostgreSQL Global Development Group, 2006) with its spatial add-on PostGIS (Refractions Research Inc., 2006). Workflows, i.e. processing and analysis algorithms, are written in the scripting language Python (Python Software Foundation, 2006), which offers a great variety of scientific libraries (Jones et al., 2001) and database connectors (Cain, 2006). The single programs are provided as GRASS GIS commands. The integration of all commands into GRASS GIS offers i) a good usability, ii) full access to the standard functionality of GRASS and iii) many interfaces, such as GDAL (Warmerdam, 2007), to common spatial data formats. As described above, the laser scanning point cloud is managed using PostGIS, but can be easily accessed from the GRASS GIS client side. The DBMS offers a client-server-architecture; therefore the large datasets are stored only once. The laser scanning data can be either retrieved directly, i.e. as 3D vector points, or indirectly by prior rasterization of the point cloud.

5.3.2 Concept of an integrative approach

The requirement to use the synergy of vector and raster algorithms, as well as the different level of detail in the point cloud and the additional information of the rasterized ALS derivatives, lead to the demand of an object-based analysis approach, which can handle both raster cells and vector points. Due to the complexity (e.g. definition of neighborhood; cf. Filin and Pfeifer, 2005) and computational effort (e.g. neighbor searching, feature derivation) of area wide point cloud analysis, the combination of raster and vector analysis is the method of choice. In the sense of a "classification-based segmentation" the target class is derived in the raster domain, while the OBPA, offering higher resolution, is done only for those selected objects. The workflow presented here consists of a modular architecture for segmentation, feature calculation and error assessment running iteratively until an acceptable classification result is reached.

5.3.2.1 Workflow

The object-based analysis workflow comprises two main traces. The first one is the raster-based object derivation in 2.5D and the second one is the point-based object derivation using the planimetrically defined objects to derive 3D objects in higher detail (Fig. 5.2).

However, both follow the same basic processing chain of segmentation, feature calculation and classification. The specific selection of the parameters and features for the single processing steps is described in Sec. 5.4.2.

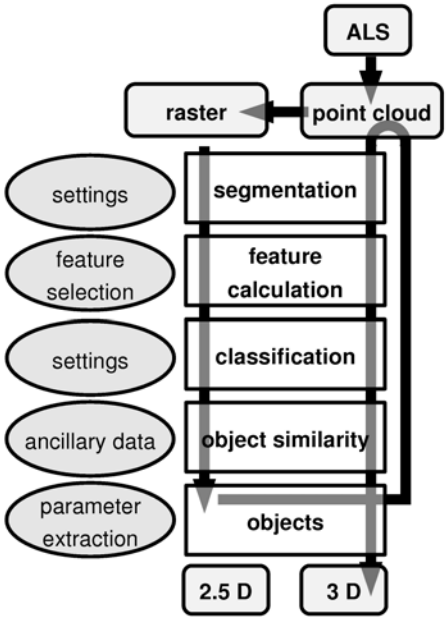

Figure 5.2: *Integrated object-based analysis workflow for raster and point cloud.*

The first derivatives from the point cloud are digital elevation models such as first echo and last echo DSMs. A first/last echo difference model (FLDM), which is an additional input in the raster segmentation, is calculated per laser shot (not per cell) using the possibility to reconstruct the flight geometry in the DBMS. The segmentation returns either polygon or line segments, depending on the segmentation method. For these segments topological, shape, raster or point cloud based features are calculated. The selected features are the input for the object classification. The classification can be done either supervised or unsupervised with the built-in classifiers of GRASS GIS or rule-based. For the latter value ranges are applied to a set of object features to define the target class. All segments within the value ranges are labeled with a weight. In the end the weights for each segment are summed up in order to get a quality measurement specifying the degree of membership of a segment to the target class. Additionally, a tool for object comparison and similarity is used either to compare multi-temporal datasets or to apply error assessment using ancillary data. The comparison of classified objects considers changes in spatial distribution, shape, and topology. Ancillary data or digitized objects in a training area are used to optimize the parameters of the raster-based workflow (Pfeifer et al., 2007a).
The objects derived from the raster models are primary results, which can be used in further applications (e.g. building polygons in urban planning or line objects for semi-automatic

mapping) (Rutzinger et al., 2006b).

In the integrative approach the objects derived in the raster domain are used to individually extract the original laser points for each object (i.e. building) from the spatial database. Then these points are grouped into segments. Each set of points generated in the segmentation is considered as one object primitive. Based on this, 3D point set features like slope, aspect, area, etc. are computed. These features are more accurate than features computed on the basis of rasterized images, because mixed pixels along the boundary deteriorate the results. With typical pixel sizes of 1 m, the number of boundary pixels makes a significant contribution. Another advantage is that the influence of the method of aggregation (i.e. taking the highest, lowest, etc. point per grid cell) does not influence the result. From the segmented points the outline of the 3D polygons is constructed and the final objects are classified by their 3D features.

5.3.2.2 Segmentation and classification in the raster domain

The raster-based segmentation is carried out independently for every target class and thus differs for specific applications. Due to the different object properties, individual segmentation approaches are used for the object of interest.

In the case of building classification, the best segmentation and classification settings are estimated for a representative training area with reference data. The parameters are estimated in a brute-force manner within user-defined intervals. Then these estimated parameters are used to segment and classify the whole data set. It is crucial that the reference data set is complete and equivalent to the object representation in the ALS data set. In case of buildings it is advisable to use manual digitized areas rather than polygons of a Digital Cadastral Map (DCM) as training data because of the fact that buildings derived from ALS contain roof overhangs, which are not present in a DCM (cf. Pfeifer et al., 2007a). In an ideal case digitized training areas and an independent reference data set with the same object representation are used for parameter estimation and error assessment respectively. The segmentation method used for building detection is based on a hydrological approach implemented in GRASS GIS (Arge et al., 2003; Rutzinger et al., 2006a). In a first step high vegetation is masked out using the information on first/last echo difference. Then a fill sink algorithm is applied to the inverted DSM in order to segment the remaining high objects. The final segment outline is defined by a height threshold (segHeight), which suppresses low non-building objects. Furthermore the segment shape is adapted by morphological opening (segOpening, radius of the structure element) and finally very small segments considered as noise are erased by a minimum area criterion (segArea).

The user selected features (standard deviation of height, shape index, area, mean first/last echo difference, etc.) are first derived for the training data set to estimate the classification rules. Then the rules are adjusted automatically in order to keep errors between training and classified polygons as small as possible. A quality map is generated from the applied weights to each feature layer. Only those objects reaching a particular, defined quality criterion are used for the final, crisp classification. The other areas could be used in a second classification with adjusted settings in the next iteration. Finally, the classified objects are used to select the corresponding points in the spatial database.

5.3.2.3 Object generation in 3D

Point cloud segmentation

Segmentation is a process to aggregate information originating in digital image processing. Here, it is applied to point sets, which require that concepts applicable to images are transferred to point clouds (Haralick and Shapiro, 1992).

The purpose of segmentation is to split a set of spatially distributed measurement icons (originally pixels) into disjoint sets. The union of the generated sets is the original. Grouping of the original measurements is done on the basis of a homogeneity criterion (e.g. gray value for pixels, or belonging to the same plane for points, etc.) requiring that such a set is spatially connected. Additionally, there is a constraint that joining two neighboring sets will violate the homogeneity criterion. This requires that neighborhood is defined, which is trivial for images using the 4- or 8-neighborhood. For point clouds it can be the set of fixed distance neighbors or the k nearest neighbors. A detailed discussion on neighborhoods in point clouds of airborne laser scanning can be found in Filin and Pfeifer (2005). The definition above normally requires the additional definition of a rejection set, i.e., a set of points, which do not belong to any other segment. Of course, the points in that set are spatially not connected.

The segmentation method applied is based on region growing and uses the neighborhood definition of k nearest neighbors for each point. We chose the latter because it adapts to variations in point density and for reasons of computational efficiency. These neighbors are used in the first preprocessing step to estimate the normal vector for each point. This is done by least squares fitting of a plane (regression) to each point and its neighbors, which can be interpreted as estimating the tangent plane of that surface point. This plane's normal is the normal vector to each point. Therefore the inputs to the region growing are the points and their normal vectors.

The region growing randomly picks a seed point and then examines the k nearest neighboring points, termed the candidate points. Random seed point selection is justified because

it can be assumed that all points belong to the same target class due to the pre-processing and selection of the OBIA approach (Sec. 5.2.2). Furthermore the parameters are updated during region growing (see below). A number of criteria are checked. During region growing an adjusting plane is also estimated for the points of a segment. This is basically the same estimation process as before. However, now each point that is accepted as belonging to the segment is used to renew the estimated normal vector. Plane estimation can only be initiated after a segment has grown to at least three points, so first the plane is instantiated by the seed point and its normal vector. If a candidate point is accepted as belonging to the segment, its k nearest neighbors become new candidate points.

Candidate points will be connected to the segment if they fulfill three criteria:

- similarity of normal vectors (a)
- distance of candidate point to the adjusting plane (r)
- distance between current point and candidate point (d)

The first criterion (similarity of the normal vectors) determines that the angle difference between the segment normal and the point normal should be under a predefined threshold (e.g. 10°). The second criterion, the distance of the candidate point to the segment plane, must also fall below a threshold (e.g. 15 cm). Finally, each point and the candidate points must not be further apart than a defined distance, measured in 3D. Growing continues until no further points, which fulfill the criteria, can be found.
This means that segments will constitute planar patches. They are spatially connected (distance d), and points on rounded edges are excluded because of the normal vector similarity requirement. This process is governed by four parameters: k, a, r, and d. The density and noise of the data can be considered by setting the number of neighbors and the maximum distance for accepting points. Points in the vegetation, on cars, traffic signs, overhead cables, chimneys, etc. typically form one point segments and are put in the rejection set. Of course, this is also a question of point density, and the above holds for point sets with approximately one point per square meter.

Triangulation

The corresponding points of each segment are triangulated separately in iterations over all segments. A triangulation of a point set results in a convex hull and therefore information about the segment shape is lost. A shape adjustment is applied to every segment by removing the longest edges of the triangulated segment. As shown in Fig. 5.3a, the minimum length of the triangle edge to be removed must be larger than the average point distance. If it is smaller, holes within the segment appear. If the chosen value for the minimum length

is too high, the segment area is overestimated and the shape at concave outline sections is not well defined. After the shape adjustment, the remaining triangles are merged to the final segment (Fig. 5.3b). The triangulation is done only in 2D, but the vertices of the final segment outline are 3D points.

The features for the classification are calculated on the basis of the 3D point cloud used in the triangulation. These are the average point distance to the estimated plane, slope and aspect, and area in 3D (projected on the segment plane) and 2D respectively.

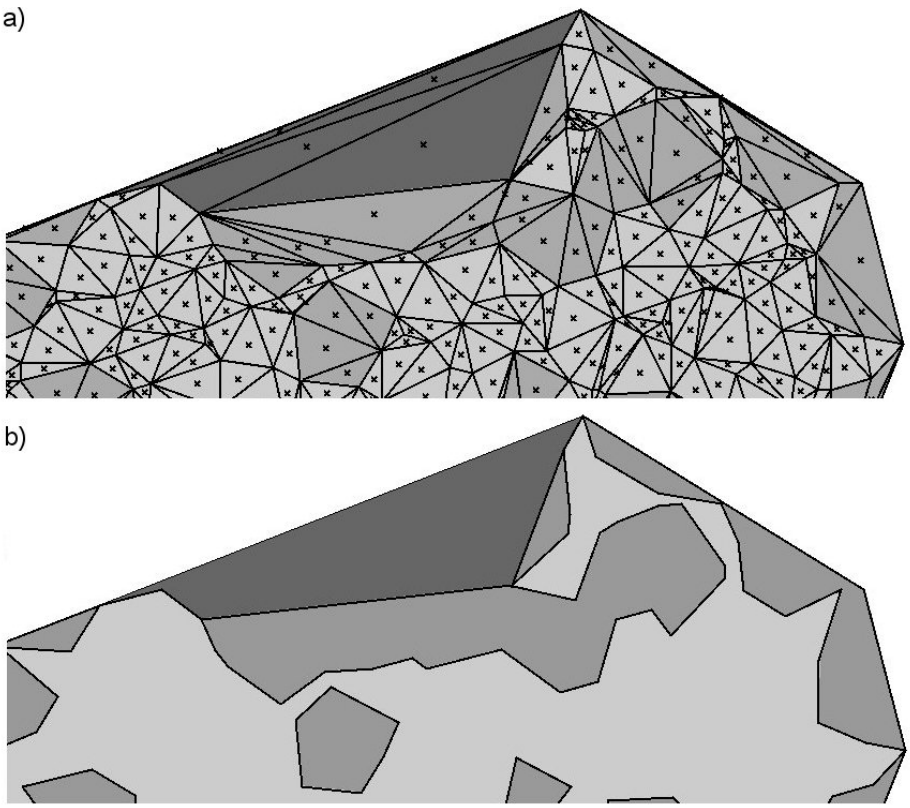

Figure 5.3: *a) Object outline determined by the minimum triangle edge length (dark gray – convex hull, medium gray – 5 m, light gray – 1 m), b) final segments from merged triangles.*

5.4 Application: Classification of roof facets

5.4.1 Test site

The tested data is a subset of the ALS acquisition campaign of the city of Innsbruck (Tyrol/Austria), which was carried out with an ALTM 3100 Optech scanner in 2005. An area of 269.6 km^2 is covered by 110 flight strips with an average point density of 4 shots/m^2. From the raw data point cloud, which is stored in the LISA system, a last echo DSM and a FLDM, both in 1 m resolution, are used as input elevation models in further processing.

5.4.2 Parameter settings

The parameters for the detection of building footprints (Sec. 5.3.2.2) are estimated for a test area where a DCM is available (segHeight=0.5 m, segArea=50 m^2, segOpening=2). For these building footprints, the last echoes are selected from the spatial database in order to segment the point cloud by region growing. The chosen parameters for the roof segmentation (k=70, a= 20°, r=2 m, d=7 m) are explained in Sec. 5.3.2.3. Additionally, the features slope, aspect, noise, 3D and 2D area are calculated for every point segment. The optimal shape representation of the roof facets is produced with a minimum triangle edge length of 5 m. Finally, the roof facets are classified by their slope into five classes (from 0 to 40° in 10° steps and one class for more than 40°).

5.4.3 Results

Figs. 5.4 and 5.5 show the results of the integrative approach for two selected samples. Fig. 5.4c shows that the shape adjustment also works for extreme concave objects such as the X-shaped building on the lower left site. The comparison of the DCM (Fig. 5.4a) and the detected building outlines (Fig. 5.4b) show that it is possible to use the OBIA approach on ALS data for map updating. The W-shaped building on the upper left could be detected, even though it was not included in the DCM. The different object representation of buildings in the DCM and in ALS data becomes apparent at the left roof edge of the largest building. The single 3D roof facets from the OBPA on the basis of the OBIA are seen in Figs. 5.4c and 5.4d.

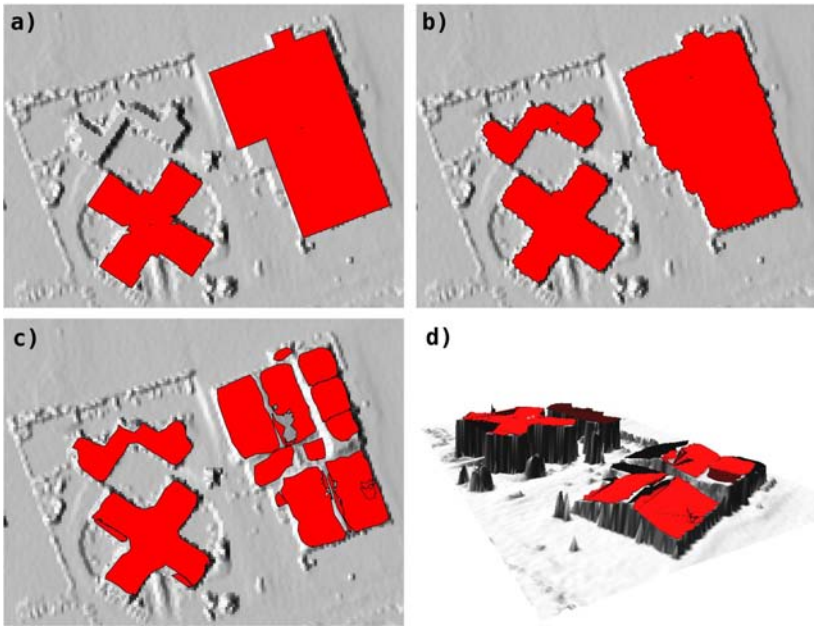

Figure 5.4: *a) DCM, b) buildings from OBIA, c) roof facets from OBPA, d) 3D view of roof facets.*

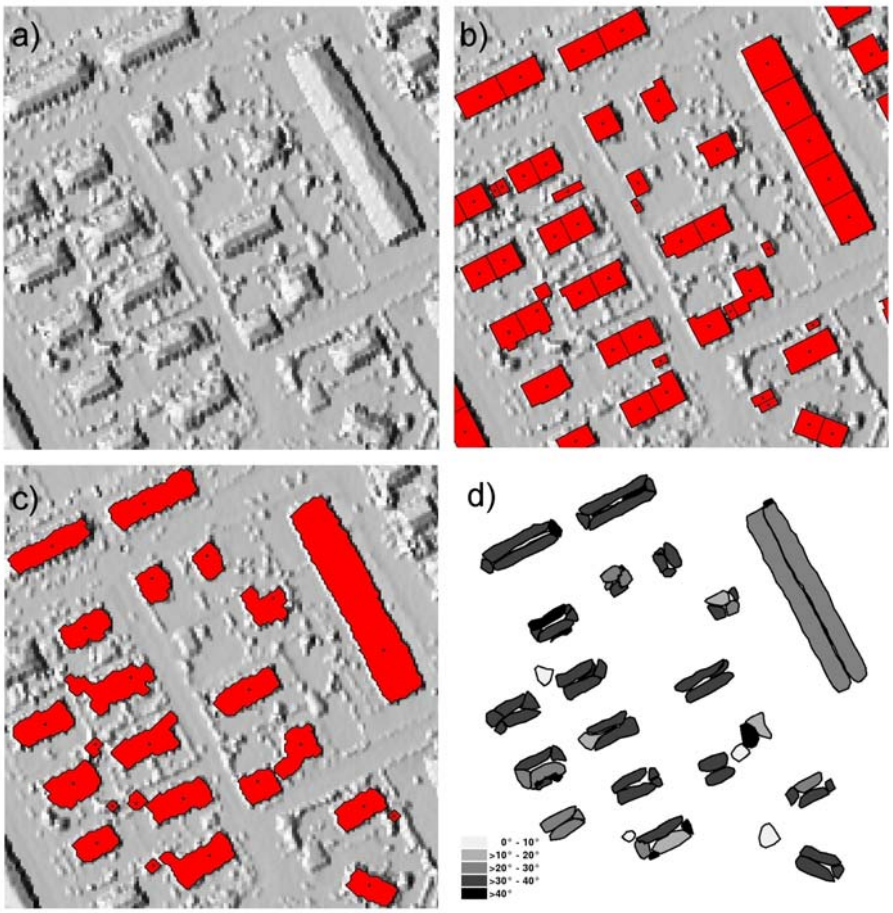

Figure 5.5: *a) Last echo DSM, b) DCM, c) buildings from OBIA, d) roof facets from OBPA classified by slope.*

For a test site containing 340 buildings located in the city of Innsbruck (Sec. 5.4.1) error assessment was calculated. A subsample is shown in Fig. 5.5. Comparing the total building areas between reference data (DCM) and buildings derived by the OBIA approach (Sec. 5.3.2.2) a user's accuracy of 84.89% and a producer's accuracy of 91.87% could be reached. These error values still suffer from uncertainties caused by the different object representation in ALS data and DCM (e.g. roof overhangs or missing reference buildings). The 3D roof facets and the derived slope classes look very promising but could not be evaluated because of lacking reference data.

5.5 Conclusion

This paper demonstrates the demand to extend the OBIA approach to 3D data sources like ALS data. The OBIA approach must not be limited to "image" analysis, but must also handle irregular distributed point clouds (OBPA). The combination of image analysis tools and GIS lead to new innovative solutions in handling high resolution data, and in classifying and determining objects in 3D. This enables the use of highly accurate products in several applications. The point cloud segmentation by region growing is already showing convincing results, although its application and settings are still subject to further research. The core function of the integrative approach is the iterative access to the original point cloud, making this approach a flexible solution. Vosselman et al. (2005) state "the future's information society will require up-to-date object-oriented three-dimensional geo-information". ALS, as well as TLS, with different data structures, demands a development in the concept of OBIA in order to provide methods for irregular distributed point data handling and 3D object classification.
New sensors in the field of laser scanning, such as full-waveform analysis, require new innovative concepts where integrative approaches can contribute to design efficient strategies for full- and semi-automatic object analysis.

6 Results and discussion

This chapter aims to give more insight into the results of the single aspects of this cumulative thesis as well as to expose new considerations in a critical review. The single topics discussed here represent the state-of-the-art in their respective domain.

6.1 LISA information system

The first paper (Chapter 2) introduced a new strategy for managing very large ALS point cloud datasets within a GIS environment solely using Open Source components. In the very last years the necessity of handling ALS datasets and having access from standard GIS software was also discovered by commercial GIS software companies as new implementations show, such as Geomatica LidarEngine by PCI Geomatics (2007) and LIDAR Analyst for ESRI ArcGIS by Visual Learning Systems (2007). A detailed list of commercial/non-commercial ALS software can be found in the Appendix (Geist and Höfle, 2007). In comparison to other software the LISA system utilizes an open spatial database management system instead of creating an own proprietary internal data structure, such as the new *terrain data type* of ESRI ArcGIS. This leads to a great variety of possibilites for linking the LISA database to external software applications (e.g. all GIS software supporting to read and access OGR vector formats). The well-defined and standardized Structured Query Language (SQL) serves as *lingua franca* between database and connected applications.

6.1.1 Spatial database management

This section (Sec. 6.1.1) intends to give detailed insight into the latest developments concerning LISA's data management. As a rapid development takes place, major improvements originating from the findings of Chapter 2 are pointed out (e.g. implementation of multi-point geometries and table partitioning, as well as increased performance of importing and selecting data).

The aim of LISA's spatial database management is not to create a new spatial data type but to optimize existing functionality (spatial data types and indices of PostgreSQL/PostGIS) for the purpose of managing ALS point measurements. As mentioned before, the used DBMS offers well-defined interfaces for data access and exchange. Within this thesis GRASS GIS was chosen as GIS backend because new modules can be implemented very easily.

6.1.1.1 Data model

The developed data model, i.e. table structures and relationships, is the core for successful data management. Therefore, it is important to consider the process of ALS data acquisition as well as the typical structure of ALS raw data delivered to end-users. The simplified data model introduced in Chapter 2 accomplishes these requirements. Storing huge amounts of laser points is always a trade-off between performance, functionality and data volume. It was chosen to have a data model as flexible and extensible as possible while accepting small losses in performance. Functionality, i.e. what analyses are supported, mainly depends on what data is provided in or along with the point cloud. For example, the timestamp of each laser shot is needed to interpolate the current scanner position. But if no flight trajectory is delivered, it is maybe not necessary to store time for each shot. For most multi-temporal analyses time attached to each strip is sufficient. Performance has to be seen relative because it mainly depends on what kind of queries (e.g. 2D/3D spatial, temporal, attribute search) are made. Anyway, intelligent indexing of table columns is essential when working with large databases. Indices drastically increase query performance but also increase data volume. As the horizontal extent (x, y) of common ALS data campaigns exceeds the vertical extent (z) many times, two-dimensional spatial indexing is the first choice. This means that only x- and y-coordinate are present in the spatial index but limiting the result by z-coordinate still remains possible, i.e. query by defining a 2D object (e.g. polygon) with a minimum and maximum z-coordinate (resulting in a right prism).

6.1.1.2 Spatial indexing and multi-point geometries

In PostGIS a R-Tree index implemented on top of a Generalized Search Tree (GiST) is utilized for geometry columns. This spatial index only stores the 2D Minimum Bounding Box (MBB) of each spatial object, regardless of which dimensionality the objects are. Spatial index queries are based on 2D bounding boxes followed by a distance query if necessary. This clearly shows the limits of directly working with the spatial index put on the laser points. It is designed to allow for the selection of laser point subsets defined by any attribute search criterion but only spatially defined by a 2D geometry object. This restricts spatial queries to polygon queries followed by a distance query (e.g. distance to a point, line or polygon). Nearest neighbor and fixed distance queries therefore are not very well supported but still possible. Therefore, a common procedure applied in the LISA system is to extract laser points lying within the area of interest (e.g. polygon selection) and afterwards building a temporary spatial index (e.g. ANN-tree (Arya et al., 1998), KD-tree or 3D R-tree (cf. Zhu et al., 2007)), which is better suited for point cloud segmentation and 3D modeling.
PostGIS's spatial index is applied on geometry columns that can contain points, lines, polygons and multi-geometries. In our case only points (single echoes) and multi-points (mul-

tiple echoes) are indexed. Each table entry leads to exactly one appearance in the spatial index. This behavior can be used to reduce index elements by grouping adjacent points into a single geometry object (multi-point object). Multi-point objects are built by grouping all echoes of one laser shot, hence referenced only once in the index, which decreases the number of index leaf tuples and as a consequence reduces the total size of the index.

But good query performance can only be guaranteed if the MBB of the echoes belonging to one shot is not too large. With a scan angle of 20° and an object height of 20 m a maximum horizontal displacement between first and last reflection would theoretically be around 7 m. The average horizontal displacement for first and last reflections in our datasets turned out to range from 1.7 m to 2.9 m, whereas the percentage of multi-echo shots to single echo shots ranged from 7% to 17%, which strongly depends on the predominant land cover, i.e. the more trees the more multiple echo shots and therefore larger MBBs slowing down query performance. If the number of multi-echo shots does not exceed the number of single echo shots, indexing of multi-point objects is favored over spatially indexing each echo in one and the same index. In any case multi-point indexing requires much less disk space. An individual index on each echo, i.e. one index on first echoes and one on last echoes, would be fastest but would also require much more disk space and more complex spatial queries (one query on each index/echo followed by union of the subresults).

Another trade-off between performance and disk usage is how PostGIS stores bounding box coordinates. Actually it is a trade-off between accuracy and disk usage because the in the spatial index the MBB coordinates are stored as 4 byte float (in comparison to the 8 byte double coordinates used for the geometry object). The type truncation (from 8 to 4 byte) leads to an overestimation of the MBBs, which guarantees that no objects are missed but also results in more overlapping of the MBBs in the respective index levels slowing down spatial queries. Fig. 6.1a shows what happens if UTM coordinates without False Easting and Northing (e.g. 32673471.2027 E, 5241018.7467 N) are indexed. In this case the MBB for a point using 4 byte floats is minimum 2 x 0.5 m large, and even larger for multi-points. Therefore, overlapping of MBBs is more the rule than the exception causing many index tuples be accessed by a spatial query. Introducing a reduction of digits (e.g. False Easting, Northing) can easily avoid this problem without losing accuracy (Fig. 6.1b).

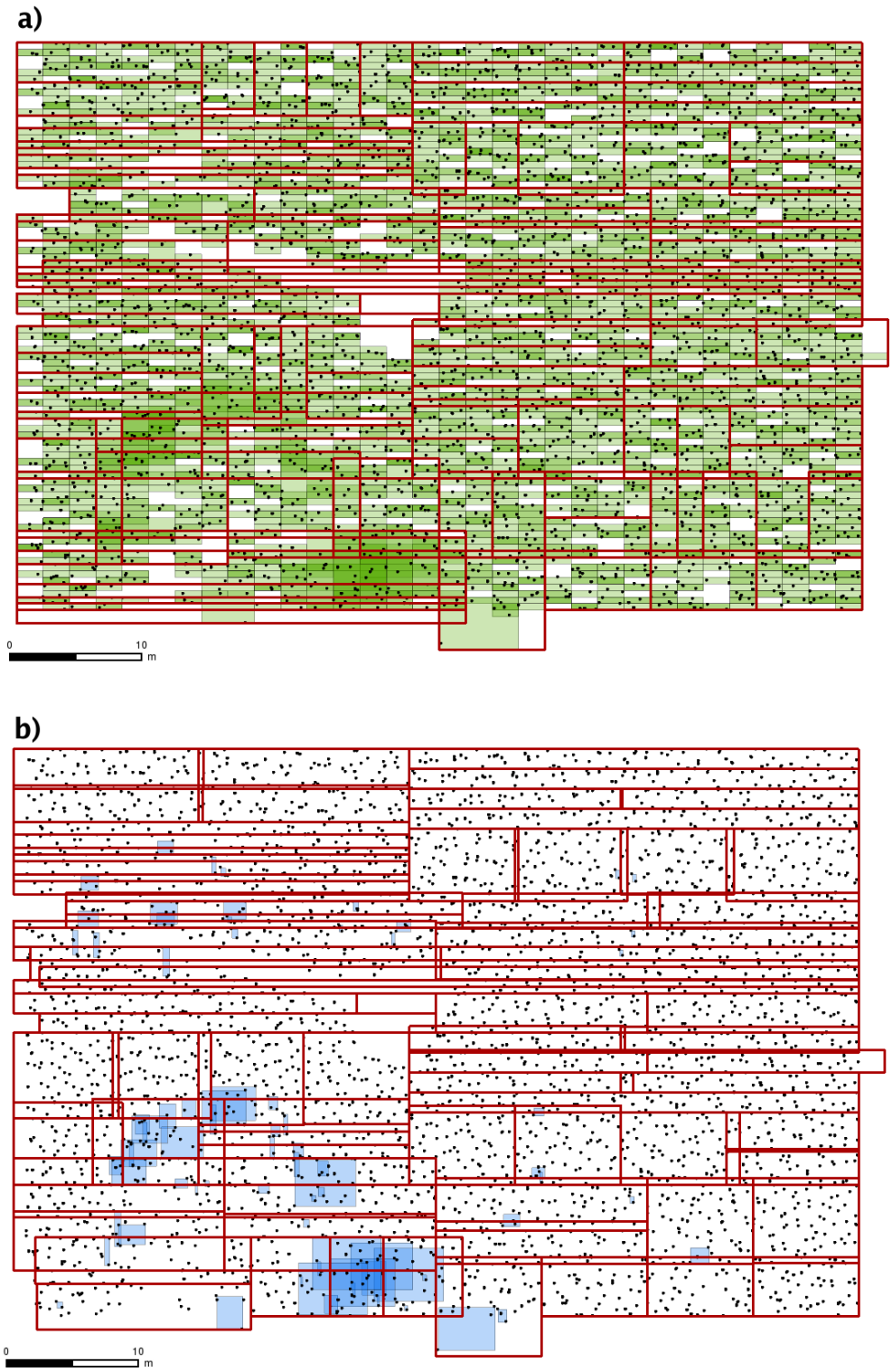

Figure 6.1: *Visualization of GiST index levels (cf. Höfle, 2006). The red rectangles are the highest (first) and the green and blue boxes, respectively, the lowest (second) index level. a) Effect of overlapping MBBs due to 4 byte type truncation of long double coordinates (the darker the colors, the more overlap). b) Reducing number of coordinate digits avoids overestimation of MBBs. Just a few multi-point MBBs overlap and are large enough to be seen. The area covered by MBBs is drastically reduced.*

Multi-point geometry objects do not have a limit on the number of points stored in one object. Despite all performance issues of indexing on multi-points (i.e. echoes belonging to one shot), the fact that the data model is easily extensible underlines the applicability for data acquired by state-of-the-art airborne laser scanners, such as full-waveform recording systems. Spatial indexing of hundreds of intermediate echoes, spatially located in a small horizontal extent, is therefore avoided without losing performance and full access on all measurements is assured. Furthermore, the connection between laser shot information (e.g. time, scanner position) and echo is never lost, which is a major advantage over spatial index strategies implemented in existing software, which work solely on x, y and z.

6.1.1.3 Data partitioning

As emphasized before, spatial indexing is crucial when working with large amounts of laser points. In established database design all spatial objects are stored in one table column and hence one spatial index is applied. But a large number of elements (e.g. if all laser points are stored in one column) results in many index tree levels (index depth), which have to be accessed when querying the geometry. Further, dynamic insertion of new elements slows down with increasing number of index tuples because index balancing and reorganization take longer. The fact that ALS data already underlies an inherent hierarchical structure (flight–strip–shot–echo) can be used for improving database design particularly for storing country-wide ALS data. It is definitely not optimal to store country-wide ALS laser points in one GiST index. Therefore, a hierarchical data partitioning was chosen, which allows for query performance almost independent of the number of laser points accumulated in one database. Data partitioning can be seen as an extension to the GiST index because it introduces another spatial hierarchy on top of the regular index.

In LISA ALS data is partitioned by flight strips, which means that every strip has its own table and indices. This drastically reduces the depth and total size of the spatial index applied to a single flight strip. The highest spatial hierarchy consists of the oriented minimum bounding boxes (oMBB) of the flight strips. An oMBB is the minimum, rectangular but possibly tilted bounding box of all laser echoes of one flight strip (Fig. 6.2). The orientation of the oMBB is derived by calculating the principal components of x and y (eigenvectors of the covariance matrix). The oMBB also overestimates the actual coverage of a flight strip but still covers much less area than the MBB, most evidently for flight paths not going N-S or W-E.

The major advantage of introducing oMBBs on top of the GiST is that a precise preselection, i.e. spatial check with oMBB polygon, of strips affected by a spatial query can be

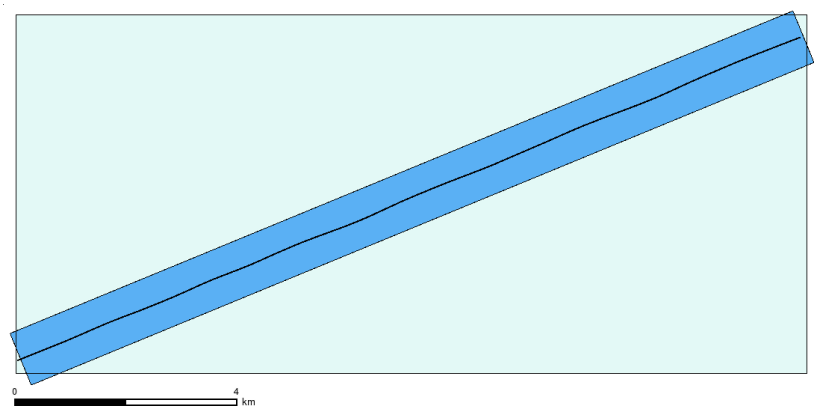

Figure 6.2: *Example of a MBB (green) versus oriented MBB (blue) of a flight strip. Flight path is drawn as black line.*

made. After that only few parts of the whole ALS database have to be accessed in their respective spatial indices (i.e. GiSTs of affected strips). Finally, the results of all subqueries just have to be put together. One may state that many flight strips slow down this preselection but an ordinary GiST index on the oMBBs guarantees good performance even with thousands of strips. Hence, query performance mainly depends on the number of selected laser points and not on the total size of the database. These logical units, i.e. partitioning by strips, offer even more possibilities for intelligent and fast queries on large ALS databases. Additionally to the spatial extent all other information, such as number of points, start time, end time, flying altitude etc., can be used to preselect certain strips. Especially for multi-temporal analyses where the spatial query may deliver many overlapping strips, a constraint on time can be included in the preselection ignoring strips of non-relevant epochs. The here presented data partitioning method reduces data volume (e.g. reduction of index sizes and no need for saving the strip ID for each shot) and increases performance due to the spatial and temporal preselection as well as the smaller index sizes. Many ALS datasets do not have information about flight strips but are organized in tiles (e.g. 5 x 5 km). Without changing the data model such datasets also benefit from data partitioning. Instead of the oMBBs the tile polygons are used for preselection.

6.1.1.4 Performance issues

Performance tests have been carried out to prove the enhancement of data partitioning versus the traditional approach of using one table with one spatial index for all laser points. A test environment was established using a desktop computer with AMD Athlon 2.0 GHz CPU, 3 GB RAM and PostgreSQL 8.2.3. To get representative results, a test dataset with 100 million laser points consisting of two different flight epochs was chosen.

Performing a polygon selection returning 8 million points and affecting 8 of 30 strips shows a query performance improvement by

- 3 times if using data partitioning and even
- 5 times if using an additional time constraint on one epoch.

During import of ALS point cloud data into the LISA system the oMBBs are automatically derived for each strip and multi-point geometries are built for each laser shot. Altogether, the import of 10 million echoes from LAS format with deriving all necessary information (oMBBs), spatial index building and set up of relationships between strip and flight as well as between echo and shot takes approximately 9 minutes (2 min 48 s for import and 6 min 3 s for building of single GiST indices).

6.1.2 Special feature

The developed data management system offers not only a fast and easy-to-access storage of large ALS point clouds but also allows for extracting useful information provided by the sophisticated data model. An example will show the added value of storing the full information coming along with the point measurements, such as timestamps and plane positions. Generally, timestamps for each shot and plane positions are available because they are needed for post-processing after ALS data acquisition but most often not delivered to end-users (maybe because not requested). In LISA both laser points with and without timestamp can be management but if time is present for each shot, additional functionality can be applied.

6.1.2.1 Missing points

Missing points, also known as laser return losses or drop-outs, occur when no backscattered signal of a laser shot has been recorded. Many reasons for the appearance of a missing point exist, such as strong absorption in the atmosphere and at the target (low reflectance), specular reflection (e.g. smooth surface) not directed towards the scanner, large distance between scanner and target (range) and a lot of small reflecting areas causing too weak echoes to be detected (e.g. vegetation). If most of the reasons are not present, i.e. atmospheric attenuation, angle of incidence and range are kept small, missing points are a feature describing surface characteristics. The modeling of missing points is only possible if timestamps are available and the pulse repetition frequency (PRF) is known.

The identification of missing points is based on the following steps:

1. sort laser shots ascending by time and strip ID
2. sequential scan over all laser shots
    - calculate time differences between temporal neighboring shots
    - divide by PRF and get number of missing points
    - linearly interpolate location of missing points using recorded last pulse before and after data gap
    - if time gap is larger than PRF but different strip IDs are found, no missing points are modeled

Due to the change of scan direction at strip edges, small time gaps always appear (when using Optech's ALTM series). An additional check on current scan direction that recognizes when the direction is changed, avoids systematic missing points modeling at strip edges. A problem can occur if a large area of missing points is located at the strip edge because linear interpolation does not deliver reliable results if the two interpolation points have different scan directions. Hence, these areas are not mapped by the proposed procedure. Missing points can easily be selected and exported, respectively, using the LISA system, just the same as the "existing points".

Primarily water bodies (ponds, lakes, rivers) with clear water and smooth surface cause missing points. Water is a strong absorber (in NIR) but also a good specular reflector (with higher incidence angles). But also ice surfaces have low reflectance in the laser wavelength (1064 nm with Optech's ALTM). This can be used to identify glacier ice areas and water bodies by calculating a value called *missing point density* (portion of missing points to existing points in certain neighborhood). Fig. 6.3 shows an example of missing points modeling at Hintereisferner, a glacier in the Ötztal valley, Tyrol. The glacier terminus is clearly highlighted by the high density of missing points occurring within the ice area. Furthermore, the large glacial stream flowing north-east and some small trenches with surficial runoff can be seen.

Another example demonstrating the information provided by missing point modeling can be found in Fig. 6.4. The river Inn is visually clearly defined by a high number of missing points, except the parts where the flight trajectories cross the river (low incidence angles). But also roof facets and cars with specular reflecting materials and vegetation are marked by missing points. The large swimming lake (Baggersee) and the small round basins of the

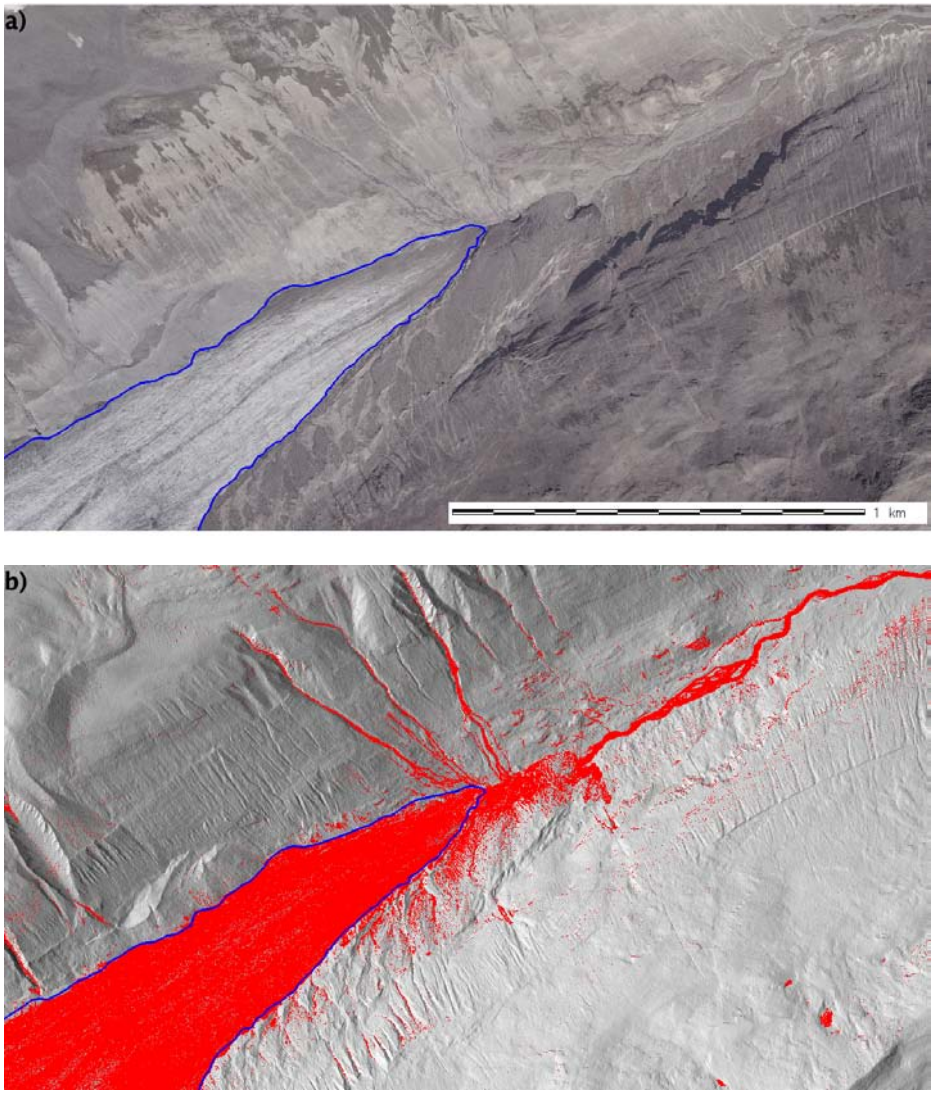

Figure 6.3: *Result of missing points modeling at Hintereisferner: a) orthophoto overlaid with manual glacier delineation (blue) and b) shaded relief map overlaid with missing points (red) and manual glacier delineation (blue).*

waste water plant are also highlighted by a large amount of missing points.

Missing points – made "alive" by LISA – establish a great potential for surface classification, especially in areas where a low measurement density complicates traditional point cloud segmentation methods, such as region growing, because only existing points are (can be) classified. The information provided by missing points, despite the problems mentioned before, should not be ignored and should be taken into consideration when working on water body and glacier surface delineation.

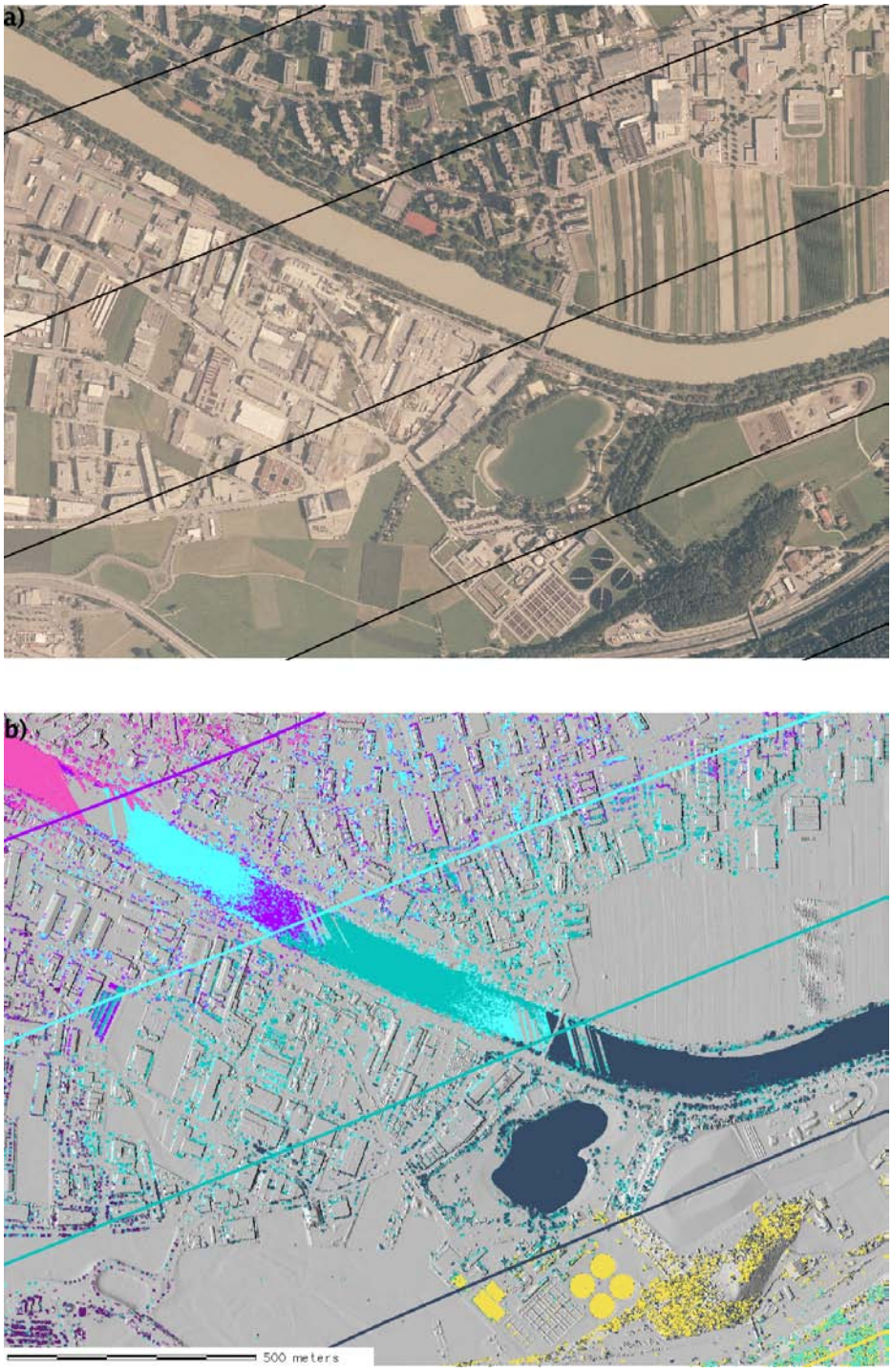

Figure 6.4: *Result of missing points modeling in the city of Innsbruck: a) orthophoto (not concurrent with ALS scan) overlaid with flight trajectories, b) shaded relief map overlaid with missing points and flight trajectories, both colored by strip.*

6.1.3 Future work

In general, a database management system (DBMS), such as PostgreSQL/PostGIS, can never be as efficient as an internal data structure explicitly designed for one purpose. But

the large pool of existing functionality (e.g. client-server-architecture, multi-user capabilities, transaction management, well-defined interfaces, security and high availability) definitely justifies the loss of some percents of performance. By implementing the management strategies developed in this thesis and taking the special structure of ALS data into consideration, allows for utilizing an existing DBMS for managing country-wide ALS point clouds. Future work concerning data management should concentrate on extending the GiST index to the third dimension. It should be arbitrary, which dimension of spatial index is applied to a flight strip or a whole campaign. This would open the possibility to store also TLS data (3D-indexed) together with 2D-index ALS data.

The LISA database is not yet designed for fast and lossy visualization of large areas/point clouds. Multiple level of details (LODs) are mostly used for that purpose (e.g. Zhang et al., 2007). In LISA, a tool for thinning of DEM grid points by defining a maximum deviation (based on TIN densification) already exists. This tool could be used to assign the original point cloud to the respective LODs. This would allow for fast visualization of large areas with specified accuracy.

Up to now the classification of laser points (e.g. ground, non-ground, vegetation) is stored as additional attribute for each echo (similar to intensity) following the LAS classification schema (LAS Specification, 2005). The relational DBMS could be used to store multiple classifications connected to each echo, for example, if different users/applications use different algorithms for point cloud classification leading to different results.

Multi-temporality is given in the LISA system, as the relative time of a shot (mostly seconds since start of week) can be easily converted into an absolute date format. But the current data management does not conform with *spatio-temporal* because one object (a laser point) cannot be connected with a corresponding object in a different epoch. If multi-temporal object-based point cloud algorithms can identify this connection, it can also be transferred and stored in the LISA database.

6.2 Intensity correction and analysis

Laser scanning intensity, airborne and terrestrial, has gained more and more attention in the last years. The lately started EuroSDR Project “Radiometric Calibration of ALS Intensity” (Hyyppä and Wagner, 2007) underlines this trend. The added value contained in the intensity has been realized and hence the need for intensity correction methods rises, which can be applied by end-users.

6.2.1 From intensity to surface reflectance

The second paper (Chapter 3) gives an extensive state-of-the-art report of existing applications concerning signal intensity of pulsed laser scanning systems and also points out the need for intensity correction. Two methods for intensity correction – a model-driven and a data-driven approach – are developed, implemented and evaluated. The goal is to use the recorded intensity to derive a value proportional to surface reflectance. The two developed methods work with different data requirements. This is important because regular end-users may not have all information needed for a physical-based correction method, such as a modeled atmosphere or information on emitted power. A prerequisite necessary for both correction methods is to know the laser range vector (vector scanner-target). If no scanner positions or range measurements are available, the proposed methods do not work but still, image processing tools can partly enhance the "raw" intensity image. Such a procedure is for example used by Lutz et al. (2003) who simply used the maximum intensity in overlapping areas for rasterization, reducing the fading out towards strip edges mainly caused by increasing range and angle of incidence. Or for example Song et al. (2002) who applied different filters and interpolation methods (IDW, median filter, Kriging) to the intensity image reducing the high local variability (stated as "salt and pepper" noise).

In general, the correlation between corrected intensity and surface reflectance underlies a few assumptions, which also limit the utilization of corrected intensity for classification to surfaces fulfilling these assumptions. To get an intensity value proportional to surface reflectance it has to be assumed that:

1. the laser range vector is known/can be calculated
2. the entire footprint is reflected on one surface (extended target with no partial reflectors)
3. the reflectance is homogeneous within the illuminated footprint (only one surface class)
4. the surface slope and hence angle of incidence can be estimated/derived
5. the reflection function/model is known (Lambertian scattering was assumed)
6. the atmospheric conditions are known or can be modeled, and do not significantly change during data acquisition
7. the transmitted power is known or constant
8. the receiver maps incoming power linear to recorded intensity

Assumption 1 is given due to the ability to interpolate the scanner position for each echo (LISA functionality). It is tried to fulfill assumption 2 by omitting shots with multiple echoes. But still small echoes not strong enough to be detected can cause loss of energy (and smaller target area due to occlusion) and hence lead to a lower intensity. Because analog threshold detectors are not able to measure more than one pulse if target areas are on slightly different elevations (Jutzi and Stilla, 2006; Wagner et al., 2006), intensities of such superimposed echoes (of one or more surface classes) are not suitable for deriving surface reflectance. But further checks on intensity homogeneity and roughness (in a local neighborhood) can help to omit these areas (e.g. vegetation) as much as possible.

Assumption 5 is not entirely fulfilled for every surface material (but maybe to a large extent). For example Hasegawa (2006) performed a ground survey with a scanner system used for airborne data acquisition (ALTM 2050DC). Different materials were fixed in a distance of 70 m with changing orientation. It was found that intensities of soil, cement, roof tile and old asphalt decreased with incidence angle whereas intensities of brick, grass and new asphalt stayed almost constant. It has to be mentioned that these tests were performed with a footprint $<$5 cm and the results cannot directly be assigned to flight campaigns where the footprint diameter is ten to twenty times larger. Also Kasaalainen et al. (2005) state that "the variability of the recorded intensity [...] as a function of incidence angle was low" based on ground laboratory experiments using brightness targets with nominal reflectance. Our dataset (Fig. 3.5), a cross-section through grass based on real flight conditions, showed a $cos\alpha$ dependency of the recorded intensity with increasing incidence angles (α) resulting in a $cos^3\alpha$ dependency due to the additional effect of increasing range. Coren and Sterzai (2006) also assume Lambertian scattering for an asphalted road (decrease of intensity with $cos\alpha$), which was well represented in their data.

Concerning assumption 6, the atmospheric conditions can be modeled or extracted from the data (cf. Table 3.4) but it gets computationally very expensive if atmospheric conditions cannot be assumed to be constant for one flight campaign. Hence, individual atmospheric attenuation coefficients must be modeled for each strip or even each laser shot.

Assumption 7 (emitted power) plays a major role because the emitted power is strongly changed with different PRF settings. In our case the emitted energy is known for different PRFs (cf. Chasmer et al., 2005), mainly corresponding with the theory (Baltsavias, 1999c).

Assumption 8 (linearity of intensity) has been proved by Ahokas et al. (2006) for the scanning system we used but it does not mean to be universally valid for all scanning system,

as for example TLS intensity investigations by Pfeifer et al. (2007b) showed that the signal amplification does not follow a simple (linear or logarithmic) model. This "linearity criterion" includes the system transmission factor, amplification and rescaling of the incoming power to the finally recorded digital number (intensity).

The correction of intensity is an important step towards intensity calibration (radiometric calibration). Calibration means to make the corrected intensity to a comparable value when using different system settings and scanners (e.g. important for multi-temporal analyses) by adjusting it to a reference. As mentioned before, our goal was to derive a value proportional to surface reflectance. Calibration is achieved if a priori information on ground targets (standard targets) is present, either portable brightness targets with nominal reflectance and known bidirectional reflectance distribution function (BRDF) (cf. Ahokas et al., 2006; Kasaalainen et al., 2005) or natural targets with known reflectance characteristics and values.

In our case, if the reference area does not have Lambertian scattering characteristics, the equation of the backscattering cross-section (Eq. (3.5)) has to be adapted. All variable parameters (e.g. range, atmospheric attenuation, emitted power) must be used for correction (cf. Eq. (6.1)) and all constant parameters (e.g. system transmission factor, receiver aperture diameter) are summarized in the calibration constant, inverse of factor C in Eq. (6.1) (cf. Wagner et al., 2006). If a parameter that has been assumed to be constant starts changing over time, it has to be moved from the calibration constant to the intensity correction part of Eq. (6.1).

$$P_r(R) \propto \frac{\rho}{R^2} 10^{-2Ra/10000} \cos\alpha \frac{1}{f_{sys}} \cdot C \tag{6.1}$$

6.2.2 Data-driven correction

The first approach – data-driven correction – assumes that most effects (known or unknown) correlate with range. For example the atmospheric attenuation increases with range and if the terrain is flat, also the incidence angle increases with range. In comparison to that, the emitted energy is generally set higher with increasing range (lower PRF). This correction method derives all necessary parameters directly from the input data (point cloud). It utilizes the fact that surfaces with homogeneous reflectance produce the same intensity value if all other influencing factors are the same. This behavior was verified by Ahokas et al. (2006) for the same system as in our study (Optech's ALTM 3100). They concluded an

original variability in the intensity measurement of 10% by looking at the standard deviations of the intensities within one brightness target with homogeneous reflectance. After correction for known effects the target reflectance could be derived with 5% relative error.

In comparison to Ahokas et al. (2006), because no calibrated reflection targets were available, natural test targets (regular fields/cells) were used. A rough preselection was performed by digitizing areas appearing homogeneous in the intensity image (mainly shortly cut meadows). Further checks (e.g. on intensity variation) excluded unsuitable fields. These homogeneous areas were used for fitting (least squares adjustment) five empirical models including range and original intensity as well as for evaluation of the correction success (for both methods). The best results could be achieved with an empirical model accounting for range-square dependency, reducing the relative intensity variation in homogeneous fields from higher than 30% to lower than 10%. The offset in intensity between strips could be reduced to nearly 5%. The influence of topographic correction was found to be very small due to the relatively flat terrain in the test site. The assumptions 6 and 7 do not have to be fulfilled in case of using a data-driven correction, but as mentioned before these effects have to correlate with range and are therefore included in the correction model.

The main drawback of the data-driven correction can be seen in the requirement of a high number of overlapping strips in different flying altitudes over homogeneous areas, which is generally not given in standard ALS campaigns. Nevertheless, the method has been proved to deliver satisfying results without the need for knowledge/data of atmosphere and emitted energy.

6.2.3 Model-driven correction

The second aproach – model-driven correction – is derived from the radar equation (cf. Jelalian, 1992; Wagner et al., 2006). Every intensity measurement is corrected independently for the effects mentioned in Sec. 6.2.1. A value proportional to surface reflectance is calculated using Eq. (3.15). The evaluation of the correction results showed a similar success as the data-driven approach. Intensity variation within homogeneous fields was reduced to 9% and the strip offsets to below 9%.
It can be concluded that the model-driven approach has less requirements on the flight campaign (no multiple flying altitudes needed) and the scanned surface (no homogeneous targets necessary) but atmospheric modeling has to be done and the emitted power has to be known or at least be constant. Resulting corrected intensity images of the model-driven correction are presented in Figs. 4.2, 4.4 and 6.5.

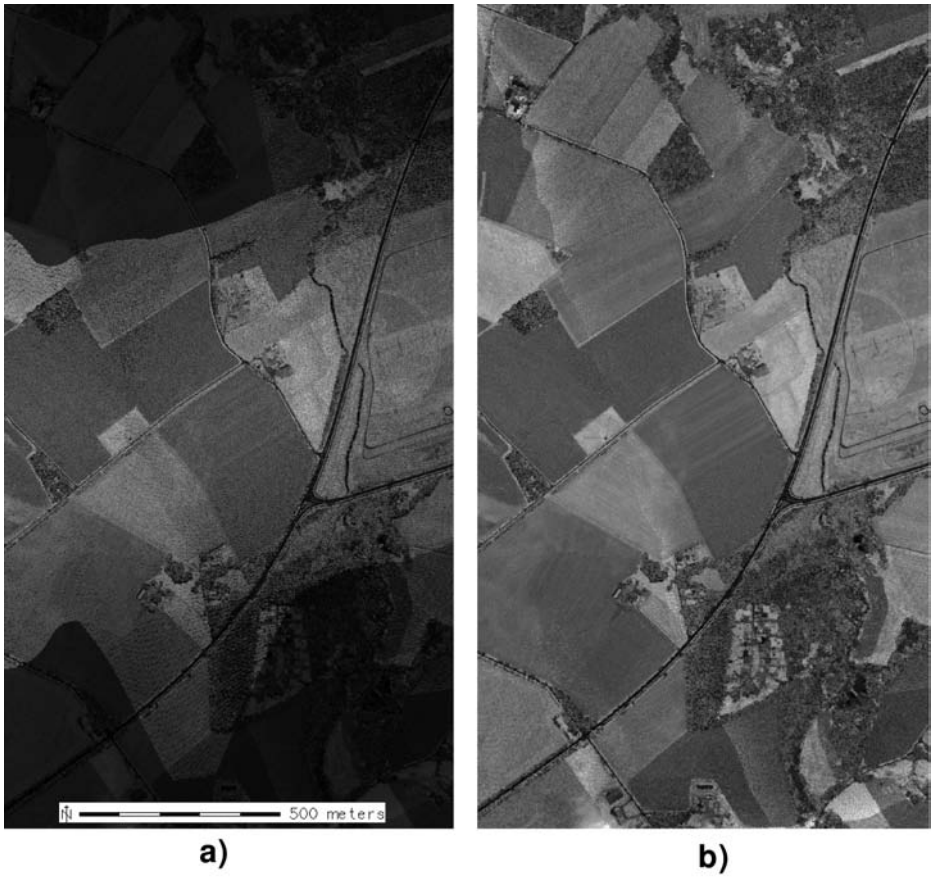

Figure 6.5: *Digital Intensity Models (DIMs) of a test site near the city of Innsbruck: a) uncorrected DIM representing original recorded intensity values and b) DIM corrected for influences of scan geometry, topography and atmosphere applying the model-driven correction approach (source: Geist et al., accepted).*

6.2.4 Résumé

The investigated datasets show that the original recorded intensity is virtually unusable if not corrected but a high information content is released if a correction method is applied (either data or model-driven). Intensity correction is a crucial step to increase the usability of the intensity information. For many applications it is sufficient to have a value proportional to surface reflectance, i.e. if the values are relatively corrected but not absolutely calibrated. Data-driven correction seems to be a good alternative to the prevalent model-driven approaches (e.g. Ahokas et al., 2006; Coren and Sterzai, 2006). As both methods are implemented in the LISA system, the end-user can choose, dependent on the flight campaign design, which correction method to use. Hence, succeeding applications can work with corrected intensity images or with a point cloud with corrected intensity as point attribute (cf. Chapter 4).

In this research ALS systems with recording up to four distinct echoes were used. In comparison to these analog threshold detectors, full-waveform (FWF) systems record the full backscattering cross-section, i.e. the quantity of σ in Eq. (3.3) can be determined directly. Further advantages of FWF systems are that pulse detection can be applied in the post-processing with repeatable, open and variable algorithms, and that also the pulse shape (i.e. width and amplitude) can be used for surface description (cf. Wagner et al., 2006). Nevertheless the superimposed effects of target size, reflectance, and directional backscatter affecting the backscattering cross-section still cannot be resolved if not two of three variables are known. The accuracy of area-wide reflectance maps by means of ALS could be improved if the bidirectional reflectance distribution function (BRDF, cf. Hapke, 1993) of the scanned surface is known, i.e. better approximation to real BRDF than assuming only Lambertian scatterers, as for example snow exhibits rather anisotropic reflectance (Rees, 2005). But at the moment it is a "chicken-and-egg question" because exactly the corrected intensity (measure for reflectance) should be used for surface classification but a surface classification with defined BRDFs is necessary to enhance reflectance mapping solely using ALS. If thinking in practical, it is justified to classify surfaces using the corrected intensity for extended targets with a simplified BRDF (e.g. choose an empirical model), if the "spectral" separability of the surface classes is higher than the errors caused by over- and under-correction due to the chosen BRDF.

6.3 Object-based analysis of ALS data

In comparison to recent object-based applications, mainly based on the commercial software eCognition (Benz et al., 2004; Definiens, 2007), the Chapters 4 and 5 propose two new concepts for object-based analysis of ALS data fully integrated in GRASS GIS. The major goals are i) to combine the spatial and intensity information of the ALS point cloud (Chapter 4) and ii) to combine the strengths of image and point cloud analysis (Chapter 5). The two ways of ALS data processing presented in Fig. 6.6 come together in the object-based analysis. ALS data analysis starts with the point cloud, which is the root dataset for all further analyses. Basically, Fig. 6.6 shows that objects can be extracted in the raster domain (which is derived from the point cloud), in the point cloud only or using a combination of both domains. Traditionally, remote sensing algorithms are written for images, i.e. rasters, whereas applications requiring the third dimension (e.g. reverse-engineering with TLS) directly utilize the 3D point cloud because a 2.5D data model is not sufficient. A combination, for example, would be the segmentation in the raster domain but deriving segment features for classification from the point cloud, or to completely segment and classify in the raster but consequently perform a point cloud based delineation using the higher degree of

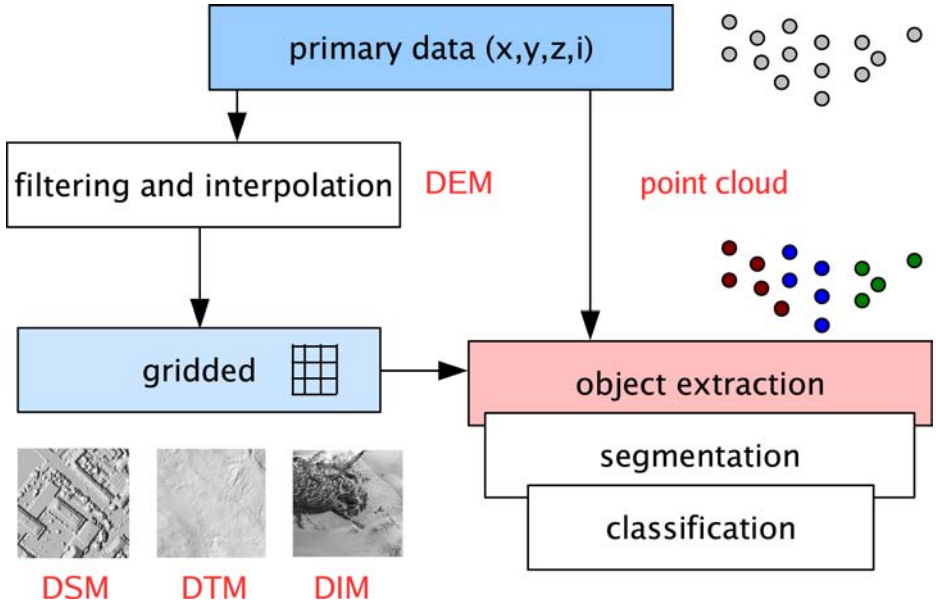

Figure 6.6: *Simplified workflow of object-based ALS data processing (source: Geist et al., accepted).*

knowledge about the target object. The common denominator for this powerful combination of vector and image processing techniques is the GIS component of the LISA system. Benz et al. (2004) mention that the creation of vector information (e.g. polygon of objects) bridges remote sensing and geo-information systems. As LISA additionally bridges GIS and point cloud management, the third dimension is employed (3D segmentation, feature calculation and delineation).

As also described in the chapters before, the object extraction relies on a segmentation and classification task (Fig. 6.6) where the object primitive can be either a pixel or a point (Fig. 6.7). Calculating features for the primitive "point" is more elaborate because neighborhood has to be defined beforehand (usually kNN or fixed distance, cf. Filin and Pfeifer, 2005). If segments fulfilling the homogeneity criteria are built (i.e. compact objects are delineated due to spatial connectivity constraint), descriptive segment/object features can be derived from underlying raster and point cloud data, as well as from the polygon geometry, the topological and contextual relationships to other objects. These features are then used for classification (e.g. supervised rule-based classification method was used in this thesis).

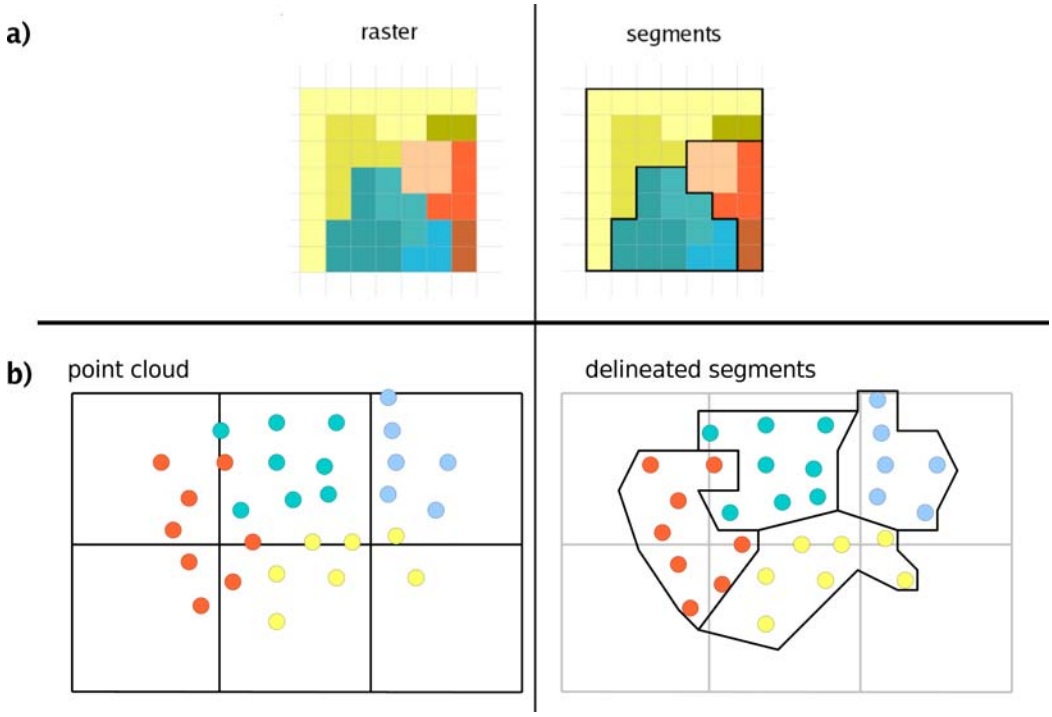

Figure 6.7: *Segmentation in a) the raster domain and b) the point cloud. The point cloud is overlaid with a raster to show the subpixel accuracy possible with high point densities (courtesy of M. Rutzinger, modified).*

6.3.1 Integrative approach – geometry and corrected intensity

This section provides additional information on the available data sources (visual comparison of ALS data and orthophoto), the intensity correction (e.g. correction factors) and the error assessment (e.g. error matrices) of Chapter 4. Additionally, the ALS data classification is compared with a supervised orthophoto classification.

Glacier mapping and surface classifications are mostly based on aerial/satellite imagery or radar measurements (Gao and Liu, 2001; Rees, 2005). Most mentioned problems – such as topographic shadows, cloud cover and lack of texture (e.g. due to saturated optics) – are generally not present when using ALS. Gao and Liu (2001) state that the accuracy of remotely sensed glacier mapping in literature varies between 70% and over 90%, and even higher accuracies are reached for snow/ice differentiation. It is also clearly emphasized that digital elevation models provide useful support for glacier mapping (e.g. topographic correction), or are even essential, such as for volume and mass balancing. The combination of the high resolution and high accurate spatial information of ALS data together with the already located intensity information establishes a great potential for applications in glaciology by using only one data source, namely ALS (cf. Arnold et al., 2006).

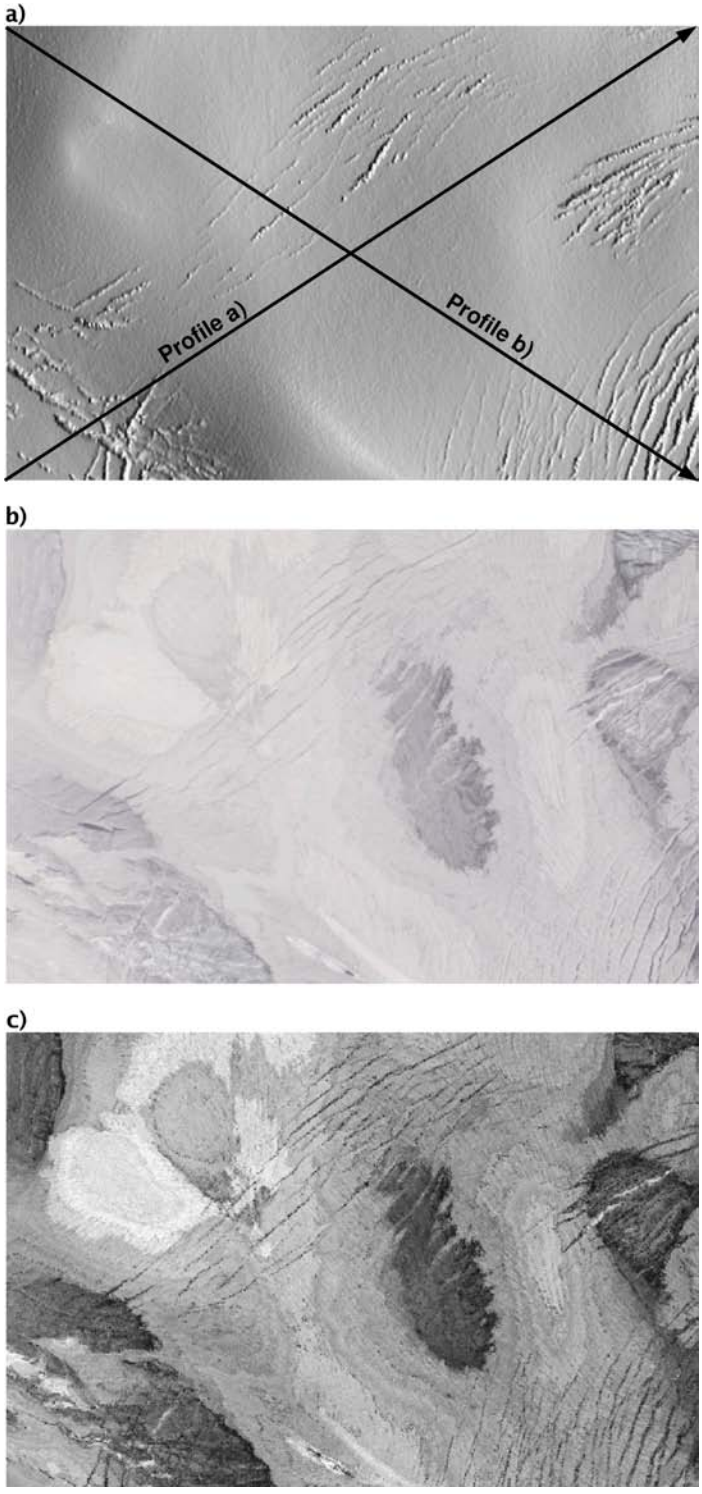

Figure 6.8: *Visual comparison of different data sources at Hintereisferner test site: a) shaded relief map of ALS elevation model overlaid with profiles of Fig. 6.9, b) orthophoto and c) corrected intensity image.*

The visual comparison (Fig. 6.8) of the shaded relief map of the digital elevation model (1 m resolution), the orthophoto (0.5 m) and the corrected intensity image (1 m) clearly indicates the different advantages of the single data sources. Except for the crevasses zones the glacier surface is relatively smooth (Fig. 6.9), hence the elevation model does not support to distinguish surface classes using surface derivatives (in the scale of a few meters), such as roughness and curvature. In contrast, the corrected intensity and the orthophoto allow for a good discrimination of surfaces. The intensity shows better separability on the glacier (e.g. between ice and firn). The orthophoto yields better separability between glacier and non-glacier surfaces (e.g. between rock and ice, or firn and grass) due to the two additional channels. The corrected intensity image shows even more classes (i.e. stages) of snow/firn but for a more detailed classification ground truth has to be collected (e.g. snow density and grain size measurements).

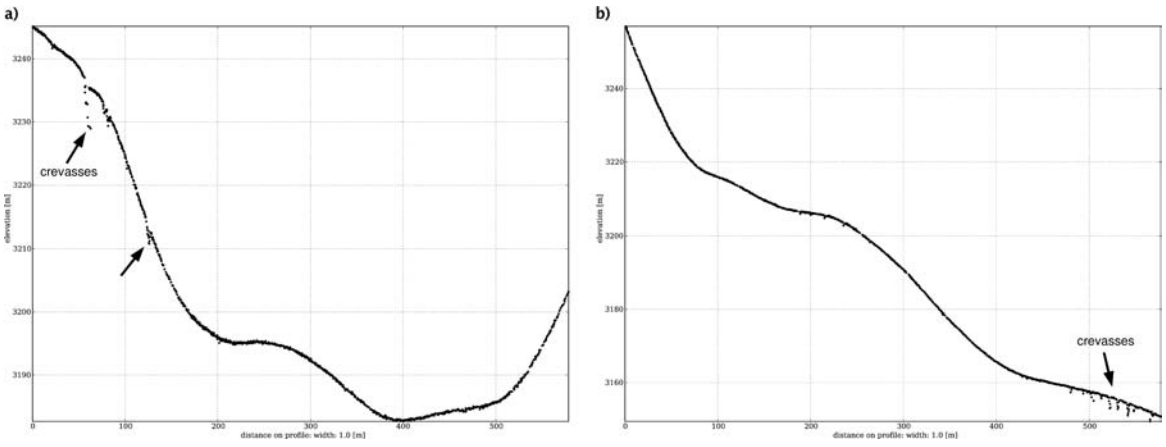

Figure 6.9: *LISA point cloud profiles of glacier test site (Fig. 6.8): a) across SW to NE corner of test site and b) NW to SE corner. Glacier surface is characterized by smooth transitions but also step edges (mainly crevasses; some marked with arrows).*

Intensity correction has been performed using the model-driven approach because of the lack of multiple flying altitudes within this flight campain and because no empirically determined correction function was available for the used scanner system and similar flight conditions. Arnold et al. (2006) found in a regression analysis including range and slope for the surface types bare ice, snow, bare rock and moraine that the effect of surface slope on the intensity value is rather small compared to the dependence on range. After applying an empirical correction accounting for the power-law dependence on range they conclude that ice/snow and ice/moraine boundaries are clearly delineated in the "corrected" intensity image. In our test site spherical, topographic and atmospheric effects have been corrected. The scanner system settings (e.g. PRF) did not change, so the emitted energy was assumed to be constant. Using a normalizing range of 960 m (min. range in the test site) an average correction of 55.6% due to range differences was necessary. Assuming Lambertian

scattering characteristics an average topographic correction of 7.1% was applied. With the given vertical atmospheric attenuation coefficient of 0.15 dB/km an average atmospheric correction of 8.6% turned out. Altogether the model-driven correction resulted in an average intensity correction factor of 1.63 for the whole test site due to the relatively small range differences (from 969 m up to 1428 m, mean range: 1189 m) compared to the correction values derived in Chapter 3.

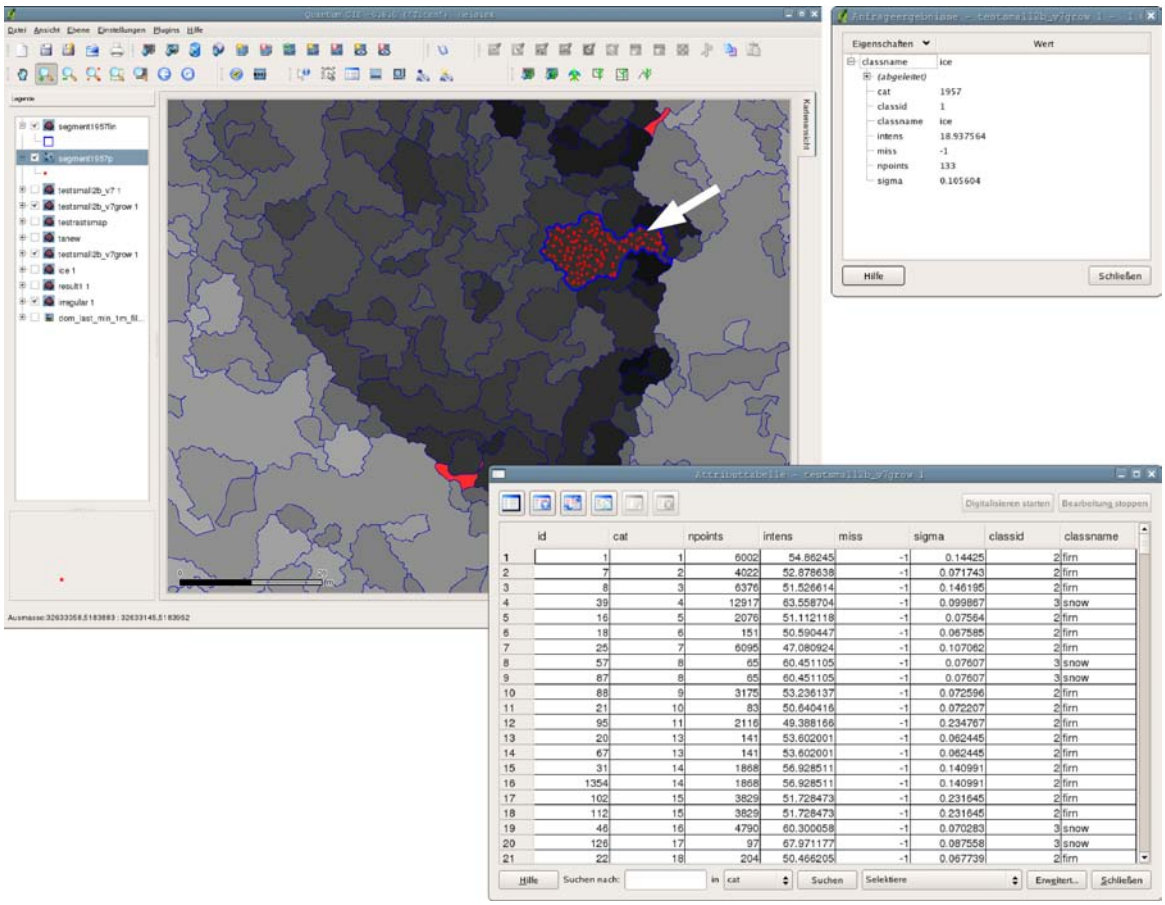

Figure 6.10: *Integration of point cloud segmentation into easy-to-use standard GIS software (QGIS and GRASS GIS): Large upper left window displays the current QGIS project with polygon segments colored by mean intensity and original laser points for one segment (marked with arrow). Small upper right window shows attributes of selected segment (e.g. no. of points, mean intensity, roughness). Lower right window displays a part of the attribute table for all segments.*

The glacier surface segmentation explained in Chapter 4 utilizes both, the 3D surface geometry represented by the original point cloud (x, y, z) and the corrected intensity value that is available for each laser point. The result of the segmentation are laser points labeled by segment ID and segment polygons as GIS layer including all segment statistics and attributes. The GIS polygon layer and the segmented point cloud are connected by the unique segment ID. Therefore, the topological (e.g. neighbors) features of the polygons can be used concurrently with the segmented point cloud. The rule-based classification

of the segment polygons is more or less a database query task in feature space. And the merge of segments belonging to the same class is a standard functionality of GRASS GIS (*v.dissolve*). Fig. 6.10 shows the integration of the developed point cloud segmentation and segment classification into QGIS (QGIS, 2007), which directly connects to GRASS GIS where all GIS data layers are stored. This integration is made possible because the segmentation algorithm works with OGC conform vector layers and uses the GRASS vector topology. This offers not only better usability but also allows for connecting existing GIS functionality with one's own developments (e.g. vector dissolving).

Table 6.1: *Error matrix resulting from ALS point cloud and intensity segmentation/classification.*

Classified data	Reference					
	Ice	Firn	Snow	Surface Irreg.	Total	User's accuracy
Ice	40990	6691	32	998	48711	84.2%
Firn	11234	202481	1931	1741	217387	93.1%
Snow	129	2310	30722	44	33205	92.5%
Surface Irregularities	1732	665	14	1374	3785	36.3%
Total	54085	212147	32699	4157	303088	
Producer's accuracy	75.8%	95.4%	94.0%	33.1%		
Overall accuracy: 90.9%			Kappa ($\hat{\kappa}$): 0.80			

In order to assess the quality of the surface classification, a simple point wise accuracy check was applied, which is comparable with the pixel wise approach in the raster domain (cf. Lillesand et al., 2004). A detailed error matrix (Table 6.1) was computed for the reference data (manual delineation) covering the whole test site. As mentioned in Chapter 4 an overall accuracy of 90.9% was reached with a $\hat{\kappa}$ value of 0.80. The class "surface irregularities" has the lowest accuracy (33.1% producer's accuracy), which can be explained by the performed closing of small gaps (hence also crevasses) and the difficulty of digitizing crevasses on basis of the 1 m shaded relief. Better parameter tuning can improve the result for this class, such as using a lower surface normal and distance-to-plane tolerance, as well as avoid filling of crevasse gaps (e.g. do not fill gaps with high surface roughness). The classes "firn" and "snow" can be detected with quite high accuracy (>90%). Ice areas are the most heterogeneous areas because many small spots of other surface classes (e.g. small crevasses, firn and snow spots) can be found within ice objects. Due to the generalized

reference data (as it is manually digitized), such small objects fall into the class "ice" and cause misclassification. It can also be seen that the ice/firn boundary is hard to define (for training areas and reference data) without ground truth.

If it is aimed to classify the laser points, the chosen error assessment method is justified, as it checks the classification at the location of each laser point. But if a complete ("gapless") surface mapping shall be reached, it is also necessary to take into account the delineation accuracy (cf. alpha shapes and filling of gaps), which is influenced by the effective average point spacing (cf. more missing points in ice) at the object boundaries. Lower delineation accuracies occur where a low point density or even no points are present (e.g. lower density in ice areas and no points in water areas). With concurrent ground truth (e.g. GPS tracks along object boundaries) and ALS data acquisition, the classification and delineation accuracy can be assessed dependent on the surface types building the boundary.

Table 6.2: *Error matrix resulting from orthophoto segmentation/classification.*

Classified data	Reference				
	Ice	Firn	Snow	Total	User's accuracy
Ice	30397	7476	40	37913	80.2%
Firn	21686	199025	2706	223417	89.1%
Snow	274	4986	29939	35199	85.1%
Total	52357	211487	32685	299317	
Producer's accuracy	58.1%	94.1%	91.6%		
Overall accuracy: 86.7%			Kappa ($\hat{\kappa}$): 0.70		

Additionally to the glacier segmentation using the ALS point cloud, an image segmentation algorithm – the sequential maximum a posteriori (SMAP) estimation that is implemented in GRASS GIS (GRASS Development Team, 2007; McCauley and Engel, 1995) – was applied to the orthophoto. The same training areas and reference dataset as for the ALS classification were used. In contrast to the algorithm working on the point cloud, the image segmentation cannot identify surface irregularities due to the lack of the third dimension. To get comparable error assessment results, the laser points were labeled according to the surface class determined by the image segmentation. Furthermore, the crevasse points had to be excluded because this class was not targeted. The calculated error matrix (Table 6.2) shows an overall accuracy of 86.7% with a $\hat{\kappa}$ value of 0.70. The greatest problem occurred

in the "ice" class that was only detected with 58% producer's accuracy for the benefit of the "firn" class. This leads to the assumption that the ice/firn boundaries are more distinct in the corrected intensity image than in the orthophoto. Fig. 6.11 shows the results of the point cloud segmentation and the orthophoto segmentation.

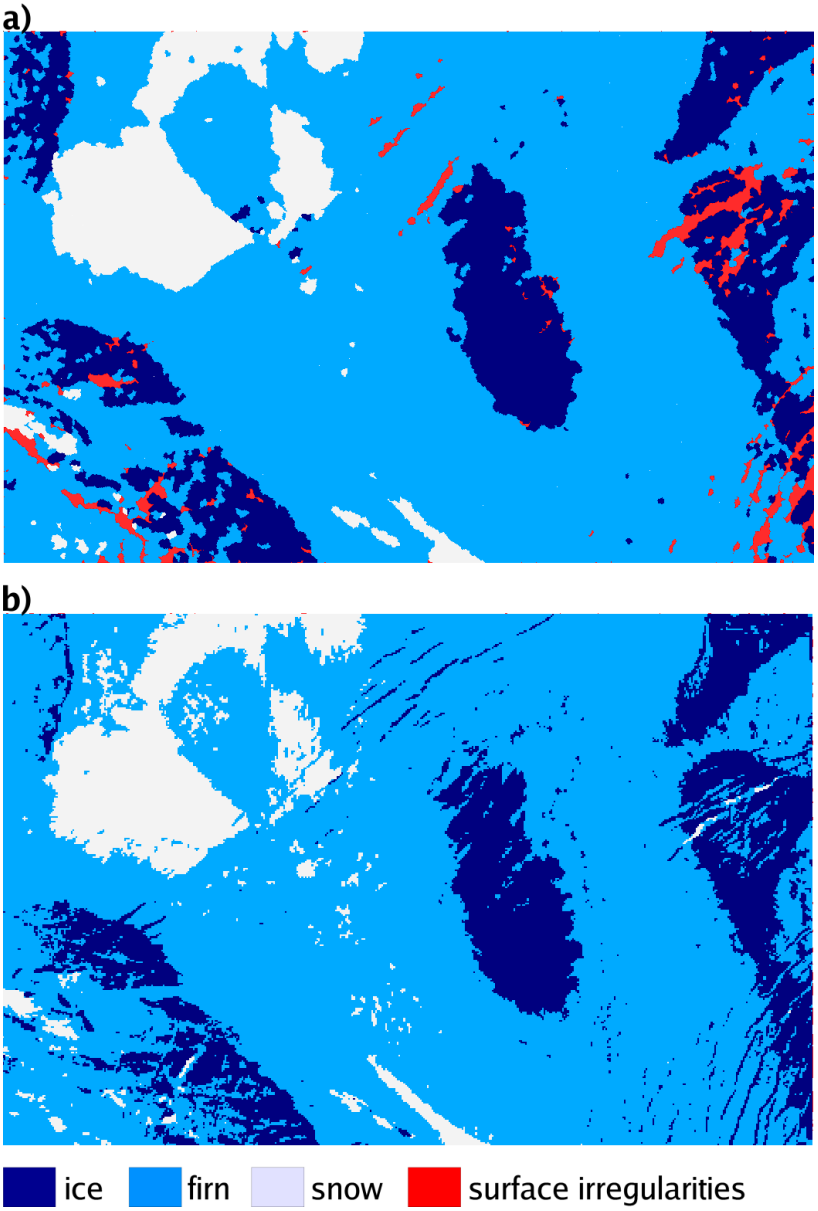

Figure 6.11: *Comparison of glacier surface classification based on a) ALS data and b) orthophoto.*

It has to be clarified that the derived classification accuracy values just show the agreement with the present reference data and do not reflect the "true" accuracy of the results. The effective accuracy may be higher than the effective accuracy of the reference data due to the inaccuracies caused by manual digitization and due to the generalization effect inherent

in human interpretation. Furthermore, the developed method guarantees replicability, repeatability and comparability of the results in contrast to the subjective method of manual delineation, which is still frequently used (e.g. glacier inventory).

Further improvements of the glacier point cloud segmentation should concentrate on including additional features for segmentation and classification, such as missing point density and roughness (e.g. SD of plane fitting), which will become important if more surface classes are present in the area of interest. For example, missing point density and roughness could support to discriminate between ice and rock, which have similar intensities. If the segmentation is applied to other glaciers with a rougher surface (e.g. with seracs, icefalls and steep edges), the need for high density 3D ALS data will increase, even terrestrial investigations (TLS campaigns) may be necessary (e.g. vertical walls at margins of plateau glacier system of Kilimanjaro, Cullen et al., 2006).

The developed methodology, which allows nearly fully automatic surface classification, can be used to systematically study the effects of different ALS settings (e.g. flying altitude above ground, max. scan angle, PRF, point density) on classification and delineation accuracy (e.g. reconstruction of crevasses) of different glacier features. Additionally, the influence of time (e.g. time of day and season) on the classification success should be assessed. For example, melting during the day may increase water-content in sun-exposed areas, and hence lead to lower intensities compared to shaded areas with the same surface cover. As always "the means are adapted to the end", i.e. dependent on the application different "packages" of system settings and flight campaign planning will be found out to be optimal.

The implementation of the glacier surface classification into Open Source GIS software (and hence into the LISA system) opens many new analysis possibilities, such as multi-temporal comparisons of classification results (e.g. vector intersection). Further, a basis is provided for linking glacier surface changes to topographic and environmental variables (cf. Gao and Liu, 2001) by using the full information of ALS along with other spatial datasets (GIS layers). But a major problem of current GIS software that is still not solved, is the limitation of the vector topology on 2D. In most GIS programs it is possible to store 3D coordinates but calculating 3D features, such as area in 3D or working with 3D neighborhood (cf. Billen and Zlatanova, 2003), is not yet available. Hence, there exists a drawback when using GIS because 3D segments have to be converted into clean 2D GIS vector topology.

The presented glacier surface classification method emphasizes that ALS data has already

reached a level for glaciological applications that is beyond the scope of a simple provider of digital elevation models. Hopkinson and Demuth (2006) state that "airborne lidar data have the ability to map all areas of a glacier surface at high accuracy and high resolution". Future work should concentrate on the integrated utilization of geometry and intensity to identify glacier features. Many authors have already stated the "great potential" of ALS intensity but never implemented this valuable combination of spatial information for glacier surface mapping (e.g. Arnold et al., 2006; Geist, 2005; Hopkinson and Demuth, 2006; Kodde et al., 2007; Lutz et al., 2003). Furthermore, future studies should also assess the added value of using full-waveform laser scanning for glacier surface model generation but also glacier surface classification, as it is already investigated for 3D vegetation mapping (e.g Wagner et al., in press).

6.3.2 Integrative approach – raster and point cloud

The building detection and the roof face modeling – starting from the rasterization of the point cloud to the final 3D roofs patches – are fully integrated in the LISA system. The original point cloud is accessed two times, namely for rasterization (OBIA) and for 3D segmentation (OBPA). The building detection is performed in the raster domain (based on the Digital Surface Model) and results in compact objects identified as buildings represented as 2D polygons. The OBIA algorithm will not be discussed here any further (see Pfeifer et al., 2007a; Rutzinger et al., 2006a,b). The application of the OBIA building delineation reduces the area of interest to areas with buildings, which are further investigated by the roof facet modeling and classification. Firstly, this initial segmentation and classification of buildings reduces data volume and hence computation time, and secondly, drastically increases the a priori information (contextual information) on the target object. It is assumed that the laser scanner mainly hits the roof of a building if the scanner views from above (bird's-eye view). Therefore all points lying within a building polygon are very likely part of the roof, i.e. belong to a roof sub-object (roof facet). This fact can be compared with the so-called "classification-based segmentation" of Benz et al. (2004). The laser points are a high-level input for an additional segmentation and classification in a different scale and spatial dimension (3D). Hence, the combination of OBIA and OBPA can be seen as "multi-scale" (i.e. two-scale) approach that works from 2D (2.5D) coarse to 3D fine.

Using the 3D information of the laser points in detailed scale allows not only for further differentiation (derivation of sub-objects) of the preliminary object but also allows for more accurate delineation (sub-pixel delineation, cf. Fig. 6.7), which is mainly dependent on point density (and spatial distribution of the points) and not on the chosen cell size, interpolation/aggregation method or orientation of the building in relation to the raster orientation.

The presented roof facet modeling is a first attempt to combine image and point cloud analysis, but has already specific applications in mind, such as snow load capacity modeling and photovoltaics site analysis. The chosen point cloud segmentation (region growing) and delineation (triangulation) delivers already promising results. But it has to be mentioned that it is not yet designed for deriving "esthetic" building or roof models (e.g. with straight gutter edges and ridges; cf. "object beautification"), which are suitable, for example, for the integration into city models (cf. Kaartinen et al., 2005). Basically two different strategies can be found in the literature, namely i) fitting of parametric primitives to point cloud subsets and ii) detection of planar faces (in raster and point cloud), which are further combined in a model representing the more or less complex roof geometry. Concerning 3D building and roof reconstruction it shall be referred to Baltsavias (2004); Hofmann et al. (2003); Maas and Vosselman (1999); Rottensteiner et al. (2005b); Schwalbe et al. (2005); Vosselman (1999).

In comparison to the glacier segmentation, the roof segmentation utilizes only the spatial component of the point cloud. Further improvements concerning the roof segmentation should investigate if taking into account the corrected intensity and the multi-echo information can enhance the segmentation result, e.g. identify and remove overlapping vegetation points or better differentiation of roof materials (e.g. roof tiles, tin roofs or glass parts). Regarding the delineation promising results have been experimentally reached by applying 2D alpha shapes to the laser points projected onto the segment adjusting plane, which means that also segments on steep faces can be delineated. The points belonging to the alpha shape (i.e. segment outline) could be used as input for an edge generator (e.g. fitting straight lines and intersect planes to get building ridges; cf. Rottensteiner et al., 2005b). By obtaining ground truth (not the digital cadastre map) the quality of the fitted roof planes can be assessed concerning height and planimetric errors of ALS (cf. Ahokas et al., 2004), which influence height determination, roof delineation and hence roof inclination determination (cf. Ahokas et al., 2005). But also the effect of different point densities and flying altitudes on the proposed roof modeling algorithm as well as the impact of roof complexity have to be studied.

7 Conclusion

7.1 Contributions

In this doctoral thesis new aspects of airborne laser scanning point cloud management and analysis have been proposed. The developed management system LISA (conceptually introduced in Höfle et al., 2005) provides the necessary basis for working with huge amounts of laser points (Chapter 2). The system allows even more than just the import, storage and export of defined laser point subsets because it *bridges the gap between ALS point cloud and Geographic Information System (GIS)*. This bridge is made possible by using existing Open Source components with well-defined interfaces and data standards. *Open Source* has also allowed implementing all developed algorithms as easy-to-use GIS modules, which opens the possibility to test and further enhance the algorithms *in* and *extra academia* (e.g. alpS-Centre).

Primarily, the full data have to be regarded if aiming at utilizing the full information potential of ALS data. The experience showed that often timestamp and signal intensity are delivered to end-users. The *intensity information*, already used in several research studies, yields even more value if a correction (or even calibration) procedure is applied. Two considerably different (concerning methodology and data requirements) *intensity correction* approaches were developed and evaluated (Chapter 3). The added value of using the timestamp of each laser shot was exemplarily shown by modeling missing points (Chapter 6) and on-the-fly interpolation of laser scanner positions used for range vector calculation.

In order to demonstrate the capabilities of the developed ALS/GIS framework, as well as to prove the usefulness of the corrected intensity two practical examples have been selected. Methodically, *two integrative object-based point cloud approaches* were successfully applied to the unclassified ALS point cloud, i.e. i) combination of geometry and intensity (Chapter 4), and ii) combination of raster and point cloud (Chapter 5). Regionally, two very diverse target objects (i.e. glacier features and building roofs) were chosen for point cloud classification, intending to point out the flexibility and portability of the developed package of methods and algorithms.

The innovative findings of this thesis can be summarized as following:

- By using solely Open Source software (mainly PostgreSQL/PostGIS and GRASS GIS) it is possible to manage large volumes of ALS point clouds ($> 10^9$ laser shots) at a performance that allows an operational use for scientific and non-scientific end-users (e.g. natural hazard management at alpS).

- The developed data model and spatial indexing system, specially designed for ALS data, guarantees performance with increasing data volume and at the same time provides an extensible and well-defined framework for new applications development embedded in a standard GIS. Hence, it is easily possible to realize GIS applications working on raster and/or point cloud data (as two selected but also many other examples show).

- The intensity value of ALS (and TLS) contains beneficial information, if it is converted to a measure proportional to surface reflectance using intensity correction methods. Spatial and corrected intensity information (originating from one data source) complement one another. In areas with no or low surface roughness, intensity can support surface classification and object detection (if objects differ in reflectance), and in areas with high roughness (e.g. vegetation, crevasses) geometry may be better suited than the intensity of non-extended targets.

- That ALS intensity is a good discriminator for glacier facies has already been stated by many authors (Chapter 4). The proposed glacier surface classification integrates the state-of-the-art methods of glacier remote sensing and ALS data analysis. For the first time, point cloud object segmentation and rule-based classification (implemented in a GIS) are successfully applied to a test site at Hintereisferner (Ötztal/Tyrol) resulting in a high quality glacier surface map (>90% classification accuracy and <2 m location accuracy). It can be concluded that ALS can/will take over most tasks of remote glacier monitoring where high accuracy is required (cf. Arnold et al., 2006; Geist, 2005) and can provide high resolution input for glaciological models (e.g. energy balance modeling, ice flow modeling, snowmelt runoff modeling).

- The fusion of object-based image processing and object-based point cloud analysis in one application is made possible by the LISA system, which allows extracting point cloud subsets for analyzing in the highest level of detail and in 3D. This hierarchical approach expands the GIS with 3D capabilities but still delivers GIS-ready data layers. It can be pointed out that the multi-resolution approach of OBIA and OBPA embedded in the GIS (exemplified in this thesis by building detection and roof delineation) was found to solve many problems occurring when working with ALS

point cloud data (e.g. reduces data volume that has to be processed; a priori object information decreases effort of analyzing the points). The given link between the different hierarchical levels is certainly a fact that let think of many other enhancements (e.g. count roof facets per building; use raster object features for setting point cloud segmentation parameters).

7.2 Future work

Detailed suggestions for future research activities have already been discussed in Chapter 6. More general, the following research/implementation demands directly arise from this thesis:

- The increasing utilization of terrestrial laser scanning requires strategies for connecting existing datasets (e.g. aerial imagery, ALS point cloud and elevation models) with TLS datasets. Such as image and ALS point cloud analysis have been connected, the LISA system could be expanded to support the management of TLS data (e.g. new data model designed for TLS data; extension of the spatial index hierarchy and spatial query possibilities to the third dimension). For example, for detailed object reconstruction the TLS point cloud could be accessed, if available, instead or together with the ALS point cloud. The fact that LISA organizes the data also in time would also enhance the usability of multi-temporal TLS datasets (e.g. landslide monitoring). In principle, intensity correction and point cloud segmentation can likewise be applied to TLS data.

- The newest laser scanner systems provide full-waveform digitization. LISA supports unlimited echo storage but until now no full-waveform data were tested in our research project. Before utilizing full-waveform data in the LISA system, it is necessary to implement algorithms for waveform modeling (decomposition) and discrete echo extraction (e.g. Reitberger et al., 2006; Wagner et al., 2006). Evidently, with full-waveform echo extraction the attributes of a laser echo have to be extended (e.g. pulse width, backscattering cross-section). However, using full-waveform ALS data will increase data management effort. But recent studies show promising results for point cloud based surface classification (e.g. of vegetation; Wagner et al., in press), which should be further investigated for other land cover types (e.g. glaciers). And also improvements in DTM filtering have been reached by using full-waveform data (e.g. Doneus and Briese, 2006).

- Object-based analysis requires new methods for quality validation because pixel-by-pixel or point-by-point error assessment is not sufficient and because the generated

datasets even make more sophisticated methods possible, as for example Pfeifer et al. (2007a) demonstrate for buildings. Hence, the derived object information should also be included in the validation process. The same is true for multi-temporal object-based analysis, which is not yet satisfactorily solved (cf. Blaschke, 2005).

- Blaschke and Lang (2006) state that only few papers utilizing OBIA for ALS data are published so far. The advantages of having object-based features (e.g. object geometry and topology) as well as the possibility of integrating hierarchical and contextual information into the analysis process are clearly visible but not often used because of the lack of easy-to-use software, which can handle rasters (e.g. ALS elevation models) and point cloud data. The two application examples of this thesis showed the large potential of implementing the object-based approach (raster and point cloud) in an easy-to-use standard GIS (cf. Lang and Blaschke, 2006). Future research efforts should make use of this "concept", which will lead to more potential users (scientific and non-scientific) and results in a broader field of applications. In return new research questions will come up and stimulate new innovative developments. In Fig. 1.1 this "backwards connection" is indicated, from decision makers and users respectively to developers of analysis tools and methods, as well as to developers of new/better remote sensing techniques and sensors.

7.3 Last paragraph

It was shown that ALS is more than the state-of-the-art technique for topographic data acquisition. This thesis has taken some steps towards the main objective *"Detection and Utilization of the Information Potential of Airborne Laser Scanning Point Cloud and Intensity Data"*. Added value was generated to the original point cloud by increasing data availability and using the full information delivered to end-users. Nevertheless, spatial data management and analysis will always lag behind the newest technology, which opens new challenges for future research.

"Measure what is measurable, and make measurable what is not so."

Galileo Galilei (1564-1642)

References

Internet links were last visited: 01.07.2007

Abdalati, W., Krabill, W., Frederick, E., Manizade, S., Martin, C., Sonntag, J., Swift, R., Thomas, R., Wright, W., Yungel, J., 2002. Airborne laser altimetry mapping of the Greenland ice sheet: application to mass balance assessment. Journal of Geodynamics 34 (3), 391-403.

Ahokas, E., Kaartinen, H., Hyyppä, J., 2004. A quality assessment of repeated airborne laser scanner observations. International Archives of Photogrammetry, Remote Sensing and Spatial Information Sciences 35 (Part B3), 237-242.

Ahokas, E., Yu, X., Kaartinen, H., Hyyppä, J., Kaasalainen, S., Matikainen, L., Honkavaara, E., Hyyppä, H., Rönnholm, P., Soininen, A., 2005. Quality of laser scanning. EARSeL Workshop "3-D Remote Sensing", June 2005, Porto, Portugal, (on CDROM).

Ahokas, E., Kaasalainen, S., Hyyppä, J., Suomalainen, J., 2006. Calibration of the Optech ALTM 3100 laser scanner intensity data using brightness targets. International Archives of Photogrammetry, Remote Sensing and Spatial Information Sciences 36 (Part 1), (on CDROM).

Arge, L., Chase, J., Toma, L., Vitter, J., Wickremesinghe, R., Halpin, P., Urban, D., 2003. Efficient flow computation on massive grid terrain datasets. GeoInformatica 7 (4), 283-313.

Arnold, N.S., Rees, W.G., Devereux, B.J., Amable, G.S., 2006. Evaluating the potential of high-resolution airborne LiDAR data in glaciology. International Journal of Remote Sensing 27 (5-6), 1233-1251.

Arya, S., Mount, D.M., Netanyahu, N.S., Silverman, R., Wu, A.Y., 1998. An optimal algorithm for approximate nearest neighbor searching. Journal of the ACM 45 (6), 891-923.

Asselen, S., Seijmonsbergen, A.C., 2006. Expert-driven semiautomated geomorphological mapping for a mountainous area using a laser DTM. Geomorphology 78 (3-4), 309-320.

Baltsavias, E.P., 1999a. A comparison between photogrammetry and laser scanning. ISPRS Journal of Photogrammetry and Remote Sensing 54 (2-3), 83-94.

Baltsavias, E.P., 1999b. Airborne laser scanning: existing systems and firms and other resources. ISPRS Journal of Photogrammetry and Remote Sensing 54 (2-3), 164-198.

Baltsavias, E.P., 1999c. Airborne laser scanning: basic relations and formulas. ISPRS Journal of Photogrammetry and Remote Sensing 54 (2-3), 199-214.

Baltsavias, E.P., Favey, E., Bauder, A., Bösch, H., Pateraki, M., 2001. Digital Surface Modelling by Airborne Laser Scanning and Digital Photogrammertry for Glacier Monitoring. Photogrammetric Record 17 (98), 243-273.

Baltsavias, E.P., 2004. Object extraction and revision by image analysis using existing geodata and knowledge: current status and steps towards operational systems. ISPRS Journal of Photogrammetry and Remote Sensing 58 (3-4), 129-151.

Bamber, J.L., Kwok, R., 2004. Remote sensing techniques for observing land and sea ice. In: Mass balance of the cryosphere: observations and modelling of contemporary and future changes. Cambridge University Press, pp. 59-113.

Bartunov, O., Sigaev, T., 2006. GiST for PostgreSQL. URL: `http://www.sai.msu.su/~megera/postgres/gist/`

Beazley, D., et al., 1995. SWIG: Simplified Wrapper and Interface Generator. URL: `http://www.swig.org`

Benz, U.C., Hofmann, P., Willhauck, G., Lingenfelder, I., Heynen, M., 2004. Multi-resolution, object-oriented fuzzy analysis of remote sensing data for GIS-ready information. ISPRS Journal of Photogrammetry and Remote Sensing 58 (3-4), 239-258.

Berk, A., Bernstein, L.S., Anderson, G.P., Acharya, P.K., Robertson, D.C., Chetwynd, J.H., Adler-Golden, S.M., 1998. MODTRAN cloud and multiple scattering upgrades with application to AVIRIS. Remote Sensing of Environment 65 (3), 367-375.

Billen, R., Zlatanova, S., 2003. 3D spatial relationships model: a useful concept for 3D cadastre? Computers, Environment and Urban Systems 27 (4), 411-425.

Blaschke, T., 2005. Towards a framework for change detection based on image objects. Göttinger Geographische Abhandlungen 113, Göttingen, pp. 1-9.

Blaschke, T., Lang, S., 2006. Object based image analysis for automated information extraction – a synthesis. Measuring the Earth II ASPRS Fall Conference, 6-10 November 2006, San Antonio, Texas, (on CDROM).

Blaschke, T., Lang, S., Hay, G., 2007. Object-Based Image Analysis – Spatial concepts for knowledge-driven remote sensing applications. Springer Lecture Notes in Geoinformation and Cartography.

Boulanger, A., 2005. Open-source versus proprietary software: Is one more reliable and secure than the other? IBM Systems Journal 44 (2), 239-248.

Brennan, R., Webster, T.L., 2006. Object-oriented land cover classification of lidar-derived surfaces. Canadian Journal of Remote Sensing 32 (2), 162-172.

Brenner, C., 2005. Building reconstruction from images and laser scanning. International Journal of Applied Earth Observation and Geoinformation 6 (3-4), 187-198.

Brinkhoff, T., 2004. Spatial access methods for organizing laserscanner data. International Archives of Photogrammetry, Remote Sensing and Spatial Information Sciences 35 (Part B4), 98-102.

Brovelli, M.A., Cannata, M., Longoni, U.M., 2002. Managing and processing LIDAR data within GRASS. Proceedings of the GRASS Users Conference 2002, Trento, Italy, pp. 1-29.

Burman, H., 2000. Adjustment of laserscanner data for correction of orientation errors. International Archives of Photogrammetry, Remote Sensing and Spatial Information Sciences 33 (Part B3/1), 125-132.

Cain, D.J.M., 2006. PyGreSQL – PostgreSQL module for Python. URL: `http://www.pygresql.org`

Charaniya, A.P., Manduchi, R., Lodha, S.K., 2004. Supervised parametric classification of aerial lidar data. IEEE Workshop on Real Time 3D Sensor and Their Use, June 2004, Washington DC. URL: `http://www.soe.ucsc.edu/~amin/research/cvpr04.pdf`

Chasmer, L., Hopkinson, C., Smith, B., Treitz, P., 2005. Examining the influence of laser pulse repetition frequencies on conifer forest canopy returns. Proceedings of the Silviscan Conference, Blacksburg, 2005, Virginia, USA. URL: `http://cears.fw.vt.edu/silviscan/presentations/Author24.pdf`

Clode, S.P., Kootsookos, P., Rottensteiner, F., 2004. The automatic extraction of roads from lidar data. International Archives of Photogrammetry, Remote Sensing and Spatial Information Sciences 35 (Part B3), 231-236.

Clode, S.P., Rottensteiner, F., Kootsookos, P., 2005. Improving city model determination by using road detection from lidar data. International Archives of Photogrammetry, Remote Sensing and Spatial Information Sciences 36 (Part 3/W24), 159-164.

Clode, S.P., Rottensteiner, F., 2005. Classification of trees and powerlines from medium resolution airborne laserscanner data in urban environments. Proceedings of the APRS

workshop on digital image computing (WDIC), 2005, Brisbane, Australia, 191-196. URL: http://www.aprs.org.au/wdic2005/fullproceedings.pdf

Conway, J.E., 2006. PL/R – R Procedural Language for PostgreSQL. URL: http://www.joeconway.com/plr/

Coren, F., Sterzai, P., 2006. Radiometric correction in laser scanning. International Journal of Remote Sensing 27 (15-16), 3097-3104.

Cullen, N.J., Mölg, T., Kaser, G., Hussein, K., Steffen, K., Hardy, D.R., 2006. Kilimanjaro Glaciers: Recent areal extent from satellite data and new interpretation of observed 20th century retreat rates. Geophysical Research Letters 33 (L16502), doi:10.1029/2006GL027084.

Da, T.K.F., 2006. 2D Alpha Shapes. In: CGAL-3.2 User and Reference Manual (CGAL Editorial Board). URL: http://www.cgal.org/Manual/3.2/doc_html/cgal_manual/contents.html

Definiens, 2007. eCognition User Guide, Technical report, Definiens Imaging GmbH, Munich. URL: http://www.definiens-imaging.com

Doneus, M., Briese, C., 2006. Full-waveform airborne laser scanning as a tool for archaeological reconnaissance. From Space to Place, Proceedings of the 2nd International Conference on Remote Sensing in Archaeology, December 2006, Rome. BAR International Series 1568, pp. 99-105.

Donoghue, D., Watt, P., Cox, N., Wilson, J., 2006. Remote sensing of species mixtures in conifer plantations using LiDAR height and intensity data. Oral presentation at International Workshop 3D Remote Sensing in Forestry, February 2006, Vienna. URL: http://www.rali.boku.ac.at/fileadmin/_/H857-VFL/workshops/3drsforestry/presentations/6a.5-donoghue.pdf

Dorninger, P., 2004. A Topographic Mars Information System – Concepts for Management, Analysis and Visualization of Planet-Wide Data. Doctoral thesis at the Institute of Photogrammetry and Remote Sensing, Vienna University of Technology, Vienna. URL: http://www.ipf.tuwien.ac.at/phdtheses/pdo/diss_pdo.pdf

Edelsbrunner, H., Mücke, E.P., 1994. Three-dimensional alpha shapes. ACM Transactions on Graphics 13 (1), 43-72.

ESRI, 2006. ArcGIS Data Interoperability Extension supported formats. URL: http://www.esri.com/software/arcgis/extensions/datainteroperability/about/supported-formats.pdf

European Commission – IDABC work programme, 2006. Open Source Observatory. URL: `http://europa.eu.int/idabc/en/chapter/452`

European Petroleum Survey Group, 2006. EPSG Geodetic Parameter Dataset. URL: `http://www.epsg.org`

Filin, S., 2003. Recovery of systematic biases in laser altimetry data using natural surfaces. Photogrammetric Engineering & Remote Sensing 69 (11), 1235-1242.

Filin, S., Pfeifer, N., 2005. Neighborhood systems for airborne laser scanner data. Photogrammetric Engineering & Remote Sensing 71 (6), 743-755.

Filin, S., Pfeifer, N., 2006. Segmentation of airborne laser scanning data using a slope adaptive neighborhood. ISPRS Journal of Photogrammetry and Remote Sensing 60 (2), 71-80.

Gao, J., Liu, Y., 2001. Applications of remote sensing, GIS and GPS in glaciology: a review. Progress in Physical Geography 25 (4), 520-540.

Geist, T., Lutz, E., Stötter, J., 2003. Airborne laser scanning technology and its potential for applications in glaciology. International Archives of Photogrammetry, Remote Sensing and Spatial Information Sciences 34 (Part 3/W13), 101-106.

Geist, T., 2005. Application of airborne laser scanner technology in glacier research. Doctoral thesis at the Institute of Geography, University of Innsbruck.

Geist, T., Höfle, B., Rutzinger, M., Stötter, J., 2005. Der Einsatz von flugzeuggestützten Laserscanner Daten für geowissenschaftliche Untersuchungen in Gebirgsräumen. Photogrammetrie, Fernerkundung, Geoinformation 3/2005, 183-190.

Geist, T., Höfle, B., Rutzinger, M., Pfeifer, N., Stötter, J., accepted. Laser scanning – a paradigm change in topographic data acquisition for natural hazard management. In: Veulliet, E., Stötter, J., Weck-Hannemann, H. (eds.): Sustainable natural hazard management in alpine environments. Springer.

Geist, T., Höfle, B., 2007. Technical Report: Existing software products for the management and analysis of laser scanning data. Institute of Geography, University of Innsbruck.

GiST Project, 2006. Generalized Search Tree (GiST) at UC Berkeley. URL: `http://gist.cs.berkeley.edu/`

Goodchild, M., 1992. Geographical Information Science. International Journal of Geographical Information Systems 6 (1), 31-46.

GRASS Development Team, 2006. GRASS 6.0 Users Manual. ITC-irst, Trento, Italy. URL: http://grass.itc.it/grass60/manuals/html_grass60/

GRASS Development Team, 2007. GRASS 6.3 Users Manual. ITC-irst, Trento, Italy. URL: http://grass.itc.it/grass63/manuals/html63_user/index.html

Hapke, B., 1993. Theory of reflectance and emittance spectroscopy. Cambridge Univ. Press, Cambridge, U.K..

Haralick, R.M., Shapiro, L.G., 1992. Computer and Robot Vision. Addison-Wesley Longman Publishing Co., Boston Massachusetts.

Hasegawa, H., 2006. Evaluations of LIDAR reflectance amplitude sensitivity towards land cover conditions. Bulletin of the Geographical Survey Institute 53, 43-50.

Hay, G.J., Castilla, G., 2006. Object-based image analysis: strengths, weaknesses, opportunities and threats (SWOT). International Archives of the Photogrammetry, Remote Sensing and Spatial Information Sciences 36 (Part 4/C42), URL: http://www.commission4.isprs.org/obia06/papers.htm

Höfle, B., Geist, T., Heller, A., Stötter, J., 2005. Entwicklung eines Informationssystems für Laserscannerdaten mit OpenSource-Software. Angewandte Geoinformatik 2005. Beiträge zum 17. AGIT-Symposium Salzburg, Wichmann Verlag, Heidelberg, pp. 277-286.

Höfle, B., 2006. Visualising GiST index geometry with PostGIS and GRASS GIS. URL: http://www.sai.msu.su/~megera/oddmuse/index.cgi/PosGIS_and_Grass.

Höfle, B., Rutzinger, M., Geist, T., Stötter, J., 2006. Using airborne laser scanning data in urban data management – set up of a flexible information system with open source components. Proceedings UDMS 2006: Urban Data Management Symposium, Aalborg, Denmark, pp. 7.11-7.23, (on CDROM).

Höfle, B., Pfeifer, N., in press. Correction of laser scanning intensity data: data and model-driven approaches. ISPRS Journal of Photogrammetry and Remote Sensing, doi:10.1016/j.isprsjprs.2007.05.008.

Höfle, B., Geist, T., Rutzinger, M., Pfeifer, N., 2007. Glacier surface segmentation using airborne laser scanning point cloud and intensity data. International Archives of the Photogrammetry, Remote Sensing and Spatial Information Sciences 36, Espoo, Finland, (on CDROM).

Hofmann, A.D., Maas, H.-G., Streilein, A., 2003. Derivation of roof types by cluster analysis in parameter spaces of airborne laserscanner point clouds. International Archives of the Photogrammetry, Remote Sensing and Spatial Information Sciences 34 (Part 3/W13), (on CDROM).

Hollaus, M., Wagner, W., Kraus, K., 2005. Airborne laser scanning and usefulness for hydrological models. Advances in Geosciences 5, 57-63.

Hollaus, M., Wagner, W., Eberhöfer, C., Karel, W., 2006. Accuracy of large-scale canopy heights derived from LiDAR data under operational constraints in a complex alpine environment. ISPRS Journal of Photogrammetry and Remote Sensing 60 (5), 323-338.

Hook, S.J., 2007. ASTER Spectral Library. Jet Propulsion Laboratory, Californian Institute of Technology, URL: `http://speclib.jpl.nasa.gov/`

Hopkinson, C., Demuth, M.N., 2006. Using airborne lidar to assess the influence of glacier downwasting on water resources in the Canadian Rocky Mountains. Canadian Journal of Remote Sensing 32 (2), 212-222.

Hug, C., Wehr, A., 1997. Detecting and identifying topographic objects in laser altimeter data. International Archives of Photogrammetry, Remote Sensing and Spatial Information Sciences 32 (Part 3-4/W2), 19-26.

Hyyppä, J., Hyyppä, H., Litkey, P., Yu, X., Haggrén, H., Rönnholm, P., Pyysalo, U., Pitkänen, J., Maltamo, M., 2004. Algorithms and methods of airborne laser-scanning for forest measurements. International Archives of Photogrammetry, Remote Sensing and Spatial Information Sciences 36 (Part 8/W2), 82-88.

Hyyppä, J., Wagner, W., 2007. EuroSDR Project – Radiometric Calibration of ALS Intensity. URL: `http://www.eurosdr.net`

Jackson, M., Sharov, A.I., Geist, T., Elvehøy, H., Pellikka, P., 2001. OMEGA – User Requirement Document. Project Report.

Jelalian, A.V., 1992. Laser Radar Systems. Artech House, Boston London.

Jonas, D., 2002. Airborne laser scanning: developments in intensity and beam divergence. Proceedings of the 11th Australasian Remote Sensing and Photogrammetry Conference, September 2002, Brisbane, Australia.

Jones, E., Oliphant, T., Peterson, P., et al., 2001. SciPy: Open Source Scientific Tools for Python. URL: `http://www.scipy.org`

Jutzi, B., Stilla, U., 2006. Range determination with waveform recording laser systems using a Wiener Filter. ISPRS Journal of Photogrammetry and Remote Sensing 61 (2), 95-107.

Kaartinen, H., Hyyppä, J., Gülch, E., Vosselman, G., Hyyppä, H., Matikainen, L., Hofmann, A.D., Mäder, U., Persson, Å., Söderman, U., Elmqvist, M., Ruiz, A., Dragoja, M., Flamanc, D., Maillet, G., Kersten, T., Carl, J., Hau, R., Wild, E., Frederiksen, L., Holmgaard, J., Vester, K., 2005. Accuracy of 3D city models: EuroSDR comparison. International Archives of Photogrammetry, Remote Sensing and Spatial Information Sciences 36 (Part 3/W19), 227-232.

Kager, H., 2004. Discrepancies between overlapping laser scanning strips – simultaneous fitting of aerial laser scanner strips. International Archives of Photogrammetry, Remote Sensing and Spatial Information Sciences 35 (Part B1), 555-560.

Kaasalainen, S., Ahokas, E., Hyyppä, J., Suomalainen, J., 2005. Study of surface brightness from backscattered intensity: calibration of laser data. IEEE Geoscience and Remote Sensing Letters 2 (3), 255-259.

Kennett, M., Eiken, T., 1997. Airborne measurement of glacier surface elevation by scanning laser altimeter. Annals of Glaciology 24, 293-296.

Kim, I.I., McArthur, B., Korevaar, E., 2001. Comparison of laser beam propagation at 785 nm and 1550 nm in fog and haze for optical wireless communications. Proceedings of SPIE – The International Society for Optical Engineering, Vol. 4214, pp. 26-37. URL: `http://www.systemsupportsolutions.com/WhitePapers/Comparison_Of_Beam_in_Fog.pdf`

Kodde, M.P., Pfeifer, N., Gorte, B.G.H., Geist, T., Höfle, B., 2007. Automatic glacier surface analysis from airborne laser scanning. International Archives of the Photogrammetry, Remote Sensing and Spatial Information Sciences 36, Espoo, Finland, (on CDROM).

Kraus, K., Pfeifer, N., 1998. Determination of terrain models in wooded areas with airborne laser scanner data. ISPRS Journal of Photogrammetry and Remote Sensing 53 (4), 193-203.

Kraus, K., 2004. Photogrammetrie, Band 1: Geometrische Informationen aus Photographien und Laserscanneraufnahmen, De Gruyter Verlag, Berlin.

Kraus, K., Briese, C., Attwenger, M., Pfeifer, N., 2004. Quality measures for digital terrain models. International Archives of Photogrammetry, Remote Sensing and Spatial Information Sciences 35 (Part B2), 113-118.

Lang, D.T., 2006. R/SPlus – Python Interface. URL: http://www.omegahat.org/RSPython/

Lang, S., Blaschke, T., 2006. Bridging remote sensing and GIS – what are the main supportive pillars? International Archives of the Photogrammetry, Remote Sensing and Spatial Information Sciences 36 (Part 4/C42), URL: http://www.commission4.isprs.org/obia06/papers.htm

LAS Specification, 2005. ASPRS LIDAR Data Exchange Format Standard Version 1.1. URL: http://www.lasformat.org

Lillesand, T.M., Kiefer, R.W., Chipman, J.W., 2004. Remote sensing and image interpretation. Fifth Edition, Wiley & Sons, pp. 586-593.

Lim, K., Treitz, P., Baldwin, K., Morrison, I., Green, J., 2003. Lidar remote sensing of biophysical properties of tolerant northern hardwood forests. Canadian Journal of Remote Sensing 29 (5), 658-678.

Luethy, J., Stengele, R., 2005. 3D mapping of Switzerland challenges and experiences. International Archives of Photogrammetry, Remote Sensing and Spatial Information Science 36 (Part 3/W19), 42-47.

Lutz, E., Geist, T., Stötter, J., 2003. Investigations of airborne laser scanning signal intensity on glacial surfaces – Utilizing comprehensive laser geometry modeling and orthophoto surface modeling (A case study: Svartisheibreen, Norway). International Archives of Photogrammetry, Remote Sensing and Spatial Information Sciences 34 (Part 3/W13), 143-148.

Luzum, B.J., Starek, M., Slatton, K.C., 2004. Normalizing ALSM intensities. Geosensing Engineering and Mapping (GEM) Center Report No. Rep_2004-07-001, Civil and Coastal Engineering Department, University of Florida, URL: http://www.aspl.ece.ufl.edu/reports/GEM_Rep_2004_07_001.pdf

Luzum, B.J., Slatton, K.C., Shrestha, R.L., 2005. Analysis of spatial and temporal stability of airborne laser swath mapping data in feature space. IEEE Transactions on Geoscience and Remote Sensing 43 (6), 1403-1420.

Maas, H.-G., Vosselman, G., 1999. Two algorithms for extracting building models from raw laser altimetry data. ISPRS Journal of Photogrammetry and Remote Sensing 54 (2-3), 153-163.

Maas, H.-G., 2001. On the use of pulse reflectance data for laserscanner strip adjustment. International Archives of Photogrammetry, Remote Sensing and Spatial Information Sciences 34 (Part 3/W4), 53-56.

Maas, H.-G., 2002. Methods for measuring height and planimetry discrepancies in airborne laserscanner data. Photogrammetric Engineering & Remote Sensing 68, 933-940.

Maier, B., Tiede, D., Dorren, L., 2006. Assessing mountain forest structure using airborne laser scanning and landscape metrics. International Archives of the Photogrammetry, Remote Sensing and Spatial Information Sciences 36 (Part 4/C42), (on CDROM).

Matikainen, L., Hyyppä, J., Hyyppä, H., 2003. Automatic detection of buildings from laser scanner data for map updating. International Archives of Photogrammetry, Remote Sensing and Spatial Information Sciences 34, (Part 3/W13), 218-224.

McCauley, J.D., Engel, B.A., 1995. Comparison of Scene Segmentations: SMAP, ECHO and Maximum Likelyhood. IEEE Transactions on Geoscience and Remote Sensing 33 (6), 1313-1316.

Moffiet, T., Mengersen, K., Witte, C., King, R., Denham, R., 2005. Airborne laser scanning: Exploratory data analysis indicates potential variables for classification of individual trees or forest stands according to species. ISPRS Journal of Photogrammetry and Remote Sensing 59 (5), 289-309.

Neteler, M., Mitasova, H., 2004. Open Source GIS: A GRASS GIS Approach. 2nd Edition, Boston, Dordrecht.

OGC Inc. – Open Geospatial Consortium, 1999. OpenGIS Simple Features Specification for SQL, Revision 1.1. URL: `http://portal.opengeospatial.org/files/?artifact_id=829`

Oude Elberink, S., Maas, H.-G., 2000. The use of anisotropic height texture measures for the segmentation of laserscanner data. International Archives of Photogrammetry, Remote Sensing and Spatial Information Sciences 33 (Part B3/2), 678-684.

OSI – Open Source Initiative, 2006. The Open Source Definition. URL: `http://www.opensource.org`

PCI Geomatics, 2007. Geomatica LidarEngine. URL: `http://www.pcigeomatics.com/products/lidarEngine.html`

Pebesma, E.J., Bivand, R., 2006. Spatial data in R. URL: `http://r-spatial.sourceforge.net/sp-manual.pdf`

Persson, Å., Söderman, U., Töpel, J., Ahlberg, S., 2005. Visualization and analysis of full-waveform airborne laser scanner data. International Archives of Photogrammetry, Remote Sensing and Spatial Information Sciences 36 (Part 3/W19), 103-108.

Persson, Å., Holmgren, J., Söderman, U., 2006. Identification of tree species of individual trees by combining very high resolution laser data with multi-spectral images. Proceedings of International Workshop 3D Remote Sensing in Forestry, February 2006, Vienna, pp. 91-96.

Pfeifer, N., Rutzinger, M., Rottensteiner, F., Mücke, W., Hollaus, M., 2007a. Extraction of building footprints from airborne laser scanning: comparison and validation techniques. Proceedings of the Urban Remote Sensing Joint Event, April 2007, Paris, pp. 1-9.

Pfeifer, N., Dorninger, P., Haring, A., Fan, H., 2007b. Investigating terrestrial laser scanning intensity data: quality and functional relations. Proceedings of the 8th Conference on Optical 3-D Measurement Techniques, July 2007, Zurich.

PostgreSQL Global Development Group, 2006. PostgreSQL 8.1 Documentation. URL: `http://www.postgresql.org/docs/manuals/`

Python Software Foundation, 2006. Python programming language. URL: `http://www.python.org`

Quantum GIS, 2007. Quantum GIS Open Source Geographic Information System – Community site. URL: `http://qgis.org`

R Development Core Team, 2006. R: A Language and Environment for Statistical Computing. URL: `http://www.r-project.org`

Rabbani, T., Heuvel, F.A. van den, Vosselman G., 2006. Segmentation of point clouds using smoothness constraint. International Archives of the Photogrammetry, Remote Sensing and Spatial Information Sciences 36 (Part 5), 248-253.

Rees, W.G., 2001. Physical Principles of Remote Sensing (Second Edition). Cambridge University Press, Cambridge.

Rees, W.G., 2005. Remote Sensing of Snow and Ice. Taylor & Francis.

Refractions Research Inc., 2006. PostGIS: Geographic Objects for PostgreSQL. PostGIS Manual. URL: `http://postgis.refractions.net/docs/`

Reitberger, J., Krzystek, P., Stilla, U., 2006. Analysis of full waveform lidar data for tree species classification. International Archives of the Photogrammetry, Remote Sensing and Spatial Information Sciences 36 (Part 3), 228-233.

Rigaux, P., Scholl, M., Voisard, A., 2001. Spatial Databases With Application To GIS. Morgan Kaufmann Publishers, San Francisco.

Rottensteiner, F., Trinder, J., Clode, S., Kubik, K., 2005a. Using the Dempster Shafer method for the fusion of LIDAR data and multispectral images for building detection. Information Fusion 6 (4), 283-300.

Rottensteiner, F., Trinder, J., Clode, S., Kubik, K., 2005b. Automated delineation of roof planes from lidar data. International Archives of the Photogrammetry, Remote Sensing and Spatial Information Sciences 36 (Part 3/W19), 221-226.

Rutzinger, M., Höfle, B., Geist, T., Stötter, J., 2006a. Object-based building detection based on airborne laser scanning data within GRASS GIS environment. Proceedings UDMS 2006: Urban Data Management Symposium, Aalborg, Denmark, pp. 7.37-7.48, (on CDROM).

Rutzinger, M., Höfle, B., Pfeifer, N., Geist, T., Stötter, J., 2006b. Object-based analysis of airborne laser scanning data for natural hazard purposes using open source components. International Archives of the Photogrammetry, Remote Sensing and Spatial Information Sciences 36 (Part 4/C42). URL: `http://www.commission4.isprs.org/obia06/papers.htm`

Rutzinger, M., Höfle, B., Pfeifer, N., accepted. Object detection in airborne laser scanning data – an integrative approach on object-based image and point cloud analysis. In: Blaschke, T., Lang, S., Hay, G. (eds.): Object-Based Image Analysis – Spatial concepts for knowledge-driven remote sensing applications. Springer.

Schwalbe, E., Maas, H.-G., Seidel, F., 2005. 3D building model generation from airborne laserscanner data using 2D GIS data and orthogonal point cloud projections. International Archives of the Photogrammetry, Remote Sensing and Spatial Information Sciences 36 (Part 3/W19), 209-214.

Sithole G., Vosselman, G., 2003. Report: ISPRS Comparison of Filters. URL: `http://enterprise.lr.tudelft.nl/frs/isprs/filtertest/`

Sithole, G., Vosselman, G., 2004. Experimental comparison of filter algorithms for bare-Earth extraction from airborne laser scanning point clouds. ISPRS Journal of Photogrammetry and Remote Sensing 59 (1-2), 85-101.

Sithole, G., 2005. Segmentation and classification of airborne laser scanner data. Publications on Geodesy 59, Netherlands Geodetic Commission, Delft.

Song, J.-H., Han, S.-H, Yu, K., Kim, Y.-I., 2002. Assessing the possibility of land-cover classification using lidar intensity data. International Archives of Photogrammetry, Remote Sensing and Spatial Information Sciences 34 (Part 3B), 259-262.

Stein, A., van der Meer, F.D., Gorte, B.G.H., 2002. Spatial Statistics for Remote Sensing. Kluwer Academic Publishers, Dordrecht.

Thiel, K.-H., Wehr, A., 1999. Calibration procedures of the imaging laser altimeter and data processing. Proceedings of the Joint Workshop of ISPRS WGs I/1,I/3, and IV/4: Sensors and Mapping from Space, September 1999, Hanover, Germany, (on CDROM).

Tóvári, D., Vögtle, T., 2004. Classification methods for 3D objects in laserscanning data. International Archives of the Photogrammetry, Remote Sensing and Spatial Information Sciences 35 (Part B3), (on CDROM).

Tóvári, D., Pfeifer, N., 2005. Segmentation based robust interpolation – a new approach to laser data filtering. International Archives of the Photogrammetry, Remote Sensing and Spatial Information Sciences 36 (Part 3/W19), 79-84.

UMN MapServer, 2006. UMN MapServer Homepage, University of Minnesota. URL: `http://mapserver.gis.umn.edu/`

Visual Learning Systems, 2007. LIDAR Analyst. URL: `http://www.featureanalyst.com/lidar_analyst.htm`

Vögtle, T., Steinle, E., Tóvári, D., 2005. Airborne laserscanning data for determination of suitable areas for photovoltaics. International Archives of the Photogrammetry, Remote Sensing and Spatial Information Sciences 36 (Part 3/W19), 215-220.

Vosselman, G., 1999. Building reconstruction using planar faces in very high density height data. International Archives of Photogrammetry, Remote Sensing and Spatial Information Sciences 32 (Part 3-2W5), 87-92.

Vosselman, G., 2002. On the estimation of planimetric offsets in laser altimetry data. International Archives of Photogrammetry, Remote Sensing and Spatial Information Sciences 34 (Part 3A), 375-380.

Vosselman, G., Kessels, P., Gorte, B., 2005. The utilisation of airborne laser scanning for mapping. International Journal of Applied Earth Observation and Geoinformation 6 (3/4), 177-186.

VTK, 2006. The Visualization Toolkit Homepage. URL: `http://www.vtk.org`

Wack, R., Stelzl, H., 2005. Laser DTM generation for South Tyrol and 3D visualisation. International Archives of Photogrammetry, Remote Sensing and Spatial Information Science 36 (Part 3/W19), 48-53.

Wagner, W., Ullrich, A., Melzer, T., Briese, C.,Kraus K., 2004. From single-pulse to full-waveform airborne laser scanners: potential and practical challenges. International Archives of Photogrammetry, Remote Sensing and Spatial Information Sciences 35 (Part B3), 201-206.

Wagner, W., Ullrich, A., Ducic, V., Melzer, T., Studnicka, N., 2006. Gaussian decomposition and calibration of a novel small-footprint full-waveform digitising airborne laser scanner. ISPRS Journal of Photogrammetry and Remote Sensing 60 (2), 100-112.

Wagner, W., Hollaus, M., Briese, C., Ducic, V., in press. 3D vegetation mapping using small-footprint full-waveform airborne laser scanners. International Journal of Remote Sensing.

Warmerdam, F., 2007. GDAL – Geospatial Data Abstraction Library. URL: `http://www.gdal.org`

Watt, P., Wilson, J., 2005. Using airborne light detection and ranging (LiDAR) to identify and monitor the performance of plantation species mixture. Proceedings of ForestSat 2005, Borås, Sweden, pp. 51-55.

Wehr, A., Lohr, U., 1999. Airborne laser scanning – an introduction and overview. ISPRS Journal of Photogrammetry and Remote Sensing 54 (2-3), 68-82.

Wever, C, Lindenberger, J., 1999. Experiences of 10 years laser scanning. Proceedings of the Photogrammetric Week 1999, pp. 125-132.

Wheeler, D.A., 2005. Why Open Source Software/Free Software (OSS/FS)? Look at the Numbers! URL: `http://www.dwheeler.com/oss_fs_why.html`

Wolfe, W.L., Zissis, G.J., 1993. The Infrared Handbook. Environmental Research Institute of Michigan, IRIA Series in Infrared and Electro Optics, Ann Arbor, MI.

Würländer, R., Rieger, W., Drexel, P., Briese, C., 2005. Landesweite Datenerhebung mit ALS – technologische Herausforderungen und vielseitige GIS-Anwendungen. Angewandte Geoinformatik 2005, Beiträge zum 17. AGIT-Symposium, Salzburg, pp. 800-805.

Zhang, L., Yang, C., Tong, X., Rui, X., 2007. Visualization of large spatial data in networking environments. Computers & Geosciences 33 (9), 1130-1139.

Zhu, Q., Gong, J., Zhang, Y., 2007. An efficient 3D R-tree spatial index method for virtual geographic environments. ISPRS Journal of Photogrammetry and Remote Sensing 62 (3), 217-224.

Appendix

ALS software overview

The software list is not exhaustive. Internet links were last visited 04.07.2007. Detailed list see next page.

Overview of most widely-used ALS software (source: Geist and Höfle, 2007)

Developer/Company	Software	Homepage
Airborne 1 Corporation	LiDAR XLR8R	http://www.airborne1.com/products/xlr8r.shtml
Ambercore Software	Amber IQ	http://www.ambercore.com/Amber_iQ.php
Applied Imagery LLC	QT Modeler	http://www.appliedimagery.com/products.html
*Arizona State University	LViz	http://lidar.asu.edu/LViz.html
FLI-MAP	FLIP7	http://www.flimap.com/site5.php
GeoCue Corporation	LIDAR 1 CuePac	http://www.niirs10.com/Products/lidar1.htm
GeoLAS Consulting	LAStools	http://www.geolas.com/Pages/servTools.html
*Helica, OGS	TARGET	http://www.helica.it/eng/prod/soft.asp
IPF, TU Vienna; inpho	SCOP++	http://www.ipf.tuwien.ac.at/products
Merrick	MARS	http://www.merrick.com/servicelines/gis/mars.aspx
*NOAA Coastal Services Center	LIDAR Data Handler	http://www.csc.noaa.gov/crs/tcm/lidar_handler.html
PCI Geomatics	Geomatica Lidar Engine	http://www.pcigeomatics.com/products/lidarEngine.html
*Politecnico di Torino	VELOCE	ftp://gps.polito.it/lidar/gnu/readme.txt
QCoherent Software	LP 360 Version	http://www.qcoherent.com/product.htm
Riegl	RiSCAN PRO	http://www.riegl.com/
Sanborn Map Company	FASE	http://www.sanborn.com/technologies/lidar.asp
Terrasolid	TerraScan	http://www.terrasolid.fi/en/products/terrascan
TopoSys GmbH	TopPIT	http://www.toposys.com
Visual Learning Systems Inc.	ESRI Lidar Analyst	http://www.featureanalyst.com/lidar_analyst.htm

* free/open source software